NOVA SCHOOL OF SCIENCE & TECHNOLOGY

DEPARTAMENTO DE CIÊNCIA DOS MATERIAIS

MÓNICA AVELÃS STANTON ARAU RIBEIRO

Licenciada em Ciências de Engenharia de Materiais

DEVELOPMENT OF NEW MATERIALS FOR CO_2 CONVERSION

EFFECT OF CARBONIZATION

MESTRADO INTEGRADO EM ENGENHARIA DE MATERIAIS

Universidade NOVA de Lisboa

Novembro, 2021

DEVELOPMENT OF NEW MATERIALS FOR CO_2 CONVERSION

EFFECT OF CARBONIZATION

MÓNICA AVELÃS STANTON ARAU RIBEIRO
Licenciada em Ciências de Engenharia de Materiais

Orientador: Doutora Marta Corvo, Investigadora, i3N|Cenimat, NOVA School of Science and Technology, Lisboa

Coorientadores: Doutora Marcileia Zanatta, Investigadora, i3N|Cenimat, NOVA School of Science and Technology, Lisboa

Institute of Advanced Materials (INAM), Universitat Jaume I, Espanha

Júri:

Presidente: Doutor Alexandre José da Costa Velhinho, Professor Auxiliar do Departamento de Ciência dos Materiais da NOVA School of Science and Technology | FCT NOVA

Arguentes: Engenheiro Nuno Filipe Constâncio Rodrigues, Responsável Projetos Ambientais, The Navigator Company

Vogais: Doutora Marta Cristina Parracho Cançado Corvo, Investigadora contratada do Departamento de Ciência dos Materiais da NOVA School of Science and Technology | FCT NOVA

MESTRADO INTEGRADO EM ENGENHARIA DE MATERIAIS

Universidade NOVA de Lisboa
Novembro, 2021

Development of New Materials for CO_2 Conversion: Effect of Carbonization

ACKNOWLEDGMENTS

First and foremost, I would like to thank my adviser, Dr. Marta Corvo, for all the help and support given to me in these months that we've worked together, for always being available to answer my endless doubts and for showing constant interest in my work. I also thank my co-adviser, Dr. Marcileia Zanatta, for being the one that accompanied me in my lab work, even though I was the one following her around most of the time. Thank you for all the reassurance you've given me and the availability that you always showed.

I will be forever grateful for the luck of having such amazing advisers, who had a major impact on the quality of my work.

I would like to thank Professor Márcia Vilarigues for Raman spectra acquisition, Dr. Daniela Gomes for SEM images acquisition, Professor Margarida Rolim for granting access to the Ceramics Lab, and Professor João Canejo for the sporadic, but always appreciated, kind words and smiles.

I thank CENIMAT|i3N and DCM from the NOVA School of Science and Technology of the NOVA University of Lisbon for being my second home these past five years.

I thank the GREENPILs4CO2 Project (PTDC/QUI-QFI/31508/2017) and the Rede Nacional de Ressonância Magnética Nuclear (RNRMN) for granting me access to the spectrometers, partially supported by Project PINFRA/22161/2016. I also thank LAQV/REQUIMTE – the Associated Laboratory for Green Chemistry for suppling the analysis needed.

I'm eternally grateful to my family, both close and far, for their incessant interest in all of my work and for the constant motivation to do my best. Grandma and Grandpa, I miss you like crazy and I cannot wait to be with you again so we can talk about everything that has happened these past three years in incredible detail. Obrigada Avô e obrigada Avó por terem sido a fonte de carinho e calma ao longo destes anos de trabalho.

To the Fantastic Beasts and the tightknit support system we've created for each other. Each of you have been the source of immense fulfillment in these past years and I appreciate you all.

And last but not least, to Francisco, without whom this journey would not have been the same but I can safely say that we both will be overjoyed to have finished it.

"When you've got 'em by the curiosity,
their hearts and minds will follow."
(Sir Terry Pratchett)

ABSTRACT

The alarming rise in carbon dioxide (CO_2) emissions has been met with urgent calls to the scientific community and global enterprises. One of the solutions relies on the conversion of CO_2 into added-value products, such as cyclic carbonates. The catalysts required to counteract the inevitable harsh conversion reaction conditions may be found in the carbonization of waste biomass materials into porous carbons. While corporations struggle to take action against these climate-related issues, The Navigator Company, a leading Portuguese paper manufacturer, transparently and proactively collaborated with this six-month study of applied waste materials.

Specifically, sludges and knots, kindly granted by The Navigator Company, were compared to commercially available chitosan, alongside six commercially available ionic liquids (ILs) with different anion/cation pairings for their potential as precursors to porous carbocatalysts. The ILs were selected for their use as templates, solvents, and catalysts as well as their unique properties (negligible vapor pressure, stability, and tunability). The synthesis on the carbon materials involved an initial hydrothermal carbonization in a Parr reactor, followed by carbonization with nitrogen flow in an alumina furnace. The cycloaddition reaction of CO_2 to styrene oxide using the prepared carbocatalysts was carried out in a Parr reactor.

To assess the effect of the ILs on the conversion reaction, on the carbonization yield, on the nitrogen content, on the degree of graphitization, and on the porosity, the resulting samples were characterized by elemental analysis, Scanning Electron Microscopy, nitrogen adsorption/desorption isotherms, and Raman spectroscopy. The catalytic potential of the obtained carbon materials was examined using ^1H NMR spectra.

Results of this study confirm efficient carbocatalyst production from waste biomass materials, with a maximum conversion of 81% and selectivity >99%, and further demonstrate that the choice of IL has a direct influence on the conversion. Further research will contribute to global demands for a circular economy.

Keywords: Waste biomass, Ionic liquid, Carbonization, CO_2 conversion, Styrene carbonate

RESUMO

O aumento das emissões de dióxido de carbono (CO_2) é um facto alarmante que requer respostas urgentes da comunidade científica e das grandes empresas. Uma das soluções estudadas é a conversão de CO_2 em carbonatos cíclicos. Para esta reação ocorrer sem condições agressivas, é necessário introduzir catalisadores produzidos, por exemplo, pela carbonização de resíduos à base de biomassa para a obtenção de carvões porosos. Enquanto algumas grandes empresas têm dificuldades em atuar perante estes problemas climatéricos, *The Navigator Company*, uma empresa líder na produção de papel, colaborou com este trabalho ao longo de seis meses na implementação dos seus resíduos para produzir catalisadores.

Especificamente, lama primária, lama biológica e nós incozidos, cedidos pela *The Navigator Company*, foram comparados com quitosano comercial quanto à sua capacidade de serem precursores de carvões porosos. Também foram utilizados seis diferentes líquidos iónicos (LIs) como precursores devido às suas propriedades únicas. Os materiais de partida foram inicialmente carbonizados hidrotermicamente num reator Parr, seguindo uma carbonização com fluxo de azoto num forno tubular de alumina. As reações entre CO_2 e óxido de estireno, utilizando os carvões sintetizados como catalisadores, foram realizadas num reator Parr.

De modo a determinar o efeito dos LIs no rendimento da conversão e da carbonização, na percentagem de azoto, no grau de grafitização e na porosidade, os carvões foram caraterizados por análise elementar, Microscopia Eletrónica de Varrimento, isotérmicas de adsorção/deadsorção de azoto e por espetroscopia de Raman. O rendimento da conversão foi analisado por RMN ^1H, de modo a determinar a eficiência catalítica dos carvões.

Os resultados obtidos nesta dissertação confirmam não só a possibilidade de produção de catalisadores carbonosos a partir de resíduos à base de biomassa, com um rendimento de conversão máximo de 81% e seletividade >99%, mas também demonstram que a escolha do LI afeta diretamente o rendimento da conversão.

Palavras chave: Biomassa, Resíduo, Líquido iónico, Carbonização, Conversão de CO_2, Carbonato de estireno

CONTENT

LIST OF FIGURES

LIST OF TABLES

LIST OF ABBREVIATIONS

[Bmim][Cl]	1-butyl-1methylimidazolium chloride
[Bmpyr][Cl]	1-butyl-1-methylpyrrolidinium chloride
[Bmpyr][DCA]	1-butyl-1-methylpyrrolidinium dicyanamide
[2Bmpy][Cl]	1-butyl-2-methylpyridinium chloride
[4Bmpy][Cl]	1-butyl-4-methylpyridinium chloride
BET	Brunauer-Emmett-Teller
br	broad
carbocatalyst	carbon-based, metal-free catalyst
CCS	carbon capture and storage
δ	chemical shift
CHI	chitosan
HBD	hydrogen bond donor
HTC	hydrothermal carbonization
IUPAC	International Union of Pure and Applied Chemistry
IL	ionic liquid
ITC	ionothermal carbonization
m	multiplet
MEA	monoethanolamine
NLDFT	non-local density functional theory
NMR	nuclear magnetic resonance
NTf_2	bis(trifluoromethylsulfonyl)imide
PIL	poly(ionic liquid)
PVBACl	poly(vinylbenzyltriethylammonium) chloride
PDADMACl	polydiallyldimethylammonium chloride
s	singlet
SC	styrene carbonate
SEM	scanning electron microscopy
SO	styrene oxide
t	triplet
TBABr	tetrabutylammonium bromide
TBACl	tetrabutylammonium chloride
VBACl	vinylbenzyltriethylammonium chloride

1. CONTEXT, MOTIVATION, AND OBJECTIVES

The alarming rise in carbon dioxide (CO_2) emissions has been met with urgent global demands for sustainable development and a circular economy. Among the effective solutions, the conversion of CO_2 into added-value products could respond to this need for greener chemistry. The combined characteristics of being a low-cost and non-toxic by-product of fossil fuel combustion and its abundance in nature, make the use of CO_2 very appealing to the scientific community [1].

As such, the conversion of this gas into added-value products is a topic that has gathered great interest due to the call for greener chemistry. The variety of applications ranges from plastics and resin materials to solvents for battery electrolytes and important chemical intermediates in the pharmaceutical industry [2].

Independently of the products desired from CO_2 conversion, it involves a reaction that cannot be performed on its own due to the elevated thermodynamic stability of this gas. To decrease the activation energy of the desired reaction, highly energetic starting materials (hydrogen, epoxides, amines, etc.) and catalysts are used in conjunction to curb the fact that the carbon atom in the CO_2 molecule is in its most oxidized state and, consequently, shows low molecular reactivity [3].

To promote the spirit of creating added-value products from CO_2 through green chemistry, this Master's dissertation proposes to explore carbon-based metal-free materials as catalysts (also known as *carbocatalysts* [4]), produced from the carbonization of waste biomass. To further explore the possibilities of a circular economy, successful contact with The Navigator Company, a leading Portuguese manufacturer of paper products, drew on mutual interest in developing materials for green applications. This company is part of an industry that is responsible for producing massive amounts of waste biomass, from discarded wood to sludges from wastewater treatment, which are a significant environmental concern [5]. This six-month study applied these waste materials, specifically sludges and knots, kindly granted by The Navigator Company, as precursors to porous carbon materials, which were then tested for their catalytic potential in the cycloaddition of CO_2 to styrene oxide.

Addressing the following topics should fulfill the objectives of this Master's dissertation:

- Porosity formation by the introduction of additives, such as ionic liquids (ILs);
- Influence of ILs on the chemical and structural properties of the resulting carbon materials (nitrogen content, degree of graphitization, and carbonization yield);
- Catalytic activity of the resulting carbon materials and the influence of different reaction parameters on the conversion;
- Comparison of the overall performance of the industrial waste biomass materials with that of commercially available biomass (chitosan).

2. INTRODUCTION

2.1. The problem of carbon dioxide

One of the major challenges affecting the planet today is global warming. The worldwide climate crisis caused by this phenomenon involves significant detrimental changes to all living beings.

Some of the main contributors to the climate crisis are greenhouse gases such as, carbon dioxide (CO_2), methane, and nitrous oxide. Of these, CO_2 is the most abundant, primarily released by burning fuels such as oil, natural gas, diesel, petrol, organic-petrol, and ethanol [6]. As shown in Figure 2.1, beginning with the Industrial Revolution (*circa* 1800), CO_2 emissions rose steadily until around the 1970s, when a significant increase in emissions was first recorded that has led to constant escalation over nearly five decades [7].

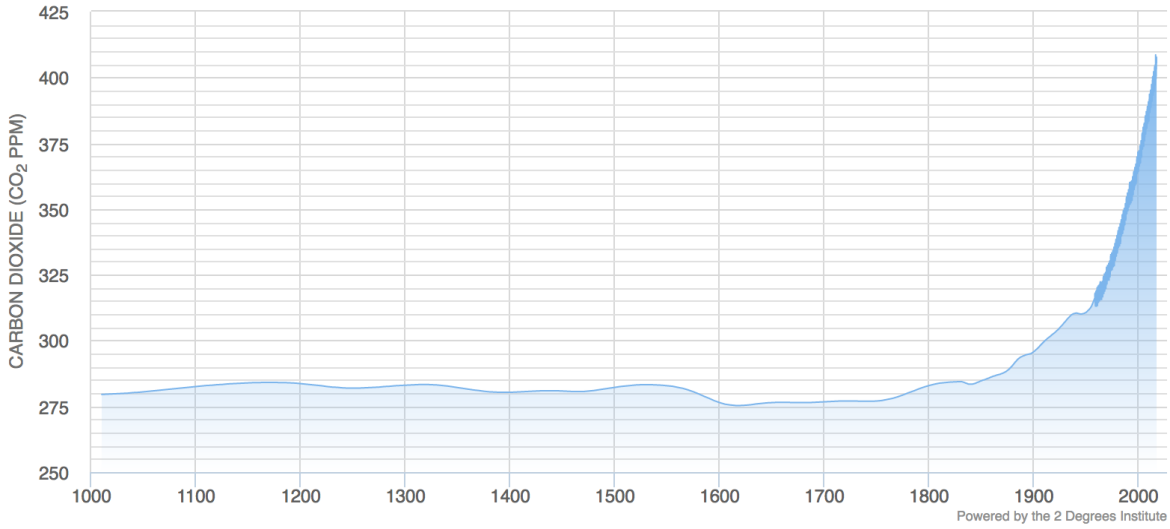

Figure 2.1. Global CO_2 levels over the years. Source: 2 Degrees Institute (https://www.co2levels.org/)

The increase in CO_2 levels has resulted in a rise in global temperature which is one of the principal concerning consequences of high emissions, recognized by many world powers that signed the 2015 Paris Climate Change Agreement [8] in a commitment to

> *"[h]olding the increase in the global average temperature to well below 2°C above pre-industrial levels and pursuing efforts to limit the temperature increase to 1.5°C above pre-industrial levels, recognizing that this would significantly reduce the risks and impacts of climate change".*

Without efforts to cap this surge, global warming can result in dire consequences, some of which are already visible today: the rise of sea levels, the growing intensity of extreme weather conditions, changes in agricultural production, permafrost thaw and glacier retreat, the extinction of species, and more diseases [6]. Technologies for carbon capture and storage

(CCS) have proven to be a key component in the mitigation of climate change. Gouveia *et al.* [9] predict a 70% increase in the overall cost of mitigation if CCS is not available during the 2020s, which further supports the need for investment in CCS so that CO_2 gas can be segregated from its sources, stored, and properly converted into useful substances [10].

2.2. Converting carbon dioxide into added-value products

CO_2, considered an economically abundant, non-toxic source of C1 to produce chemicals and energy [11], can fulfill the need for green chemistry through its transformation into added-value products such as methanol [12], dimethyl carbonate [13], urea [14], carboxylic acids [11], or, most commonly, cyclic carbonates [15]. Thorough investigation in this area shows, however, that the gas' high stability, inert properties and low reactivity in many chemical reactions make its conversion require harsh reaction conditions [3].

Based on these findings, the introduction of catalysts, whether heterogeneous or homogeneous, can make the reaction conditions less aggressive (characterized by both lower temperature and pressure) and allow for large scale transformation of CO_2 into added-value products [12]. Catalysts can be classified as heterogeneous when they are in a different phase than the reactants, or as homogeneous when they are in the same phase as the reactants [16]. Typical homogeneous catalysts for CO_2 conversion are metal complexes [17], ionic liquids (ILs) [18], superbases [19], and organocatalysts [20]. Typical heterogeneous catalysts include poly(ionic liquid)s (PILs) [21], [22], metal organic frameworks [23], porous carbons [24], silica sieves [25], and metal oxides [26].

Despite the reported higher catalytic activity of homogeneous catalytic systems, heterogeneous catalysts have not only a simpler reactor design, but also better separation, handling, stability and reusability of the catalyst. Production costs are also lowered with heterogeneous catalysts given their high efficiency [12].

Amongst the heterogeneous catalysts listed, porous carbon materials may be one of the most promising heterogeneous catalysts due to their many unique properties, which include low cost, potential for increased active sites through heteroatom doping, high surface area, and high porosity [27]. These carbon materials can even be prepared from inexpensive, highly renewable, and eco-friendly materials, such as biomass [28]–[31].

2.3. Biomass-based porous carbon materials as heterogeneous catalysts

2.3.1. The appeal of biomass for carbon dioxide conversion

"Biomass" is defined as all biological material from living or recently living organisms. Considered the only renewable organic resource and one of the most abundant ones, biomass should be used efficiently [32].

For a more sustainable future and to combat the trend towards a depletion of natural resources, biomass has drawn much attention due to its many vital properties:

inexpensiveness, renewability, non-toxicity, easy access, rapid regeneration, availability in high quality, and eco-friendliness [33], [34].

Notably, in the field of CCS, biomass materials show very promising results from commercially available materials such as chitosan [35], [36], glucose [37], algae [28], and cellulose [38], to materials derived from other industries, such as waste cow manure [27], rice husk [39]–[43], wood sawdust [44], cocoa bean shells [45], or waste sludges [46]–[50].

Biomass materials are not only a widely available and renewable resource, they can also be manipulated to allow fine-tuning of their physical and chemical properties, which makes them more appealing as heterogeneous catalysts for CO_2 conversion than expensive non-biomass-based catalysts that currently dominate this field [39], [51]–[53]. The natural abundance of functional groups in biomass materials, like hydroxyl, carboxyl, or aldehyde groups, is one of the properties that has been found to play an important role in the cycloaddition reaction of CO_2 to epoxides [54].

Regardless of the benefits, there are some drawbacks to using biomass materials in scientific research. These include, the difficulty associated with the replicability of results since the environment is ever-changing and because biomass decays and is susceptible to damage, which could alter the morphology and structure of the biomass itself. Nevertheless, the advantages outweigh the disadvantages, which makes biomass appealing for use in large-scale production in a world economy aiming to use waste and biomass materials as feedstock to promote a more circular economy [55].

2.3.2. Porous carbon materials synthesis strategies

The inherent properties of biomass, such as its high carbon content and low inorganic content, make materials of a biomass nature ideal precursors to porous carbons [56].

Porous carbons are produced by carbonization, which involves heating the starting material to eliminate volatiles and enrich the matrix in carbon. Removing the heterogenous elements results in a skeleton made primarily of carbon with a simple porous structure and increased aromaticity. The development of aromatic compounds is evidence of new empty spaces, left by the volatilized functional groups and bridged chains, which are an essential part of porous carbons [57].

Traditionally, porosity can be induced in the carbon via activation, which can be physical or chemical, leading to an activated carbon. *Physical activation* involves heating the precursors to 600-1200˚C while applying gases (CO_2, steam, or air). In *chemical activation*, the activating agents ($ZnCl_2$, NaOH, KOH, K_2CO_3, or H_3PO_4) are impregnated into the precursors and pyrolysis follows at temperatures of 450-900˚C. The final material is then washed thoroughly to remove any remaining activating agent [57].

Another technique that can be used to induce porosity in the carbon material is templating, which is classified as either *template-assisted* or *template-free*. In template-assisted carbonization, the objective is to replicate the structure and texture of the template in the carbon material by simple filling of the template and subsequent thermolysis. This technique can be divided into *hard templating*, which uses inorganic materials as templates (SiO_2, MgO, ZnO, Al_2O_3, TiO_2, zeolite, etc.), and *soft templating*, using organic materials as templates (ILs,

block polyether F127, etc.). Template-free carbonization, however, is the simplest method, involving only the direct carbonization of the precursor without any additional templates or complex procedures [58].

A different type of carbonization that also shows promising results in the production of carbon materials from biomass is *hydrothermal carbonization* (HTC), where hydrochars are produced from the application of an aqueous medium over 100 ˚C and 0.1 MPa. Hydrochars can also undergo activation to further improve their porosity [59], [60].

Although it is more common to rely on carbonization-activation methods to produce porous carbons from biomass materials, additives can also be incorporated into the system as carbon precursors in order to induce further porosity, such as ILs.

2.4. Ionic liquids

2.4.1. The unique properties of ionic liquids

ILs are organic salts that exist freely and stably in liquid form at temperatures below 100˚C. They contain positively and negatively charged ions. Usually, they are composed of a large nitrogen or phosphorous-containing cation (e.g., imidazolium or phosphonium, respectively), where the anion is much smaller and can be organic (e.g., bis(trifluoromethylsulfonyl)imide (NTf_2^-) or dicyanamide ($N(CN)_2^-$)) or inorganic (e.g., Cl^- or tetrafluoroborate (BF_4^-)) [61] (Figure 2.2).

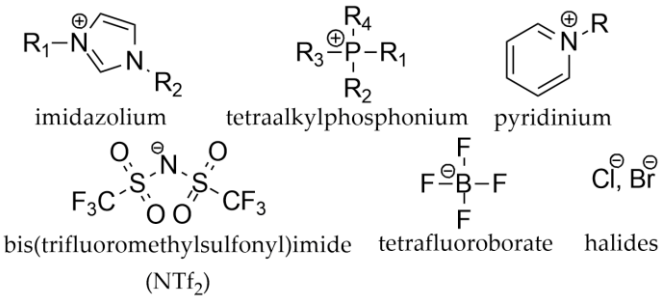

Figure 2.2. Common cations and anions in ionic liquids.

Even though ILs were discovered over a century ago, in 1914 [62], scientists continue to be interested in their unique physical and chemical properties, from their negligible vapor pressure, their thermal, photo, electro and chemical stability, and non-flammability to the fact that their anions and cations can be combined in many different ways to create numerous compounds with distinct properties that affect their CO_2 solubility and selectivity [63], [64]. Furthermore, the supramolecular structural organization of ILs is a singular property which results in the presence of non-homogenous nano-domains that can accommodate both polar and non-polar compounds [65], [66].

Another class of materials that has grown from ILs are PILs, the polymerization products of an IL monomer. This means that each repeating unit is ionic and connected through a polymeric backbone forming a macromolecular structure. As such, PILs combine the above-mentioned superior qualities of ILs and the properties of polymers, such as good

mechanical stability. Furthermore, they present improved processability and spatial controllability, when compared to their corresponding IL monomers [67].

2.4.2. Ionic liquids as carbon precursors

Just over a decade ago in 2009, Dai *et al.* [68] discovered the initial palpable connection between ILs and carbon materials, using a template-free methodology to carbonize 1-butyl-3-methylimidazolium bis(trifluoromethylsulfonyl)imide ([Bmim][NTf_2]). A year later, Yuan *et al.* [69] complemented this template-free carbonization research by first reporting the conversion of PILs into porous carbons.

Since then, ILs have been used as templates in soft-templating carbonization [70], solvents in *ionothermal carbonization* (ITC) [71] and in other variations of these techniques, such as self-templating [72], salt-templating [73], [74], and confined carbonization [75].

In template-assisted carbonization, the use of ILs is very advantageous since they are generally liquid at room temperature, which means that they are easily incorporated into the porous templates without the application of any intricate techniques prior to carbonization. Another property of ILs that facilitates their use in this type of carbonization is their energetic interactions with different surfaces, which improves homogenous coverage of the IL on the template surface without additional solvents or pressure [58], [76], [77].

For template-free carbonization, most IL-derived porous carbons either have uncontrollable porosity and pore location or low surface areas [58], [78]. Proper identification of the carbon precursor can avoid these issues and lead to successful carbonization. As such, there have been successful reports on the synthesis of porous carbons via direct carbonization of ILs resulting in higher porosities and greater surface areas [68], [69], [79].

Analogous to HTC, studies have taken an IL approach to hydrothermally carbonizing biomass materials through ITC [45], [80]–[84]. In this type of carbonization, the IL plays three key roles as soft template, solvent, and catalyst, resulting in enhanced carbon yields [71].

2.5. Approach and contributions of this study

To study a green pathway for the development of heterogeneous catalysts for CO_2 conversion, this study aims to explore the catalytic potential of carbon materials produced from biomass (chitosan, knots, and waste sludges), assessing the role that ILs and other additives have in the carbon yield, nitrogen content, porosity, and conversion for the cycloaddition reaction of CO_2 to styrene oxide (SO).

In order to do so, reports with similar conditions were compiled and are summarized in Table A.1 in the Appendix. A wide variety of conditions are applied, CO_2 pressure from 1-40 bar of, 30-150 °C, over the course of 0.5-48 h. Most carbocatalysts show conversions in the range of 70-100% and high selectivity (>90%).

Most of the studies found do not use ILs as carbon precursors, but rather immobilized them onto the surface of the biomass-based carbon. The use of both biomass and ILs as carbon precursors is, however, applied in the areas of supercapacitors [69] and CO_2 capture [36], among others. Here, we propose applying metal-free carbon materials prepared with biomass and IL precursors for the development of new materials for a solvent-free CO_2 conversion.

3. EXPERIMENTAL

The reagents and equipments used throughout the study are listed in Section A.2 in the Appendix, along with the conditions of the characterization techniques. Additional experimental procedures are mentioned in Section A.3.

3.1. Synthesis of carbon materials

3.1.1. Pre-carbonization processes

1-Butyl-1-methylimidazolium chloride ([Bmim][Cl]) was dried under vacuum for 2 h prior to use. 1-Butyl-4-methylpyridinium chloride ([4Bmpy][Cl]) was dried under vacuum overnight at 50 ^{o}C prior to use.

Paper mill waste sludges (primary and biological) and knots were dried under vacuum at 105 ^{o}C for 2 h. They were then ground and sieved to obtain uniform powders which were stored until used.

3.1.2. Carbonization

The present methodology was based on that reported by Wu *et al.* [36]. In a typical experiment, 500 mg of selected biomass material, 250 mg of additive (IL or salt mixture), and 5 mL of water were stirred at 50 ^{o}C for 60 min to obtain a suspension. This suspension was then inserted into a Parr reactor, placed into an oil bath and heated to 180 ^{o}C for 17 h. The reactor was then placed in an ice bath to cool down.

The resulting product was collected, centrifuged at 12000 rpm for 5 min, washed with water until the solution was clear, and washed one final time with ethanol. The solid was then dried overnight at 100 ^{o}C.

The resulting powder was placed in a tubular alumina furnace under nitrogen atmosphere. The furnace containing the sample was purged with nitrogen flowing at 75 mL min^{-1} for 30 min at room temperature. The nitrogen flow was then reduced to 10-20 mL min^{-1} and the furnace heated at a rate of 15 ^{o}C min^{-1} to 800 ^{o}C for 2 h. After the dwell was completed, the nitrogen flow was interrupted and, by switching off the power, the furnace cooled down to room temperature.

Carbonization of the biomass materials was also performed without additives, following all the steps described above. The completed carbonizations are listed in Table 3.1 and the chemical structures of the selected additives can be found in Table A.2 in the Appendix. The samples were then characterized through elemental analysis, nitrogen adsorption/desorption isotherms, Scanning Electron Microscopy (SEM), and Raman spectroscopy.

Table 3.1. Materials used in all completed carbonizations.

Entry	Sample designation	Biomass	Additive
1	CHI-0	CHI	−
2	Kno-0	Knots	−
3	PriS-0	Primary sludge	−
4	BioS-0	Biological sludge	−
5	BioS-ImCl	Biological sludge	[Bmim][Cl]
6	CHI-ImCl	CHI	[Bmim][Cl]
7	CHI-PyrCl	CHI	[Bmpyr][Cl]
8	CHI-PyrDCA	CHI	[Bmpyr][DCA]
9	CHI-PDADMACl	CHI	PDADMACl
10	CHI-2PyCl	CHI	[2Bmpy][Cl]
11	CHI-4PyCl	CHI	[4Bmpy][Cl]
12	CHI-DES	CHI	LiCl/KCl[a]
13	CHI-DES-F[b]	CHI	LiCl/KCl[a]

[a] 45:55 by weight.

[b] Carbon obtained from washing and filtering sample CHI-DES.

3.1.3. Post-carbonization treatment of LiCl/KCl-based carbon

After carbonization, the sample prepared from chitosan (CHI) and the salt mixture LiCl/KCl (CHI-DES) was washed and filtered with sufficient water to remove any remaining salt. The sample was then dried at 40 ^{o}C under vacuum for over 42 h and designated CHI-DES-F.

3.2. Cycloaddition of CO_2 and recyclability

In a typical experiment, a certain amount of SO, catalyst and co-catalyst were placed in a Parr reactor. The reactor was purged three times with cycles of vacuum and CO_2, in order to evacuate the air from the inside of the equipment, and then charged to 5 bar of CO_2. The reactor was placed in an oil bath previously heated to 100 ^{o}C for a designated time. When the reaction time was complete, the reactor was placed into an ice bath to cool down.

After this, all the product from the reaction was transferred from the reactor to an Eppendorf tube, which was centrifuged, and the supernatant was separated from the carbocatalyst, into an NMR test tube. This supernatant was then analyzed by ^{1}H NMR to assess the outcome of the reaction.

To assess the recyclability of the carbocatalyst, after completing all the steps described previously, the remaining carbon material was washed, shaken, and centrifuged with 500 µL of trichloromethane twice. Both times, the supernatant was removed after centrifuging, so to eliminate all traces of the co-catalyst. The washed product was then placed under vacuum for 18 h at 40 ^{o}C, after which the carbocatalyst was reused in a subsequent reaction under the same conditions, by adding SO and co-catalyst.

The conversion of the reactions was assessed using ^{1}H NMR after every cycle.

4. RESULTS AND DISCUSSION

Metal-free carbon samples were produced by a two-step procedure, namely a hydrothermal carbonization followed by a carbonization with nitrogen flow (Figure 4.1). The samples were analyzed by elemental analysis, nitrogen adsorption/desorption isotherms, SEM, and Raman spectroscopy. Once the carbon samples were characterized, they were applied as catalysts for the cycloaddition reaction of CO_2 to SO to produce styrene carbonate (SC) in the absence of solvents. The conversion was determined by ^1H NMR spectra.

This study aimed to successfully produce carbocatalysts from (waste) biomass and ILs.

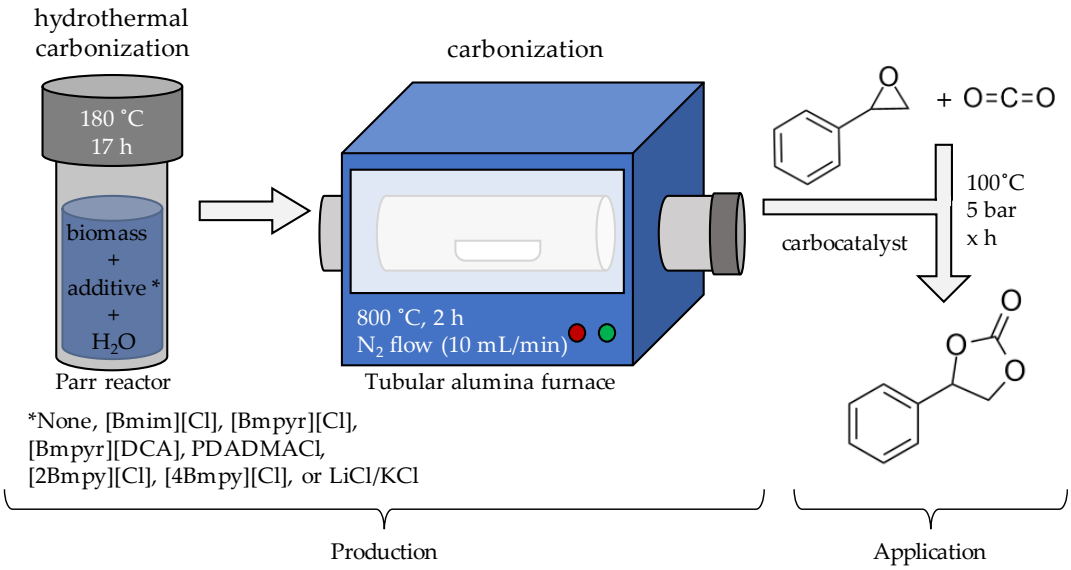

Figure 4.1. Schematic illustration of the general procedure of the present study.

4.1. Characterization of the carbocatalysts

4.1.1. Carbonization yield and elemental analysis

As a starting point for the analysis of the carbon samples, their carbonization yield (to be named carbon yield hereafter) was calculated using the following Equation (1), where W1 and W2 are the weights of the material, before and after carbonization:

$$Carbon\ yield\ (in\ wt.\%) = \frac{(W1)}{(W2)} \times 100 \quad (1)$$

Posteriorly, elemental analysis of the starting materials and of the resulting carbons was performed.

4.1.1.1. Chitosan samples

The results for the elemental analysis of the starting chitosan and chitosan-based carbons can be found in Table 4.1, along with the respective carbon yields.

Table 4.1. Elemental analysis of chitosan and chitosan-based carbons, with respective average carbon yields.

Entry	Sample	N (wt.%)	C (wt.%)	H (wt.%)	H/C[a]	N/C[a]	Average Carbon Yield (wt.%)
1	CHI	6.94	40.15	6.88	2.06	0.15	–
2	CHI-0	7.14	47.49	0.71	0.18	0.13	32
3	CHI-ImCl	6.69	74.70	1.45	0.23	0.08	30
4	CHI-PyrCl	6.91	76.97	1.06	0.17	0.08	28
5	CHI-PyrDCA	8.04	76.32	1.12	0.18	0.09	27
6	CHI-PDADMACl	7.35	73.49	0.95	0.16	0.09	28
7	CHI-2PyCl	6.89	77.40	0.99	0.15	0.08	29
8	CHI-4PyCl	7.23	78.46	1.06	0.16	0.08	32
9	CHI-DES	5.02	53.11	1.06	0.24	0.08	40
10	CHI-DES-F	6.79	70.05	0.82	0.14	0.08	29

[a] Molar ratio.

Since carbonization enriches the matrix in carbon and removes heterogenous elements, what is left behind is a skeleton with an improved carbon content and a reduced nitrogen and hydrogen content [85]. The table above shows this overall trend for the carbon and hydrogen contents. However, when looking at the nitrogen content of each sample, four samples show a higher value than that of the starting chitosan: CHI-0 with 7.14 wt.%, CHI-PyrDCA with 8.04 wt.%, CHI-PDADMACl with 7.35 wt.%, and CHI-4PyCl with 7.23 wt.% (Entries 2, 4, 6, and 8 of Table 4.1, respectively). The most significant difference is with sample CHI-PyrDCA, which could be because this is the only sample whose IL precursor anion contains nitrogen while the others contain only the ion chloride. The significant presence of nitrogen in this sample can have an influence on its catalytic activity since this heteroatom helps keep the catalytic phase well-dispersed and intervenes in the reaction mechanism [86], as discussed in Section 4.2.1.

Comparing IL cation type, the average nitrogen content of the carbonized samples increases in the following order: imidazolium < pyridinium < pyrrolidinium. Sun *et al.* [87] reported similar results to those obtained in the present study.

Regarding sample CHI-DES (Entry 9 of Table 4.1), which has the lowest nitrogen content (5.02 wt.%), this result is expected since the additive used was a salt mixture of LiCl/KCl that does not contain nitrogen. Furthermore, in samples CHI-DES and CHI-DES-F (entries, 9 and 10 of Table 4.1, respectively), the nitrogen and carbon content increases from 5.02 to 6.79 wt.% and from 53.11 to 70.05 wt.%, respectively. Being that the only step involved was washing and filtering, this change in nitrogen and carbon content is likely due to the removal of inorganic

matter, such as the excess salt [50], indicating that some of the salt mixture was still present after carbonization, as confirmed during SEM analysis.

When comparing carbon yields, all samples range from 27 to 32 wt.%, except for sample CHI-DES which yielded 40 wt.% (Entry 9 of Table 4.1). But once this sample is washed and filtered in order to obtain sample CHI-DES-F (Entry 10 of Table 4.1), the yield decreases significantly to 29 wt.%, which fits in the established range of the carbon yields. Furthermore, none of the carbons produced showed a higher carbon yield than sample CHI-0 (32 wt.%, which is similar to that found in the literature [70]), leading to the observation that, if the objective is to obtain the highest yield, it can be done by carbonizing the chitosan alone, without any additives. Nevertheless, even though the yield is lower when an IL or the salt mixture additive is used, other properties may arise, such as nitrogen content, porosity, or surface area, which are desired for applications in CO_2 capture and conversion [88], [89].

It is widely accepted that cyano or nitrile groups favor the carbon yield, due to the fact that, during the pyrolysis, nitrile groups can undergo cyclization. This process results in higher yields because it does not allow for as much molecular disorientation yet simultaneously retains a higher mass yield by converting the volatile linear structure into a ring conformation [68], [69], [87], [90], [91]. However, the sample that contains these groups, CHI-PyrDCA, has the lowest carbon yield of 27 wt.% (Entry 5 of Table 4.1). Nevertheless, even though this sample has the lowest yield value, it also shows the highest nitrogen content of all the carbons prepared, which hints at its catalytic activity, as was mentioned previously and will be discussed later.

Furthermore, the samples whose IL cation type was pyrrolidinium show the lowest carbon yields (Entries 4 to 6 of Table 4.1, resulting in yields of 27 and 28 wt.%), which is in agreement with the literature [87].

The H/C ratio indicates the presence of aromatic or aliphatic groups, being that a lower ratio indicates the presence of more aromatic groups in the sample [47], [49]. The first observation is that all carbonized samples in comparison with the starting chitosan, exhibit a higher carbonized and aromatic structure, which is expected because, in this process, while the heteroatoms are removed, the remaining carbon atoms group into stacks of flat aromatic sheets, which are randomly cross-linked [92]. Furthermore, the H/C ratios of the carbonized samples are all very similar, with samples CHI-ImCl and CHI-DES showing the highest values (Entries 3 and 9 of Table 4.1, with ratios of 0.23 and 0.24, respectively).

Relative to the N/C ratio, this value can be correlated to the polymerization degree of the organic matter of the samples, where a higher N/C ratio means that the sample is less polymerized [49]. Consequently, sample CHI-0 shows to be the least polymerized (Entry 2 od Table 4.1), with the additives having the effect of lowering the N/C ratio, thus increasing the polymerization degree. There are no significant variations of the N/C ratio amongst the carbonized samples.

4.1.1.2. Waste biomass samples

Table 4.2 shows the elemental analysis of the waste biomass samples (waste sludges and knots) and biomass-based carbons, with their respective carbon yields.

Table 4.2. Elemental analysis of waste biomass materials and waste biomass-based carbons, with respective average carbon yields.

Entry	Sample	N (wt.%)	C (wt.%)	H (wt.%)	S (wt.%)	H/C[a]	N/C[a]	Average Carbon Yield (wt.%)
1	Knots	0.11	44.18	5.04	0.56	1.37	<0.01	–
2	Primary Sludge	0.63	29.88	3.73	0.15	1.50	0.02	–
3	Biological Sludge	2.74	33.52	3.97	0.42	1.42	0.07	–
4	Kno-0	0.24	72.18	0.43	0.51	0.07	<0.01	22
5	PriS-0	0.11	7.02	0.82	0.21	1.40	0.01	37
6	BioS-0	0.15	9.07	0.44	0.59	0.58	0.01	41
7	BioS-ImCl	0.31	9.42	1.78	0.17	2.27	0.03	38

[a] Molar ratio.

The paper and pulp industry transforms significant amounts of lignocellulosic biomass, as such, their residues are mainly lignocellulosic [93], which is the case of the knots used in the present study. Regarding these samples (Entries 1 and 4 from Table 4.2), they are the only ones whose carbon and nitrogen content both increase after carbonization (from 0.11 to 0.24 wt.% and from 44.18 to 72.18 wt.%, respectively), despite the lowest carbon yield of 22 wt.%. This could be due to the decomposition of carbon in the form of CO, CO_2 and CH_4 and tar coupling with O and H atoms [94]–[96]. This low value of carbon yield could be useful for storage purposes if the aim were to reduce the volume of material.

As mentioned in the previous Section 4.1.1.1, for most carbonized organic materials, there is an increase in the carbon content. However, for sludges, the opposite is more common [46], which is the case with both of the sludges analyzed (Entries 5 to 7 from Table 4.2).

For sample BioS-ImCl, which is the biological sludge carbonized with the [Bmim][Cl] precursor, a higher nitrogen content is registered relative to sample BioS-0 (Entries 7 and 6 of Table 4.2 with nitrogen contents of 0.31 and 0.15 wt.%, respectively). This increase could be due to the nitrogen in the IL's structure remaining after the carbonization. Comparison of the carbon yields of these two samples shows that when the IL is present there is a slight decrease in this value (from 41 to 38 wt.%), which assures the economic viability of carbonizing the biological sludge, without the expense of commercial chemicals, to obtain a similar amount of carbon material.

Comparing the starting materials to their carbonized counterparts without additives (Entries 1 to 6 from Table 4.2), there is an overall decrease in the H/C ratio, which indicates the formation of highly carbonized and aromatic structures. Among the waste sludges and the knots, sample PriS-0 seems to be the one with the most aromatic structures (H/C ratio of 1.40). Furthermore, this value might also mean that it has a high amount of organic compounds like, cellulose, lignin, and the other polymeric compounds originally present in the sludge [47], [97]. Regarding samples BioS-0 and BioS-ImCl (Entries 6 and 7 of Table 4.2, respectively), there is an increase in the H/C ratio when the IL is added (from 0.58 to 2.27),

which means that sample BioS-ImCl shows more aromaticity, which is expected due to the aromatic ring present in the imidazolium.

Regarding the N/C ratios, they are all relatively low, with a highest value of 0.07 for the starting biological sludge (Entry 3 of Table 4.2), which would mean that all samples also have a high degree of polymerization.

Finally, comparing the entries from Table 4.1 and Table 4.2, there is a noticeable difference in the carbon yield. It appears that samples PriS-0, BioS-0, and BioS-ImCl have a higher yield (37, 41 and 38 wt.%, respectively) than any of the carbons produced with chitosan (ranging from 27 to 40 wt.%). This is a good indicator to the feasibility of using waste sludges from the paper and pulp industry as a carbon precursor.

4.1.2. Textural properties

The textural properties were analyzed through nitrogen (N_2) adsorption/desorption isotherm and SEM. The N_2 adsorption/desorption isotherms were first analyzed using the Brunauer-Emmett-Teller (BET) theory. However, for most of the samples analyzed, the criteria for this model were not met. It is generally accepted that the BET theory is not suitable for microporous carbons, due to the fact that it does not take into account micropore filling [98], which could be the case for the samples prepared for this study. Another attempt to obtain porosity values was carried out using another model (non-local density functional theory (NLDFT) model), which similarly could not provide values of porosity.

Nevertheless, the study continued on the basis of the N_2 adsorption/desorption isotherms (all isotherms can be found in Figure A.5 to Figure A.7 in the Appendix), which can be classified into six main types of isotherms that indicate the type of porosity of the material, according to the International Union of Pure and Applied Chemistry (IUPAC) [98]: Type I − microporosity; Types IV and V − mesoporosity; Types II, III, and VI − nonporous/macroporosity. Additionally, IUPAC also categorizes the type of porosity, based on the pore size of the material: microporosity (<2 nm), mesoporosity (2−50 nm), or macroporosity (>50 nm).

In order to overcome the problem of the porosity values, SEM images (Figure A.8 to Figure A.11 in the Appendix) were analyzed with the assistance of the software *ImageJ*, which provided an estimate of the average pore width.

The samples prepared exhibit every type of isotherm, except Types IV and V, and the average pore width also varies from sample to sample.

4.1.2.1. Chitosan samples

Samples CHI-0 and CHI-PyrCl both show a combined behavior of Type I/II isotherms, which indicates their micro/macroporous nature (Figure 4.2(a) and (b), respectively), however, they are different kinds of Type I isotherms, where sample CHI-0 is a Type I(a) and sample CHI-PyrCl is a Type I(b). The main difference in aspect of these two isotherms is at low p/p^0, where the former is steeper than the latter. This difference means that sample CHI-0 has almost exclusively narrow micropores, and their filling occurs at low p/p^0, while sample CHI-PyrCl has wider micropores, with the possibility of narrow mesopores. In both cases, the

plateau region corresponds to the formation of a monolayer. Both samples also show a hysteresis loop, where the desorption branch is higher than the adsorption branch, which means that the dimensions of the pores make the desorption more difficult. In this case, the pore width exceeds the critical width, which depends on the adsorption system and temperature when the analysis is performed [98]. Beyond this, the hysteresis loop can be more closely observed as an H4 loop, whose branches are parallel and practically horizontal, and which is typical of narrow pores that have a slit shape [57]. It was not possible to confirm these results with SEM images due to the resolution of the microscope used.

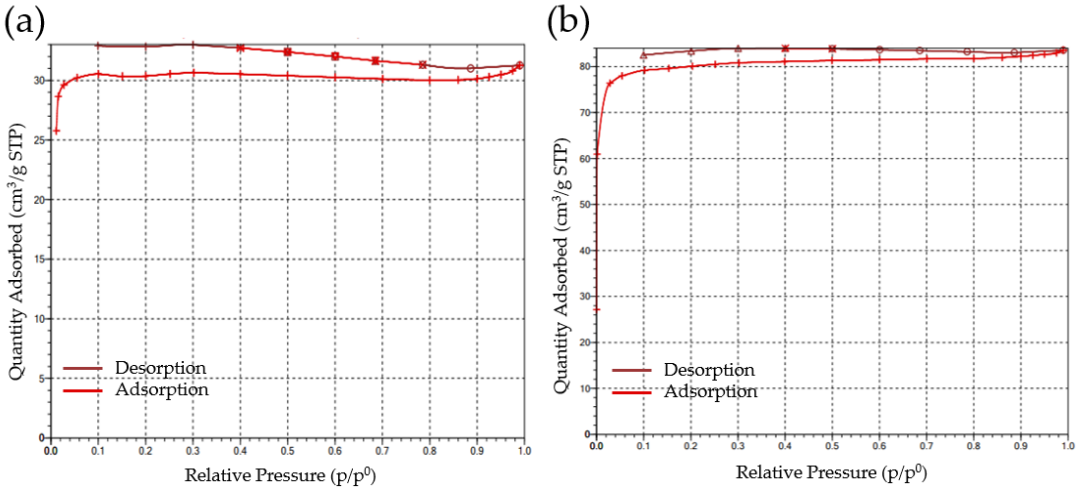

Figure 4.2. N_2 adsorption/desorption isotherm at 77 K of samples: (a) CHI-0. (b) CHI-PyrCl.

However, the bulk morphology of these and all the other carbons prepared was observed with SEM (Figure A.8 in the Appendix). In general, the samples prepared with chitosan do not differ greatly from each other and appear to fit into the description of a microporous activated carbon first provided by Stoeckli [99] (Figure 4.3), which states that:

> *"[t]he structure consists of aromatic sheets and strips, often bent and resembling a mixture of wood shavings and crumpled paper, with variable gaps of molecular dimensions between them – the micropores."*

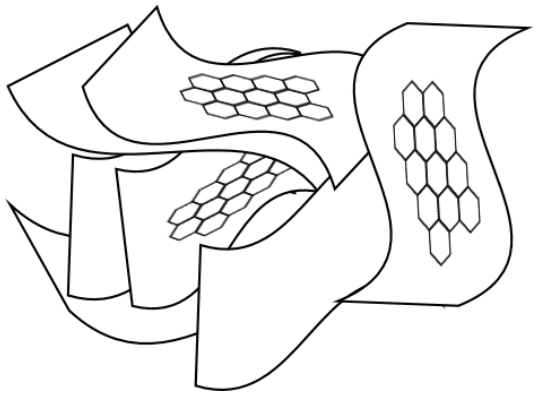

Figure 4.3. Schematic illustration of an activated carbon.

Samples CHI-DES and CHI-DES-F both present isotherms that indicate that they are nonporous or macroporous (Type III and Type II, respectively, as shown in Figure A.6(b) and

(c) in the Appendix). The SEM analysis corroborates this hypothesis as observed in Figure 4.4, where we see that sample CHI-DES is non-porous and CHI-DES-F is macroporous (average pore width of 364 nm).

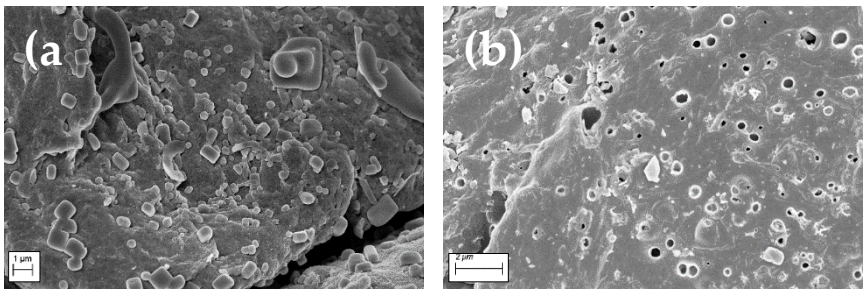

Figure 4.4. SEM images of samples: (a) CHI-DES. (b) CHI-DES-F.

While inspecting sample CHI-DES (Figure 4.4(a)), it is clear that there are additional structures present in this carbon that are not present in the other samples. It was believed that there was leftover LiCl/KCl salt mixture still present in the carbon so the sample was washed and filtered to remove the excess salt, obtaining sample CHI-DES-F (Figure 4.4(b)). Observation of this new sample with SEM shows that the excess salt was successfully removed and that whatever remains is very scattered. Furthermore, in the place of the salt crystals, pores have appeared that were not visible before washing and filtering the sample.

Samples CHI-PyrDCA, CHI-2PyCl, and CHI-4PyCl have isotherms that do not fit into any of the categories defined by IUPAC (Figure A.5(d) and (f), and Figure A.6(a) in the Appendix, respectively). But when analyzing these samples with SEM (Figure 4.5), it is clear that some porosity is present (average pore widths of 88, 122, and 84 nm, respectively), consequently they would all be categorized as macroporous carbons.

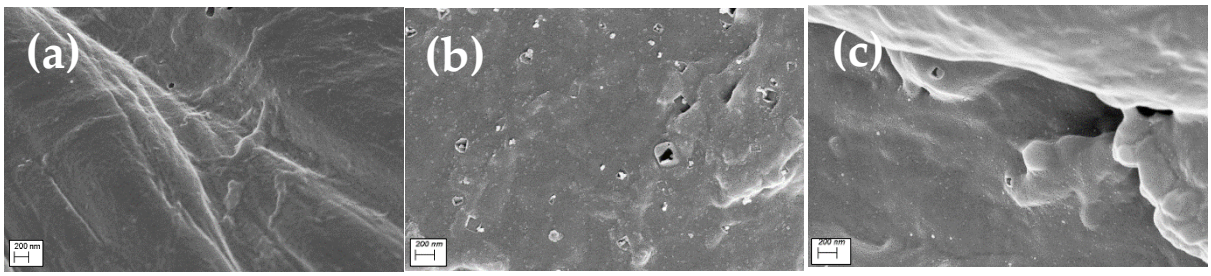

Figure 4.5. SEM images of samples: (a) CHI-PyrDCA. (b) CHI-2PyCl. (c) CHI-4PyCl.

Additionally, there is a clear difference in the abundance of pores of the two pyridinium-based carbons, with sample CHI-2PyCl showing more pores than CHI-4PyCl (Figure 4.6(a) and (b), respectively).

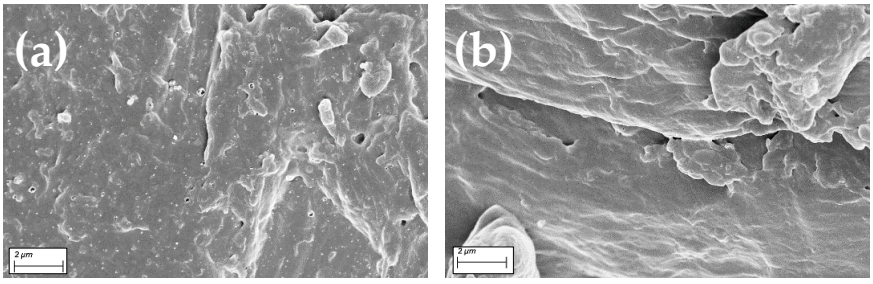

Figure 4.6. SEM images of samples: (a) CHI-2PyCl. (b) CHI-4PyCl.

Other samples that have isotherms that indicate no porosity or macroporosity are samples CHI-ImCl and CHI-PDADMACl, both of which show an isotherm Type VI although sample CHI-ImCl has a desorption branch that resembles a Type II isotherm (Figure A.5(b) and (e) in the Appendix, respectively). SEM images of the latter sample do not show much porosity, while images of sample CHI-PDADMACl actually show pores that range in width from about 40 to 80 nm (Figure 4.7(a) and (b), respectively). This means that sample CHI-PDADMACl possesses some mesoporosity that was not accounted for in the isotherm.

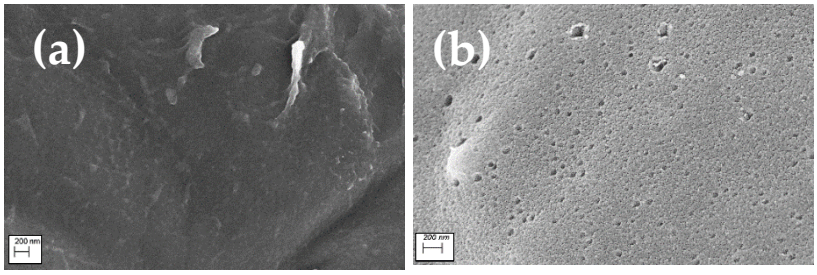

Figure 4.7. SEM images of samples: (a) CHI-ImCl. (b) CHI-PDADMACl.

By cross-referencing the information from the N_2 adsorption/desorption isotherms and the pore width values given by *ImageJ*, the pore sizes of the chitosan-based carbonized samples are shown to increase in the following order of cation type: pyrrolidinium < pyridinium < imidazolium, where the PIL with a pyrrolidinium base (sample CHI-PDADMACl) produced larger pores than its IL counterpart (sample CHI-PyrCl). A similar result can be found in the literature, and is believed to be a result of the multivalent binding power of the PIL [80]. Additionally, the salt mixture LiCl/KCl, after being washed from the carbon material, produced the largest pores of all the samples, as shown in Table 4.3.

Table 4.3. Average pore width as determined by *ImageJ*.

Sample	Average pore width (nm)[a]
CHI-PDADMACl	40−80
CHI-4PyCl	84
CHI-PyrDCA	88
CHI-2PyCl	122
CHI-DES-F	364

[a] Values obtained directly from *ImageJ*.

4.1.2.2. Waste biomass samples

Analysis of the starting waste biomass materials and comparison with SEM images of the starting chitosan shows clear structural differences between these biomasses (Figure 4.8). Their differences can be analyzed based on an understanding of the production process of the paper mill. In the present study, all waste biomass (knots and sludges) were obtained from a paper mill that works exclusively with eucalyptus wood through the kraft pulp production process.

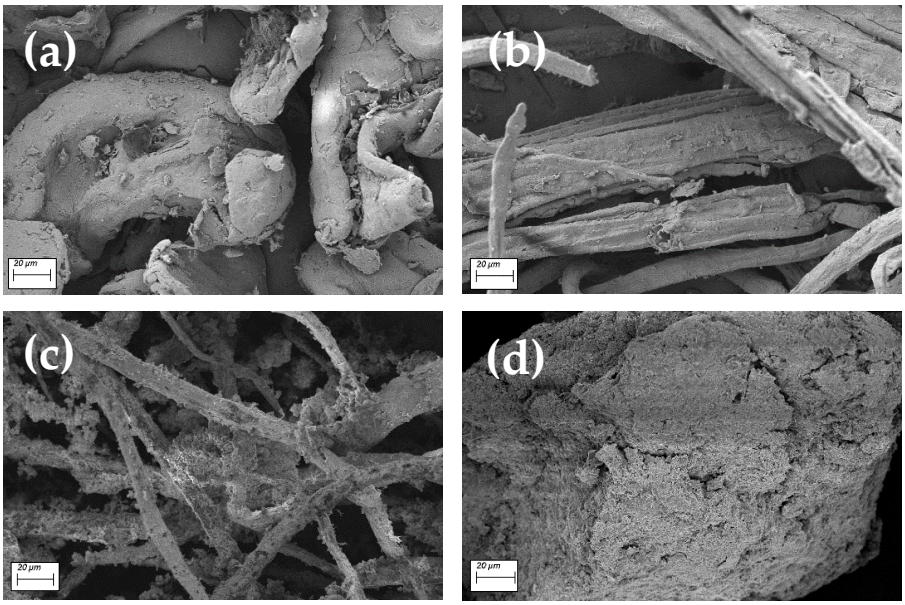

Figure 4.8. SEM images of starting materials: (a) CHI. (b) Kno. (c) PriS. (d) BioS.

Originated from the cooking process in the paper mill, knots consist of rejects from the pulp washing and screening stage (after cooking and before bleaching) that are discarded due to morphological anomalies (density, dimensions, etc.) The waste sludges, which occur during effluent treatment, are first considered primary sludge, composed mainly of fibers and other solids lost in contact with diverse equipment. The fibers consist mostly of cellulose, hemicellulose, and lignin. After primary treatment, the remaining suspended solids in the wastewater are submitted to bacterial digestion, under aerobic conditions, to reduce the organic matter content in the effluent. These biological sludges are composed of the mixture of biosolids and the remaining suspended solids [100]–[102].

Commercially available chitosan (Figure 4.8(a)) appears smooth and round, like small grains. Of the waste biomass samples, only the structure of the biological sludge (Figure 4.8(d)) compares with that of chitosan, even though it appears to have a rougher surface. This could be one of the suspended solids contained in the sludge. In contrast, the knots and the primary sludge (Figure 4.8(b) and (c), respectively) are completely different. Their more fibrous than grain-like appearance can be ascribed to their composition, since the knots are rejects from pulp washing and screening and the primary sludge consists of fibers discarded during effluent treatment.

The carbons prepared from these waste biomasses do not show porosity, as is confirmed by their isotherms (Figure A.7 in the Appendix). All the carbons prepared with the sludges show a Type III isotherm (samples PriS-0, BioS-0, and BioS-ImCl), and the one prepared with knots (sample Kno-0) has a Type II isotherm, which indicates that they are all nonporous/macroporous.

When analyzing these samples by SEM, there is an evident difference in structure between the samples carbonized from the knots (Figure 4.9(a)) and the waste sludges (Figure 4.9(b) to (d)). While the samples prepared with the waste sludges exhibit a stacked structure, the knots originated a flatter surface. Observing with lesser magnification, sample Kno-0 has kept its pre-carbonization, more fibrous structure (Figure A.10(b) in the Appendix), while

samples PriS-0, BioS-0, and BioS-ImCl (Figure A.10(d), (f), and (g) in the Appendix, respectively) have a more powder-like structure.

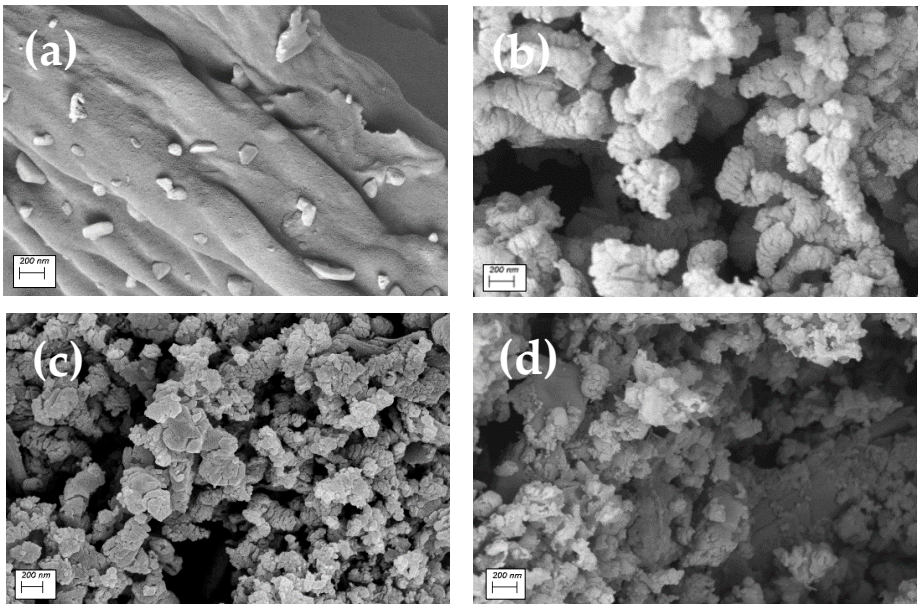

Figure 4.9. SEM images of samples: (a) Kno-0. (b) PriS-0. (c) BioS-0. (d) BioS-ImCl.

4.1.3. Raman spectroscopy

4.1.3.1. Chitosan samples

According to literature [103], [104], Raman spectroscopy is a technique that is well-suited for analysis of the structure of carbonaceous materials. One of the Raman spectra can be found in Figure 4.10, while the rest of the chitosan-based carbonized samples spectra are shown in Figure A.12 of the Appendix and Table 4.4 notes the D and G band values obtained from the Raman spectra of the carbons obtained from chitosan, along with their respective intensity values and I_D/I_G intensity ratio.

Analyzing the Raman spectra, the characteristic D and G bands are present in all the carbon samples [105]. These bands are related to the defective/disordered structure of the carbon and the in-plate vibration of the sp^2 carbon atoms, respectively. The ratio of their intensities (I_D/I_G) is used to evaluate the degree of graphitization of the carbon, such that a higher intensity ratio points to a more disordered structure [24], [36], [106], [107].

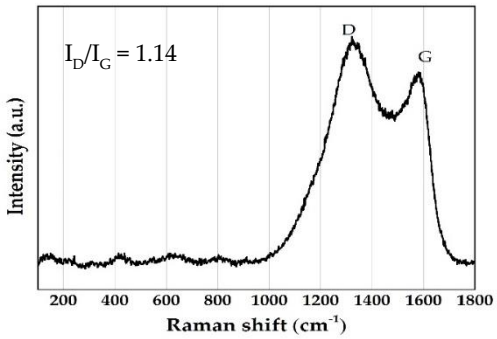

Figure 4.10. Raman spectrum of sample CHI-0.

Table 4.4. Raman structural parameters of chitosan-based carbons.

Entry	Sample	D band (cm^{-1})	G band (cm^{-1})	I_D (a.u.)	I_G (a.u.)	I_D/I_G
1	CHI-0	1330	1583	0.88	0.75	1.14
2	CHI-ImCl	1327	1585	0.82	0.69	1.19
3	CHI-PyrCl	1329	1582	0.75	0.62	1.22
4	CHI-PyrDCA	1334	1595	0.74	0.60	1.05
5	CHI-PDADMACl	1329	1568	0.70	0.66	1.30
6	CHI-2PyCl	1331	1574	0.87	0.67	1.16
7	CHI-4PyCl	1326	1579	0.85	0.73	1.17
8	CHI-DES	1332	1588	0.85	0.75	1.09

All samples in the table above show a relatively high intensity ratio, indicating a more disordered/amorphous structure [36], [107]. Comparing sample CHI-0 (Entry 1 of Table 4.4) to all the others that were carbonized with an additive, an overall increase in the intensity ratio is shown, except for samples CHI-PyrDCA and CHI-DES (Entries 4 and 8 of Table 4.4, respectively), which means that only the addition of [Bmpyr][DCA] or of the salt mixture LiCl/KCl cause an increase in the degree of graphitization and, consequently, less structural defects. A further observation based on these results is the highest I_D/I_G value of 1.30 that belongs to sample CHI-PDADMACl (Entry 5 of Table 4.4), which means that this sample has the lowest degree of graphitization. This could be related to the fact that the additive PDADMACl used as a precursor was a 20 wt.% solution in H_2O, resulting in excess water present during the hydrothermal carbonization compared to the other samples.

4.1.3.2. Waste biomass samples

Raman spectra of the waste biomass-based carbonized samples are shown in Figure A.13 in the Appendix while Table 4.5 presents the values of the D and G bands of the carbons as well as their respective intensity values and I_D/I_G ratio.

Table 4.5. Raman structural parameters of waste biomass-based carbons.

Entry	Sample	D band (cm^{-1})	G band (cm^{-1})	I_D (a.u.)	I_G (a.u.)	I_D/I_G
1	Kno-0	1327	1584	0.79	0.73	1.09
2	PriS-0	1318	1584	0.70	0.52	1.36
3	BioS-0	1322	1588	0.69	0.51	1.35
4	BioS-ImCl	1324	1579	0.75	0.62	1.22

Observing these results, the carbonized sludges (Entries 2 to 4 from Table 4.5) show similar intensity ratios and, consequently, similar degrees of graphitization. In comparison to the intensity ratio of the sample prepared from the knots (Entry 1 from Table 4.5), the latter appears to have a higher degree of graphitization, which means that it shows less structural defects.

When comparing samples BioS-0 and BioS-ImCl (Entries 3 and 4 of Table 4.5, respectively), the incorporation of the IL additive caused a reduction in the intensity ratio (1.35 to 1.22, respectively) and, therefore, a rise in the degree of graphitization, bringing it closer to the intensity ratio value of the chitosan sample prepared with the same IL additive (Entry 2 from Table 4.4). Additionally, these samples that were prepared with the biological waste sludge present a single peak at around 1080 cm^{-1}, observable in Figure 4.11, which indicates the presence of carbonate ions [108]. This presence, also encountered by Jaria *et al.* [5], can be justified by the use of calcium carbonate as a blanching agent for pulp and paper production.

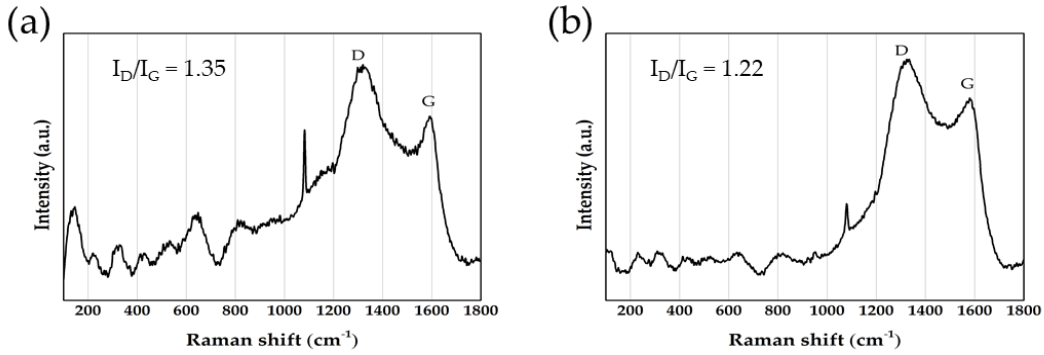

Figure 4.11. Raman spectra of samples: (a)BioS-0. (b) BioS-ImCl.

4.2. Application of the carbocatalysts in the conversion of CO_2

Once the samples were characterized accordingly, the viability for their application as carbocatalysts for the cycloaddition reaction of CO_2 to SO for the formation of SC, in the absence of solvents, was tested. All product formation was analyzed with ^1H NMR spectroscopy to identify and quantify the products of the cycloaddition reaction.

The calculation of the conversion of the reaction was based on the moles of SO and SC, which were obtained from the integration of the methylene resonance observable in the ^1H NMR spectra at a chemical shift of 3.91 and 5.71 ppm, respectively, indicated as b and b' in Figure 4.12 [109]. Equations (3) and (4) were used to obtain the conversion and the selectivity of the reaction. For all reactions, no diol was detected, so the selectivity was >99%.

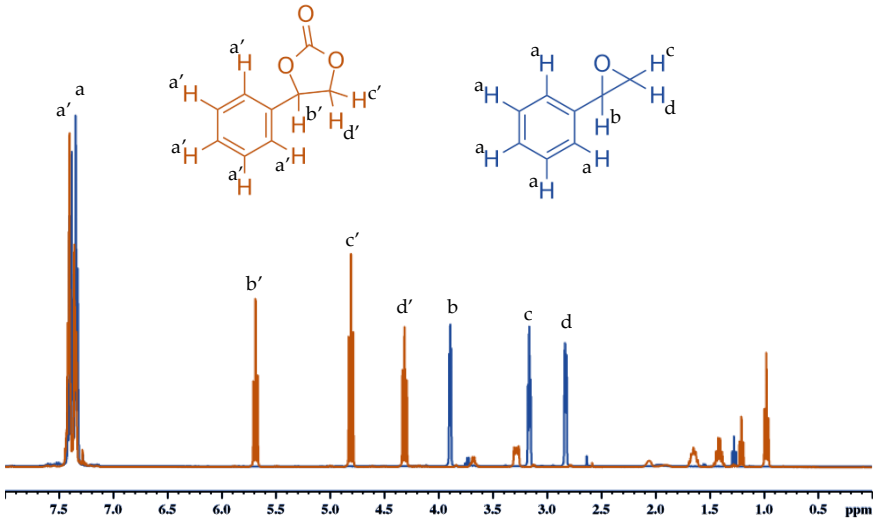

Figure 4.12. Model ^1H NMR of SO and catalytic reaction mixture with SC overlapped.

$$mol\ of\ reaction\ products = mol\ of\ SC + mol\ of\ diol\ (if\ present) \quad (2)$$

$$Conversion\ \% = \frac{mol\ of\ reaction\ products}{mol\ of\ reaction\ products + mol\ of\ unreacted\ SO} \times 100 \quad (3)$$

$$Selectivity\ \% = \frac{mol\ of\ SC}{mol\ of\ reaction\ \ products} \times 100 \quad (4)$$

To verify that the CO_2 to be introduced in the reaction would not alter the carbocatalyst structurally, CO_2 flow tests of 5 and 30 min were run. The carbon sample CHI-ImCl, before and after being subjected to a CO_2 flow, was analyzed with Raman spectroscopy. No significant structural alterations were detected in the corresponding spectra (Figure A.14 in the Appendix). A photograph and a schematic illustration created to show the flow system of the CO_2 can be found in Figure A.15 in the Appendix.

4.2.1. Synthesis of styrene carbonate

To evaluate and compare their efficiency, all the carbocatalysts that were prepared were tested under the same conditions for the production of SC from the cycloaddition reaction of CO_2 to SO. The results are detailed in Table 4.6, grouped by biomass, IL cation, and IL anion.

Table 4.6. Screening of carbocatalysts in the reaction between SO and CO_2 to obtain SC[a].

Entry	Catalyst	Conversion (%)
1	Kno-0	50
2	PriS-0	47
3	BioS-0	75
4	BioS-ImCl	81
5	CHI-0	61
6	CHI-ImCl[b]	≈0
7	CHI-ImCl@TBABr-20[c]	5
8	CHI-ImCl@TBABr-50[d]	21
9	CHI-ImCl	80
10	CHI-2PyCl	77
11	CHI-4PyCl	58
12	CHI-PyrCl	74
13	CHI-PDADMACl	56
14	CHI-PyrDCA	62
15	CHI-DES	74
16	CHI-DES-F	74

[a] Reaction conditions, unless stated otherwise: 100 °C, 3 h, CO_2 (5 bar), SO (6.66 mmol), catalyst (10 mg), co-catalyst TBABr (7 mol% in relation to SO).

[b] Without co-catalyst TBABr.

[c] Carbocatalyst CHI-ImCl impregnated with co-catalyst TBABr (12 mg), as detailed in Section A.3.2.

[d] Carbocatalyst CHI-ImCl impregnated with co-catalyst TBABr (20 mg), as detailed in Section A.3.2.

To properly analyze the conversions obtained, it is essential to have a comprehensive understanding of the conversion mechanism of the cycloaddition of CO_2 to epoxides (Figure 4.13) and potential influences. The conversion mechanism itself can be described in three key steps [110]: first, the epoxide is activated and the oxirane ring opened by a nucleophilic group; next the CO_2 molecule inserts into the oxygen anion intermediate, and finally the ring closes to form the cyclic carbonate. The nucleophilic group is then recycled for further reaction.

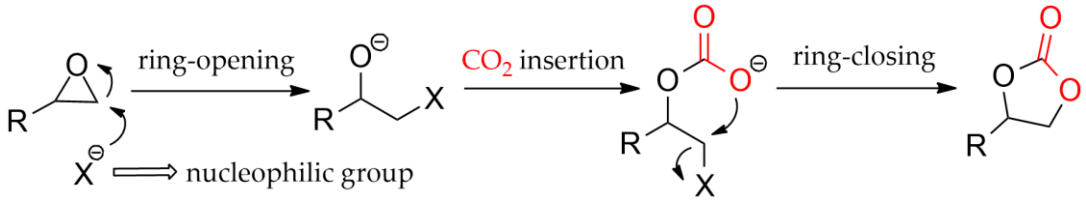

Figure 4.13. Generally accepted mechanism of the cycloaddition reaction of epoxides with CO_2.

The rate-determining step of the reaction is the epoxide ring-opening by a nucleophile [111]. The epoxide is usually activated by a Lewis acid, either a transition metal or a hydrogen bond donor (HBD). This compound binds to the oxygen atom of the epoxide through the formation of a hydrogen bond, activating the epoxide. After this, the ring can be opened by a nucleophilic attack at the less sterically hindered carbon of the epoxide [112]. Thus, it is generally accepted that an efficient catalytic system for this reaction would employ a Lewis acid center in combination with highly nucleophilic groups [113].

Biomass materials generally possess a limited number of reactive sites, most of which are HBD groups, such as hydroxyl, methoxy, aldehyde, ketone, carboxyl, among others. Lewis bases can also help speed up the conversion mechanism by activating the CO_2, as occurs with the addition of ILs and deep eutectic salt mixtures [54].

When comparing the type of biomass used to produce the carbocatalysts (Entries 1 to 3 and 5 of Table 4.6), the samples produced with primary sludge (PriS-0) and knots (Kno-0) exhibited the lowest conversions of 47 and 50%, respectively, while the sample produced from biological sludge (BioS-0) had the highest conversion of 75%, which surpassed that of the sample prepared with chitosan (CHI-0). This result might be explained by the presence of carbonate ions in sample BioS-0 detected with Raman spectroscopy (Section 4.1.3.2). It has been reported that alkali metal carbonates can be used as activating agents for inducing microporosity and increasing surface area [114], which means that the carbonates present in the biological sludge could have kickstarted some sort of chemical activation, which impacted the conversion positively.

Furthermore, when the IL additive [Bmim][Cl] was used with the biological sludge to produce sample BioS-ImCl (Entry 4 of Table 4.6), there was an improvement of the conversion from 75 to 81%, the highest conversion obtained in this study. This improvement can be attributed to the increased nitrogen content, as shown through elemental analysis (Section 4.1.1.2), and the consequent increase in active sites from the incorporation of the imidazolium-based IL. This result reenforces the possibility of using waste materials, such as the biological sludge granted by The Navigator Company, for carbocatalyst production.

In fact, there is an overall improvement of the conversion when additives are also used as carbon precursors, both in the case of the carbocatalysts produced from biological sludge or from chitosan.

When the chitosan was carbonized in the absence of any additives (Entry 5 of Table 4.6), the result was a moderate conversion of 61%. Apart from additives [4Bmpy][Cl] and PDADMACl (Entries 11 and 13 of Table 4.6) that resulted in a slight decrease in the conversion to 58 and 56%, respectively, there was a general increase of the conversion when additives were used, whether ILs or LiCl/KCl salt mixture, by the increase of basic active sites.

However, in the case the two CHI-ImCl samples that were impregnated with tetrabutylammonium bromide (TBABr) (Entries 7 and 8 of Table 4.6), these resulted in the lowest conversion of all the carbons that were tested with the presence of co-catalyst TBABr. This may be due to the fact that there was not enough co-catalyst impregnated in the carbon to make a significant difference in the reaction. In fact, in the absence of co-catalyst TBABr, no conversion was detected for the cycloaddition reaction (Entry 6 of Table 4.6).

On the other hand, the same carbocatalyst CHI-ImCl without impregnation achieved the highest conversion of 80% (Entry 9 of Table 4.6) for the samples prepared with chitosan. This result might be explained by its nitrogen atoms since these favor the interactions between the active phase and the support, and can even have direct participation in the reaction mechanism, which benefits the conversion [86]. However, the nitrogen content of this sample was relatively low (Section 4.1.1.1), so its nitrogen atoms might be better distributed throughout the carbon's surface so to act as basic active sites and promote more reaction, thus increasing the conversion.

The significant difference in conversion from the samples produced with the same pyridinium cation (Entries 10 and 11 of Table 4.6) can be ascribed to the greater abundance of pores in sample CHI-2PyCl than in sample CHI-4PyCl, as seen previously in SEM images (Section 4.1.2.1), resulting in conversions of 77 and 58%, respectively.

The samples prepared with a pyrrolidinium-based IL allowed for an inspection of the effect of the IL anion on the conversion. Sample CHI-PyrCl achieved a higher conversion of 74% in comparison to sample CHI-PyrDCA, which achieved a conversion of 62% (Entries 12 and 14 of Table 4.6, respectively), with the only difference being the anion of the IL used. Even though sample CHI-PyrDCA showed the highest nitrogen content in its elemental analysis (Section 4.1.1.1), which could bring benefits in the conversion as mentioned above, it's lower conversion is mainly due to the fact that the dicyanamide anion is less nucleophilic than the chloride anions present in the other samples [13].

The relatively low conversion of 56% resulting from sample CHI-PDADMACl (Entry 13 of Table 4.6) might be related to its low degree of graphitization, which in turn could be due to excess water present during the hydrothermal carbonization (as discussed in Section 4.1.3.1).

Regarding the sample prepared with the LiCl/KCl salt mixture, having washed and filtered the sample had no impact on the catalytic activity of the carbon (Entries 15 and 16 of Table 4.6). This means that, despite the porosity made available from washing out the salt mixture, the active sites were not significantly altered, thus leaving the conversion unchanged.

After evaluating all the carbon samples to determine the highest conversion, sample CHI-ImCl was chosen to undergo further optimization, so to have a more controlled environment.

4.2.2. Effect of the amount of carbocatalyst and co-catalyst

First the amount of carbocatalyst was varied, maintaining all other parameters constant (Figure 4.14(a)). Both the increase and decrease of the amount of carbocatalyst, respectively 50 and 5 mg, resulted in slightly lowered conversion of 72 and 77%, respectively.

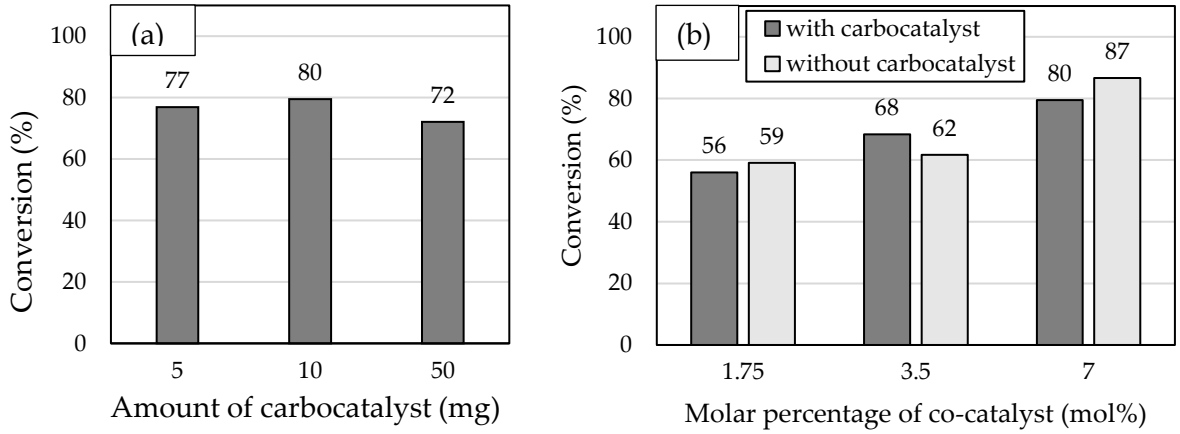

Figure 4.14. (a) Influence of the amount of carbocatalyst CHI-ImCl for 7 mol% of co-catalyst TBABr in relation to the SO on the conversion. (b) Influence of the molar percentage of co-catalyst TBABr in relation to SO for 10 mg of carbocatalyst CHI-ImCl on the conversion. Conditions: 100 °C, 3h, CO_2 (5 bar), SO (6.66 mmol).

The lower conversion resulting from the decrease to 5 mg of carbocatalyst is expected since less catalyst also implies less active sites [51]. The conversion reaction also reaches a saturation point, thus the increase of the amount of carbocatalyst to 50 mg did not favor the conversion. This phenomenon is in agreement with the study carried out by Sun *et al*. [115], where catalyst loading above 1.8 mol% resulted in a lowered conversion for the cycloaddition of CO_2 to propylene oxide. The decreased conversion for a higher amount of carbocatalyst was attributed to a not so effective dispersion of the catalyst in the reaction mixture which limited the mass transfer between the active sites and the reactants.

After the optimal amount of carbocatalyst was found for these conditions (10 mg), the molar percentage of co-catalyst TBABr was altered in the presence and absence of the carbocatalyst CHI-ImCl, maintaining all other parameters constant (Figure 4.14(b)). This parameter was tested to determine the conditions for improved conversion using a carbocatalyst.

The decrease in the amount of co-catalyst was found to cause a decrease in the conversion, which is expected. The bromide anion of the co-catalyst has strong nucleophilicity [41], which means that it facilitates the ring-opening process and effectively acts as a leaving group so to be easily displaced and ensure the formation of the cyclic carbonate [116]. As such, the increase in amount of co-catalyst being accompanied by an improvement in conversion is due to the excess of nucleophiles [17].

The alteration of the molar percentage of co-catalyst allowed to assess the effect of the carbocatalyst on the conversion. The molar percentage of co-catalyst of 3.5 mol% was the condition where the carbocatalyst improved the conversion, which is lower than the co-catalyst molar percentages used in the literature [27], [31], [39].

4.2.3. Effect of reaction time

Based on the condition of 3.5 mol% of TBABr, which showed that the carbocatalyst was performing an essential role in the conversion reaction, the evolution of the conversion was studied over time (Figure 4.15).

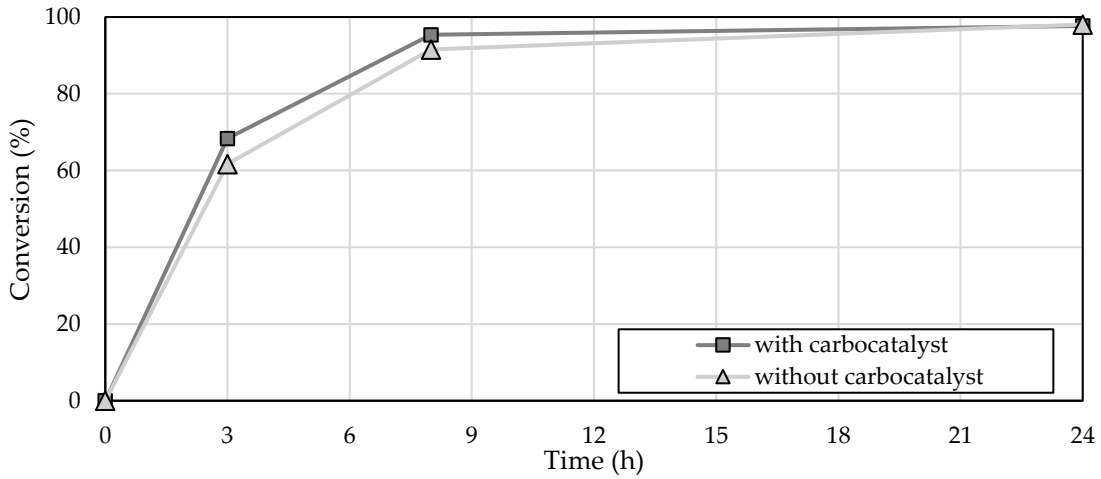

Figure 4.15. Influence of time on the conversion. Conditions: 100 °C, CO_2 (5 bar), SO (6.66 mmol), carbocatalyst CHI-ImCl (10 mg, when used), co-catalyst TBABr (3.5 mol% in relation to SO).

The maximum conversion (≈100%) was reached when the reaction lasted 24h, both with and without the carbocatalyst CHI-ImCl. For the intermediary reaction times tested (3 and 8h), the reaction containing the carbocatalyst consistently yielded greater conversion than without it, which confirms the important role of the carbocatalyst during the reaction.

Furthermore, this optimization step shows that the carbocatalyst reaches a high conversion (>95%) in, at least, eight hours. However, for the purposes of studying the influence of the other parameters on the conversion with a large margin for improvement, the optimization carried on with a reaction time of three hours.

4.2.4. Effect of co-catalyst

Once the carbocatalyst CHI-ImCl was confirmed to be a critical participant in the reaction, different co-catalysts, other than TBABr, were evaluated to assess their potential to further improve the conversion: tetrabutylammonium chloride (TBACl), vinylbenzyltriethylammonium chloride (VBACl), and poly(vinylbenzyltriethylammonium) chloride (PVBACl). All other parameters remained constant, with results in Figure 4.17.

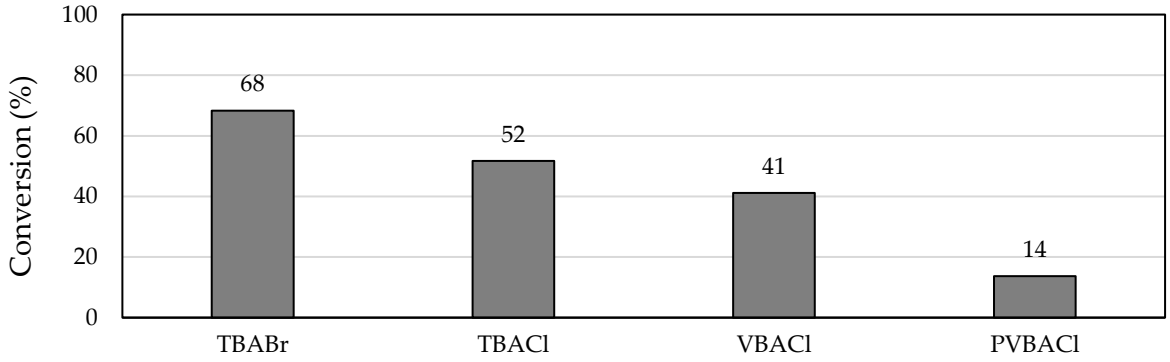

Figure 4.17. Influence of co-catalyst on the conversion. Conditions: 100 °C, 3 h, CO_2 (5 bar), SO (6.66 mmol), carbocatalyst CHI-ImCl (10 mg), co-catalyst (3.5 mol% in relation to SO).

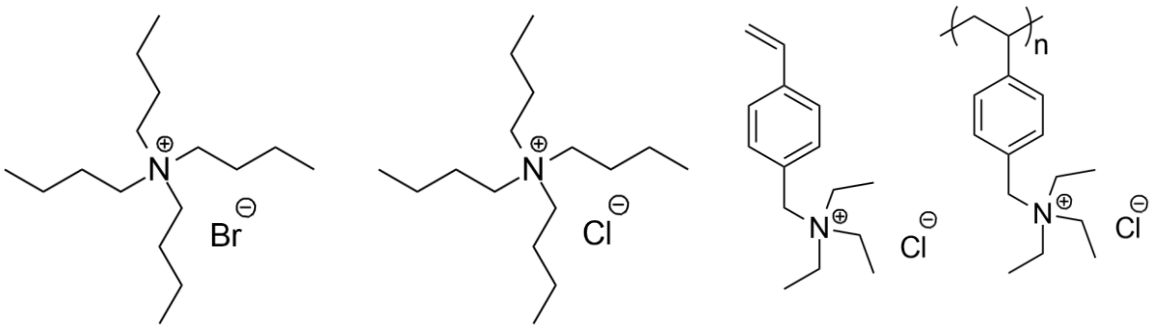

Figure 4.16. Chemical structures of TBABr, TBACl, VBACl, and PVBACl (from left to right).

When altering the anion of the tetrabutylammonium cation from bromide to chloride, the conversion drops from 68 to 52%, which is supported by the literature [18], [117]. This result is ascribed to the bulkiness of the tetrahedral ammonium ion, which forces the halide anion away from the cation. This reduced electrostatic interaction renders the halide anion (i.e., Cl^- or Br^-) more nucleophilic [118]. Since the bromide anion is bulkier than the chloride anion, when pushed away from the cation, the bromide anion reacts more quickly as a nucleophile in the attack of the epoxide ring. The bromide anion is also a better leaving group, which facilitates the ring-closing step and formation of the cyclic carbonate.

When altering the cation of the co-catalyst while maintaining a chloride anion (comparing TBACl to VBACl), the tetrabutylammonium cation renders a higher conversion than the vinylbenzyltriethylammonium cation (conversions of 52 and 41%, respectively). This result is believed to be due to the fact that VBACl has a tendency to polymerize with the increase of temperature, thus creating a competition between the polymerization reaction and the conversion reaction and due to the degradation that the co-catalyst suffered over time after having been synthesized in the laboratory.

Originally, the reaction with co-catalyst PVBACl had a conversion of around 3%. Here, the co-catalyst used formed a viscous paste when heated, which encompassed the carbocatalyst. Because of the low conversion and the fact that the carbocatalyst was lost, some of the reaction product might have gotten trapped in the viscous paste formed by the co-catalyst. As such, the reaction was repeated, and the resulting viscous paste was washed with chloroform-*d*, for the supernatant to be removed and analyzed for catalytic activity. This methodology proved to be effective, because the conversion increased to 14%, as is shown in

Figure 4.17, which confirmed that some of the reaction product could, in fact, get trapped in the paste. Furthermore, the results of this reaction can be ascribed to the viscosity of the paste, which limited the migration of the reactant to the catalytic sites and, consequently, led to a lower conversion due to poor diffusion [110].

4.2.5. Effect of carbocatalyst

To finalize the optimization, the catalytic activities of samples CHI-0, CHI-PyrCl, BioS-0, and BioS-ImCl were evaluated under the optimal reaction conditions found for the cycloaddition of CO_2 to SO, using the best co-catalyst evaluated (TBABr). The first two carbon samples prepared with chitosan were chosen because their N_2 adsorption/desorption isotherms showed the most promising results. The last two carbon samples prepared with biological waste sludge were chosen due to their high catalytic activity.

Given that the only difference between these results and those initially reported in Table 4.6 is the molar percentage of co-catalyst TBABr, similar results were expected. A side-by-side comparison of these results is shown in Figure 4.18. Indeed, observing the figure below, regardless of the carbocatalyst used, the conversion decreased with the decrease in molar percentage of the co-catalyst from 7 to 3.5 mol%, which is ascribed to the reduction in active sites available for conversion. The only sample that seems to have maintained the conversion, independent of the molar percentage of co-catalyst, is sample CHI-0. The best carbocatalysts were still CHI-ImCl and BioS-ImCl, with conversions of 68 and 62%, respectively.

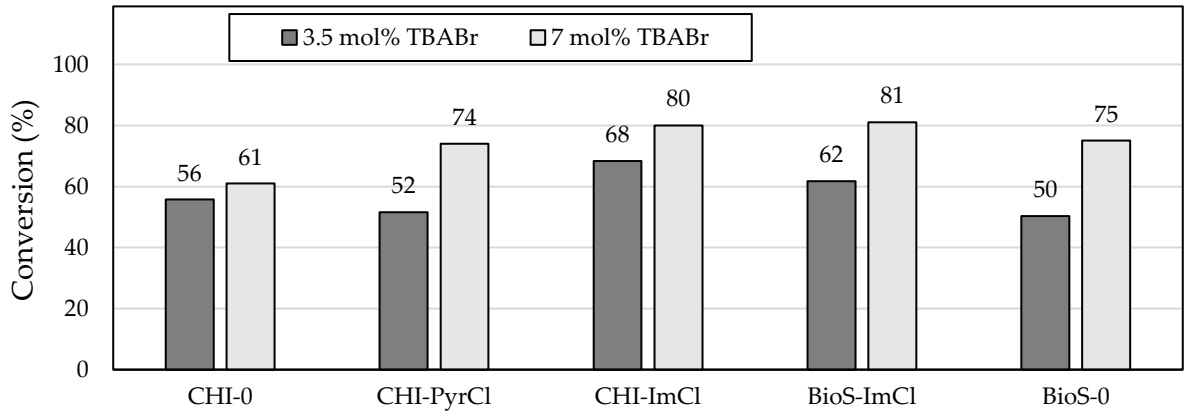

Figure 4.18. Influence of the carbocatalyst on the conversion. Conditions: 100 °C, 3 h, CO_2 (5 bar), SO (6.66 mmol), carbocatalyst (10 mg), co-catalyst TBABr.

4.2.6. Recyclability of the carbocatalyst

Based on the previous optimizations, the best combination of carbocatalyst, co-catalyst, and molar percentage of co-catalyst in relation to the substrate was used to study the recyclability of the carbocatalyst. Results can be found in Figure 4.19.

As the carbocatalyst is reused, there is no alteration in the selectivity, and is maintained constant at >99%. Nevertheless, there is a decrease in the conversion immediately after the first cycle, which can be ascribed to handling loss of carbocatalyst, since the conversion increases from the second to the third cycle when no carbocatalyst is lost.

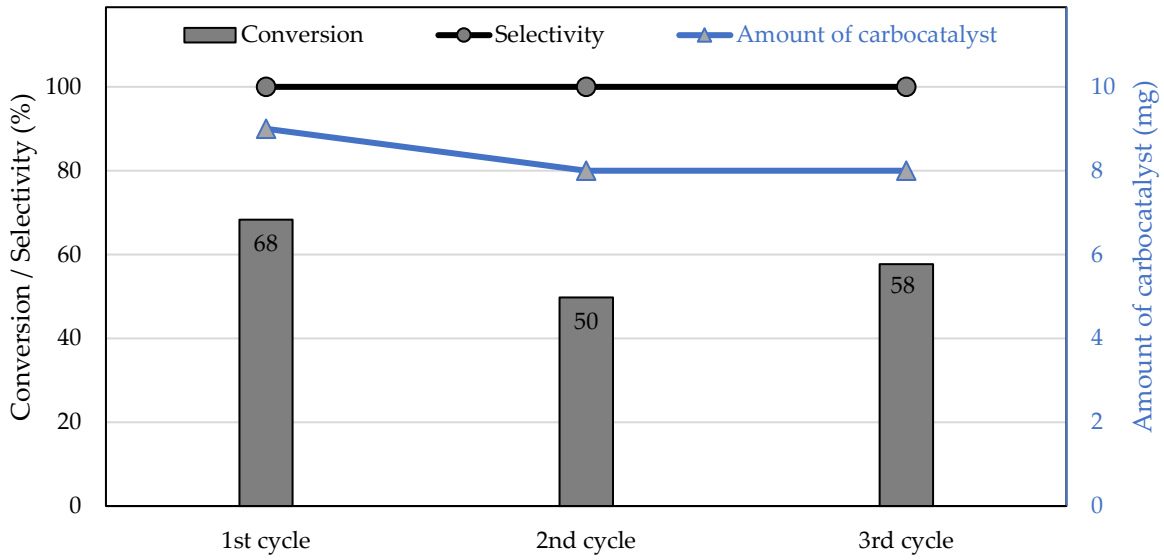

Figure 4.19. Amount of carbocatalyst, conversion and selectivity of carbocatalyst CHI-ImCl toward CO_2 cycloaddition with SO during three consecutive cycles. Conditions: 100 °C, 3 h, CO_2 (5 bar), SO (6.66 mmol), carbocatalyst CHI-ImCl, co-catalyst TBABr (3.5 mol% in relation to SO).

4.2.7. Literature comparison

Sample CHI-ImCl was the one that was most explored for its catalytic potential, as such it was chosen for comparison within the literature. The criteria for comparison was the use of biomass as a precursor to carbon materials which would posteriorly be used as heterogeneous catalysts to produce SC. A detailed excerpt of Table A.1 in the Appendix can be found in Table 4.7 with the studies that fulfill the comparison criteria.

Observing the lowest conversion obtained when sample CHI-ImCl was used as a catalyst (Entry 16 of Table 4.7), this result is fairly similar to those of Entries 1 and 3 of Table 4.7. In the case of the current study, the reaction parameters used were mostly milder than those in the literature, namely the CO_2 pressure and reaction duration, while the reaction temperature was kept at a relatively high 100 ˚C. For conversions above 90% (Entries 14 and 17 of Table 4.7), these were achieved by submitting the reaction to an extended time of at least eight hours, which is in agreement with the experimental conditions and high conversions obtained by Molla *et al.* [31] (Entries 6 and 7 of Table 4.7). For intermediate conversions, those in this study were reached with lower CO_2 pressure, and also lower substrate and catalyst amounts than the other studies. This remains true even when comparing the results obtained from the solvent-free approach taken in this study to the one carried out by Molla *et al.* [31], who used 2-propanol as solvent in all the mentioned reactions (Entries 3 to 7 of Table 4.7).

Comparing the sample prepared in this study to the ones that include immobilization techniques [27], [41], advantages are apparent. In the case of Kong *et al*. [27], they were able to achieve an intermediate conversion of 50% (Entry 1 of Table 4.7) at around room temperature, through the support of metal ions that would participate in the ring-opening step of the conversion reaction. For Appaturi *et al*. [41], a high conversion (Entries 9 and 10 of Table 4.7) was possible with the immobilization of a bromide containing compound, which is a strong nucleophile, as mentioned in Section 4.2.4.

Table 4.7. Literature comparison of the catalytic activity of carbon-based catalysts prepared from biomass for the cycloaddition of CO_2 to SO to those prepared in this study.

Entry	Catalyst (mg)	SO (mmol)	TBABr[a] (mol%)	P_{CO2} (bar)	Temp. (˚C)	Time (h)	Yield (%)	Ref.
1	Co/CMC-A-1[b] (30)	10	7	1	30	48	50	[27]
2	Co/CMC-A-1[b] (30)	10	7	1	80	48	84	
3	N-GMC[c] (20)	10	10	10	80	15	52	[31]
4	N-GMC[c] (30)	10	10	10	80	15	67	
5	N-GMC[c] (40)	10	10	10	80	15	88	
6	N-GMC[c] (50)	10	10	10	80	15	98	
7	N-GMC[c] (60)	10	10	10	80	15	98	
8	MCM-41-Imi[d] (300)	30	–	30	140	6	9	[41]
9	MCM-41-Imi/Br[e] (300)	30	–	30	140	6	84	
10	MCM-41-Imi/Br[e] (200)	30	–	40	100	4	99	
11	CHI-ImCl (5)	6.67	7	5	100	3	77	this study
12	CHI-ImCl (10)	6.67	7	5	100	3	80	
13	CHI-ImCl (10)	6.67	3.5	5	100	3	68	
14	CHI-ImCl (10)	6.67	3.5	5	100	8	95	
15	CHI-ImCl (10)	6.67	3.5	5	100	24	98	
16	CHI-ImCl (10)	6.67	1.75	5	100	3	56	
17	CHI-ImCl (50)	6.67	7	5	100	3	72	

[a] in relation to SO.

[b] Co^{2+} supported on chemically activated carbon derived from waste cow manure.

[c] Nitrogen-doped mesoporous carbon prepared by soft templating carbonization of glucose.

[d] Imidazole grafted on rice husk derived MCM-41.

[e] Imidazole and 1,2-dibromoethane grafted on rice husk derived MCM-41.

Overall, the carbocatalyst prepared in this study shows comparable results to those reported in the literature. Even though a slightly higher reaction temperature was applied here, a wide range of conversions (from 56 to 98%) were achieved with a lower CO_2 pressure, a reduced reaction time, a lesser amount of substrate, catalyst and co-catalyst, and in the absence of solvents.

5. CONCLUSIONS AND FUTURE RESEARCH

This study aimed to develop new metal-free materials for CO_2 conversion, through the carbonization of (waste) biomass materials. The methodology involved the use of biomass (chitosan, knots, and waste sludges − primary and biological) and additives (six different ILs and a salt mixture) as precursors to porous carbon materials by subjecting the precursors to a hydrothermal carbonization followed by carbonization with nitrogen flow. The carbon samples were characterized with a variety of techniques to assess their carbon yield, elemental composition, porosity, and degree of graphitization. The resulting carbon materials were then tested for their catalytic potential in the cycloaddition reaction of CO_2 to SO for the formation of SC, in the absence of solvents.

From the results of the carbonization process, the incorporation of the IL or salt mixture additives did not increase the carbonization yield. However, their introduction affected the other properties (nitrogen content, porosity, and degree of graphitization) which would influence the catalytic potential of the resulting carbocatalysts.

All carbon samples were highly selective (>99%) but differed in their catalytic activity. The carbon sample prepared with chitosan and [Bmim][Cl] (CHI-ImCl), with a conversion of 80%, proved to be the most efficient catalyst. Additionally, the use of the same IL in the preparation of the carbon sample produced with the biological sludge (BioS-ImCl) resulted in a catalyst that attained a similar conversion, in the same conditions (100 ^{o}C, 3 h, CO_2 (5 bar), SO (6.66 mol), catalyst (10 mg), co-catalyst TBABr (7 mol%)), in the absence of solvents or metals.

Due to better reproducibility of results, sample CHI-ImCl was chosen as the catalyst for further reaction optimization. The optimized conditions, which resulted in a conversion of 68%, were found to be:

100^{o}C, 3h, CO_2 (5bar), SO (6.66mol), co-catalyst TBABr (3.5mol%), carbocatalyst (10mg)

Sample BioS-ImCl was also tested with these conditions and maintained the performance as an efficient catalyst, yielding a conversion of 62%.

For the purposes of this study, the samples prepared with biological sludge showed the highest carbonization yield and conversion, the most promising results of all the waste biomass materials. This result confirms the possibility of incorporating waste biomass materials that received little to no treatment, and would have been disposed of otherwise, in the production process of carbocatalysts for the conversion of CO_2.

Overall, the carbocatalysts prepared in this study presented comparable conversions to those reported in the literature, in general, requiring milder conditions.

The improvements which could benefit this study rely on the characterization of the carbon samples and further testing:

- **Thermal Gravimetric Analysis (TGA)** so to have a proximate analysis that determines the volatile matter and ash content of the samples so to assess the influence of these parameters on the final application;
- **X-ray Photoelectron Spectroscopy (XPS)** would be advantageous to reveal the nature of the nitrogen atoms in the carbon samples since this is a parameter that can strongly influence the conversion of the cycloaddition reaction;
- **Extend the number of recycle runs** to derive accurate conclusions regarding the recyclability and stability of the carbon. This would determine whether the decrease in conversion found in this study when the carbocatalyst is reused is related to a decrease in stability of the carbocatalyst or whether the conversion stabilizes as the carbocatalyst is used for more cycles;
- **Raman spectroscopy** after every cycle that the carbocatalyst is reused could ascertain the integrity of the carbon structure;
- **Replicate the samples**, especially for the waste biomass materials (knots and sludges) to determine their replicability and the viability of using these industrial residues for green applications.

Future research could focus on the immobilization of ILs onto the carbon surface, especially for those prepared with the waste biomass materials, for the same application. As another step for an even greener pathway, waste CO_2 could be used for the cycloaddition reaction instead of pure CO_2 so to further motivate a circular economy. The exploration of the adsorbent potential of the carbon samples in the capture of CO_2 would complement the aim of this work.

BIBLIOGRAPHY

[1] C. Claver, M. Bin Yeamin, M. Reguero, and A. M. Masdeu-Bultó, "Recent advances in the use of catalysts based on natural products for the conversion of CO 2 into cyclic carbonates," *Green Chem.*, vol. 22, no. 22, pp. 7665–7706, 2020, doi: 10.1039/D0GC01870H.

[2] S. K. Shukla, S. G. Khokarale, T. Q. Bui, and J.-P. T. Mikkola, "Ionic Liquids: Potential Materials for Carbon Dioxide Capture and Utilization," *Front. Mater.*, vol. 6, no. March, pp. 1–8, Mar. 2019, doi: 10.3389/fmats.2019.00042.

[3] C. Calabrese, F. Giacalone, and C. Aprile, "Hybrid catalysts for CO 2 conversion into cyclic carbonates," *Catalysts*, vol. 9, no. 4, pp. 1–30, 2019, doi: 10.3390/catal9040325.

[4] S. Wu, L. Yu, G. Wen, Z. Xie, and Y. Lin, "Recent progress of carbon-based metal-free materials in thermal-driven catalysis," *J. Energy Chem.*, vol. 58, pp. 318–335, 2021, doi: 10.1016/j.jechem.2020.10.011.

[5] G. Jaria, C. P. Silva, C. I. A. Ferreira, M. Otero, and V. Calisto, "Sludge from paper mill effluent treatment as raw material to produce carbon adsorbents: An alternative waste management strategy," *J. Environ. Manage.*, vol. 188, pp. 203–211, Mar. 2017, doi: 10.1016/j.jenvman.2016.12.004.

[6] A. Shahbazi and B. Rezaei Nasab, "Carbon Capture and Storage (CCS) and its Impacts on Climate Change and Global Warming," *J. Pet. Environ. Biotechnol.*, vol. 7, no. 4, 2016, doi: 10.4172/2157-7463.1000291.

[7] ACS Chemistry for Life, "What are the greenhouse gas changes since the Industrial Revolution?" https://www.acs.org/content/acs/en/climatescience/greenhousegases/industrialrevolution.html.

[8] *United Nations Framework Convention on Climate & Change*. Paris: United Nations, 2015, p. 27.

[9] J. P. Gouveia, J. Seixas, M. Labriet, P. Fortes, and M. Gargiulo, "Prospective scenarios for the adoption of CCS technologies in the Iberian Peninsula," *Sustain. Energy Technol. Assessments*, vol. 2, no. 1, pp. 31–41, Jun. 2013, doi: 10.1016/j.seta.2013.02.002.

[10] J. F. Brennecke and B. E. Gurkan, "Ionic Liquids for CO 2 Capture and Emission Reduction," *J. Phys. Chem. Lett.*, vol. 1, no. 24, pp. 3459–3464, Dec. 2010, doi: 10.1021/jz1014828.

[11] P. Mao *et al.*, "Polymer nanoparticles grafted zinc-containing ionic liquids: A highly efficient and recyclable catalyst for cooperative cycloaddition of CO2 with epoxides," *J. CO2 Util.*, vol. 28, no. September, pp. 96–116, 2018, doi: 10.1016/j.jcou.2018.09.017.

[12] N. A. M. Razali, K. T. Lee, S. Bhatia, and A. R. Mohamed, "Heterogeneous catalysts for production of chemicals using carbon dioxide as raw material: A review," *Renew. Sustain. Energy Rev.*, vol. 16, no. 7, pp. 4951–4964, 2012, doi: 10.1016/j.rser.2012.04.012.

[13] Y. He *et al.*, "Efficient fixation of CO2 into carbonates by tertiary N-functionalized poly(ionic liquids): Experimental-theoretical investigation," *J. CO2 Util.*, vol. 44, no. September 2020, p. 101427, 2021, doi: 10.1016/j.jcou.2020.101427.

[14] J. N. Appaturi *et al.*, "Review on Carbon Dioxide Utilization for Cycloaddition of Epoxides by Ionic Liquid-Modified Hybrid Catalysts: Effect of Influential Parameters and Mechanisms Insight," *Catalysts*, vol. 11, no. 1, p. 4, Dec. 2020, doi: 10.3390/catal11010004.

[15] W. J. Peppel, "Preparation and Properties of the Alkylene Carbonates," *Ind. Eng. Chem.*, vol. 50, no. 5, pp. 767–770, May 1958, doi: 10.1021/ie50581a030.

[16] B. Cornils, W. A. Herrmann, C. Wong, H. Zanthoff, and R. Eds, "Catalysis from A to

Z," *Focus Catal.*, vol. 2007, no. 8, p. 8, Aug. 2007, doi: 10.1016/S1351-4180(07)70462-2.
[17] M. Cozzolino, K. Press, M. Mazzeo, and M. Lamberti, "Carbon Dioxide/Epoxide Reactions Catalyzed by Bimetallic Salalen Aluminum Complexes," *ChemCatChem*, vol. 8, no. 2, pp. 455–460, Jan. 2016, doi: 10.1002/cctc.201500856.
[18] A. Lopes do Rosário Ventura, "Utilization of ionic liquids as solvents and co-catalysts in the production of cyclic carbonates from CO 2," Universidade Nova de Lisboa, 2017.
[19] Z.-Z. Yang, L.-N. He, Y.-N. Zhao, B. Li, and B. Yu, "CO2 capture and activation by superbase/polyethylene glycol and its subsequent conversion," *Energy Environ. Sci.*, vol. 4, no. 10, p. 3971, 2011, doi: 10.1039/c1ee02156g.
[20] L. Guo, K. J. Lamb, and M. North, "Recent developments in organocatalysed transformations of epoxides and carbon dioxide into cyclic carbonates," *Green Chem.*, vol. 23, no. 1, pp. 77–118, 2021, doi: 10.1039/d0gc03465g.
[21] M. F. Rojas *et al.*, "Poly(ionic liquid)s as efficient catalyst in transformation of CO 2 to cyclic carbonate," *J. Mol. Catal. A Chem.*, vol. 392, pp. 83–88, 2014, doi: 10.1016/j.molcata.2014.05.007.
[22] Y. Wang *et al.*, "Imidazolium-based polymeric ionic liquids for heterogeneous catalytic conversion of CO2 into cyclic carbonates," *Microporous Mesoporous Mater.*, vol. 292, no. May 2019, p. 109751, 2020, doi: 10.1016/j.micromeso.2019.109751.
[23] J. Kim, S. N. Kim, H. G. Jang, G. Seo, and W. S. Ahn, "CO2 cycloaddition of styrene oxide over MOF catalysts," *Appl. Catal. A Gen.*, vol. 453, pp. 175–180, 2013, doi: 10.1016/j.apcata.2012.12.018.
[24] Y. Li, B. Zou, C. Hu, and M. Cao, "Nitrogen-doped porous carbon nanofiber webs for efficient CO2 capture and conversion," *Carbon N. Y.*, vol. 99, pp. 79–89, Apr. 2016, doi: 10.1016/j.carbon.2015.11.074.
[25] W. Cheng, X. Chen, J. Sun, J. Wang, and S. Zhang, "SBA-15 supported triazolium-based ionic liquids as highly efficient and recyclable catalysts for fixation of CO2 with epoxides," *Catal. Today*, vol. 200, no. 1, pp. 117–124, 2013, doi: 10.1016/j.cattod.2012.10.001.
[26] A. I. Adeleye, D. Patel, D. Niyogi, and B. Saha, "Efficient and greener synthesis of propylene carbonate from carbon dioxide and propylene oxide," *Ind. Eng. Chem. Res.*, vol. 53, no. 49, pp. 18647–18657, 2014, doi: 10.1021/ie500345z.
[27] W. Kong and J. Liu, "Nitrogen-decorated, porous carbons derived from waste cow manure as efficient catalysts for the selective capture and conversion of CO 2," *RSC Adv.*, vol. 9, no. 9, pp. 4925–4931, 2019, doi: 10.1039/C8RA10497B.
[28] X. Ma, B. Zou, M. Cao, S.-L. Chen, and C. Hu, "Nitrogen-doped porous carbon monolith as a highly efficient catalyst for CO 2 conversion," *J. Mater. Chem. A*, vol. 2, no. 43, pp. 18360–18366, Sep. 2014, doi: 10.1039/C4TA02734E.
[29] X. Shao *et al.*, "Renewable N-doped microporous carbons from walnut shells for CO 2 capture and conversion," *Sustain. Energy Fuels*, vol. 5, no. 18, pp. 4701–4709, 2021, doi: 10.1039/D1SE01000J.
[30] A. Samikannu, L. J. Konwar, P. Mäki-Arvela, and J. P. Mikkola, "Renewable N-doped active carbons as efficient catalysts for direct synthesis of cyclic carbonates from epoxides and CO2," *Appl. Catal. B Environ.*, vol. 241, pp. 41–51, 2019, doi: 10.1016/j.apcatb.2018.09.019.
[31] R. A. Molla, A. Iqubal, K. Ghosh, and M. Islam, "Nitrogen-Doped Mesoporous Carbon Material (N-GMC) as a Highly Efficient Catalyst for Carbon Dioxide Fixation Reaction with Epoxides under metal-free condition," *ChemistrySelect*, vol. 1, no. 12, pp. 3100–3107, Aug. 2016, doi: 10.1002/slct.201600346.
[32] C. Baskar, S. Baskar, and R. S. Dhillon, Eds., *Biomass Conversion*. Berlin, Heidelberg: Springer Berlin Heidelberg, 2012.
[33] J. Yin, W. Zhang, N. A. Alhebshi, N. Salah, and H. N. Alshareef, "Synthesis Strategies

of Porous Carbon for Supercapacitor Applications," *Small Methods*, vol. 4, no. 3, Mar. 2020, doi: 10.1002/smtd.201900853.

[34] B. Hu, K. Wang, L. Wu, S. H. Yu, M. Antonietti, and M. M. Titirici, "Engineering carbon materials from the hydrothermal carbonization process of biomass," *Advanced Materials*, vol. 22, no. 7. pp. 813–828, 2010, doi: 10.1002/adma.200902812.

[35] J. A. O. Chagas, G. O. Crispim, B. P. Pinto, R. A. S. San Gil, and C. J. A. Mota, "Synthesis, Characterization, and CO 2 Uptake of Adsorbents Prepared by Hydrothermal Carbonization of Chitosan," *ACS Omega*, vol. 5, no. 45, pp. 29520–29529, Nov. 2020, doi: 10.1021/acsomega.0c04470.

[36] Q. Wu *et al.*, "Preparation and application performance study of biomass-based carbon materials with various morphologies by a hydrothermal/soft template method," *Nanotechnology*, vol. 30, no. 18, p. 185702, May 2019, doi: 10.1088/1361-6528/ab0042.

[37] Z. Liu *et al.*, "New strategy to prepare ultramicroporous carbon by ionic activation for superior CO2 capture," *Chem. Eng. J.*, vol. 337, no. December 2017, pp. 290–299, 2018, doi: 10.1016/j.cej.2017.11.184.

[38] Y. J. Heo and S. J. Park, "A role of steam activation on CO2 capture and separation of narrow microporous carbons produced from cellulose fibers," *Energy*, vol. 91, pp. 142–150, 2015, doi: 10.1016/j.energy.2015.08.033.

[39] L. Muniandy, F. Adam, N. R. A. Rahman, and E. P. Ng, "Highly selective synthesis of cyclic carbonates via solvent free cycloaddition of CO 2 and epoxides using ionic liquid grafted on rice husk derived MCM-41," *Inorg. Chem. Commun.*, vol. 104, no. January, pp. 1–7, 2019, doi: 10.1016/j.inoche.2019.03.012.

[40] D. Li, T. Ma, R. Zhang, Y. Tian, and Y. Qiao, "Preparation of porous carbons with high low-pressure CO2 uptake by KOH activation of rice husk char," *Fuel*, vol. 139, pp. 68–70, 2015, doi: 10.1016/j.fuel.2014.08.027.

[41] J. N. Appaturi and F. Adam, "A facile and efficient synthesis of styrene carbonate via cycloaddition of CO2 to styrene oxide over ordered mesoporous MCM-41-Imi/Br catalyst," *Appl. Catal. B Environ.*, vol. 136–137, pp. 150–159, 2013, doi: 10.1016/j.apcatb.2013.01.049.

[42] F. Adam, J. N. Appaturi, and E. P. Ng, "Halide aided synergistic ring opening mechanism of epoxides and their cycloaddition to CO2 using MCM-41-imidazolium bromide catalyst," *J. Mol. Catal. A Chem.*, vol. 386, pp. 42–48, 2014, doi: 10.1016/j.molcata.2014.02.008.

[43] R. J. Ramalingam, J. N. Appaturi, T. Pulingam, N. Ibrahim S, and H. A. Al-Lohedan, "Synthesis, characterization and catalytic activity of ionic liquid mimic halides modified MCM-41 for solvent free synthesis of phenyl glycidyl carbonate," *Mater. Chem. Phys.*, vol. 233, no. December 2018, pp. 79–88, 2019, doi: 10.1016/j.matchemphys.2019.05.045.

[44] B. Adeniran and R. Mokaya, "Is N-Doping in Porous Carbons Beneficial for CO 2 Storage? Experimental Demonstration of the Relative Effects of Pore Size and N-Doping," *Chem. Mater.*, vol. 28, no. 3, pp. 994–1001, Feb. 2016, doi: 10.1021/acs.chemmater.5b05020.

[45] L. Cibien *et al.*, "Ionothermal carbonization in [Bmim][FeCl 4]: an opportunity for the valorization of raw lignocellulosic agrowastes into advanced porous carbons for CO 2 capture," *Green Chem.*, vol. 22, no. 16, pp. 5423–5436, 2020, doi: 10.1039/D0GC01510E.

[46] A. Zielińska, P. Oleszczuk, B. Charmas, J. Skubiszewska-Zięba, and S. Pasieczna-Patkowska, "Effect of sewage sludge properties on the biochar characteristic," *J. Anal. Appl. Pyrolysis*, vol. 112, pp. 201–213, Mar. 2015, doi: 10.1016/j.jaap.2015.01.025.

[47] P. Devi and A. K. Saroha, "Effect of pyrolysis temperature on polycyclic aromatic hydrocarbons toxicity and sorption behaviour of biochars prepared by pyrolysis of paper mill effluent treatment plant sludge," *Bioresour. Technol.*, vol. 192, pp. 312–320,

2015, doi: 10.1016/j.biortech.2015.05.084.
[48] V. M. Monsalvo, A. F. Mohedano, and J. J. Rodriguez, "Adsorption of 4-chlorophenol by inexpensive sewage sludge-based adsorbents," *Chem. Eng. Res. Des.*, vol. 90, no. 11, pp. 1807–1814, 2012, doi: 10.1016/j.cherd.2012.03.018.
[49] G. Gascó, C. G. Blanco, F. Guerrero, and A. M. M. Lázaro, "The influence of organic matter on sewage sludge pyrolysis," *J. Anal. Appl. Pyrolysis*, vol. 74, no. 1–2, pp. 413–420, 2005, doi: 10.1016/j.jaap.2004.08.007.
[50] A. Bagreev, T. J. Bandosz, and D. C. Locke, "Pore structure and surface chemistry of adsorbents obtained by pyrolysis of sewage sludge-derived fertilizer," *Carbon N. Y.*, vol. 39, no. 13, pp. 1971–1979, Nov. 2001, doi: 10.1016/S0008-6223(01)00026-4.
[51] M. Buaki-Sogó, A. Vivian, L. A. Bivona, H. García, M. Gruttadauria, and C. Aprile, "Imidazolium functionalized carbon nanotubes for the synthesis of cyclic carbonates: reducing the gap between homogeneous and heterogeneous catalysis," *Catal. Sci. Technol.*, vol. 6, no. 24, pp. 8418–8427, 2016, doi: 10.1039/C6CY01068G.
[52] Z. Akbari and M. Ghiaci, "Heterogenization of a Green Homogeneous Catalyst: Synthesis and Characterization of Imidazolium Ionene/Br-Cl-@SiO2 as an Efficient Catalyst for the Cycloaddition of CO2 with Epoxides," *Ind. Eng. Chem. Res.*, vol. 56, no. 32, pp. 9045–9053, 2017, doi: 10.1021/acs.iecr.7b02803.
[53] J. Sun *et al.*, "Chitosan functionalized ionic liquid as a recyclable biopolymer-supported catalyst for cycloaddition of CO2," *Green Chem.*, vol. 14, no. 3, p. 654, 2012, doi: 10.1039/c2gc16335g.
[54] L. Guo *et al.*, "The Application of Biomass-Based Catalytic Materials in the Synthesis of Cyclic Carbonates from CO2 and Epoxides," *Molecules*, vol. 25, no. 16, p. 3627, Aug. 2020, doi: 10.3390/molecules25163627.
[55] B. Szczęśniak, J. Phuriragpitikhon, J. Choma, and M. Jaroniec, "Recent advances in the development and applications of biomass-derived carbons with uniform porosity," *J. Mater. Chem. A*, vol. 8, no. 36, pp. 18464–18491, 2020, doi: 10.1039/d0ta05094f.
[56] M. A. Tadda *et al.*, "A Review On Activated Carbon: Process, Application And Prospects," *J. Adv. Civ. Eng. Pract. Res.*, vol. 2, no. 1, pp. 7–13, 2016.
[57] S. C. R. Marques, "Different approaches to the development and use of carbon materials for water treatment purposes," Universidade de Lisboa, 2017.
[58] S. Zhang, K. Dokko, and M. Watanabe, "Carbon materialization of ionic liquids: From solvents to materials," *Mater. Horizons*, vol. 2, no. 2, pp. 168–197, 2015, doi: 10.1039/c4mh00141a.
[59] W. Hao, E. Björkman, M. Lilliestråle, and N. Hedin, "Activated carbons prepared from hydrothermally carbonized waste biomass used as adsorbents for CO2," *Appl. Energy*, vol. 112, pp. 526–532, 2013, doi: 10.1016/j.apenergy.2013.02.028.
[60] N. Querejeta, M. V. Gil, C. Pevida, and T. A. Centeno, "Standing out the key role of ultramicroporosity to tailor biomass-derived carbons for CO2 capture," *J. CO2 Util.*, vol. 26, no. March, pp. 1–7, 2018, doi: 10.1016/j.jcou.2018.04.016.
[61] S. Sadjadi, Ed., *Emerging Carbon Materials for Catalysis*. Elsevier, 2021.
[62] P. Walden, "Ueber die Molekulargrosse und elektrische Leitfahigkeit einiger geschmolzenen Salze," *Bull. l'Académie Impériale des Sci. St.-Pétersbourg. VI série*, vol. 8, no. 6, pp. 405–422, 1914.
[63] M. C. Corvo *et al.*, "A Rational Approach to CO 2 Capture by Imidazolium Ionic Liquids: Tuning CO 2 Solubility by Cation Alkyl Branching," *ChemSusChem*, vol. 8, no. 11, pp. 1935–1946, Jun. 2015, doi: 10.1002/cssc.201500104.
[64] M. Zanatta, N. M. Simon, and J. Dupont, "The Nature of Carbon Dioxide in Bare Ionic Liquids," *ChemSusChem*, vol. 13, no. 12, pp. 3101–3109, 2020, doi: 10.1002/cssc.202000574.
[65] N. M. Simon, M. Zanatta, F. P. dos Santos, M. C. Corvo, E. J. Cabrita, and J. Dupont,

"Carbon Dioxide Capture by Aqueous Ionic Liquid Solutions," *ChemSusChem*, vol. 10, no. 24, pp. 4927–4933, 2017, doi: 10.1002/cssc.201701044.

[66] W. Silva, M. Zanatta, A. S. Ferreira, M. C. Corvo, and E. J. Cabrita, "Revisiting Ionic Liquid Structure-Property Relationship: A Critical Analysis," *Int. J. Mol. Sci.*, vol. 21, no. 20, p. 7745, Oct. 2020, doi: 10.3390/ijms21207745.

[67] G. Yu *et al.*, "New crosslinked-porous poly-ammonium microparticles as CO2 adsorbents," *React. Funct. Polym.*, vol. 73, no. 8, pp. 1058–1064, Aug. 2013, doi: 10.1016/j.reactfunctpolym.2013.04.005.

[68] S. Dai, J. S. Lee, X. Wang, H. Luo, and G. A. Baker, "Facile Ionothermal Synthesis of Microporous and Mesoporous Carbons from Task Specific Ionic Liquids," *J. Am. Chem. Soc.*, vol. 131, no. 13, pp. 4596–4597, Apr. 2009, doi: 10.1021/ja900686d.

[69] J. Yuan, C. Giordano, and M. Antonietti, "Ionic Liquid Monomers and Polymers as Precursors of Highly Conductive, Mesoporous, Graphitic Carbon Nanostructures," *Chem. Mater.*, vol. 22, no. 17, pp. 5003–5012, Sep. 2010, doi: 10.1021/cm1012729.

[70] Q. Wu *et al.*, "N-doped porous carbon from different nitrogen sources for high-performance supercapacitors and CO2 adsorption," *J. Alloys Compd.*, vol. 786, pp. 826–838, May 2019, doi: 10.1016/j.jallcom.2019.02.052.

[71] Z.-L. Xie, R. J. White, J. Weber, A. Taubert, and M. M. Titirici, "Hierarchical porous carbonaceous materials via ionothermal carbonization of carbohydrates," *J. Mater. Chem.*, vol. 21, no. 20, p. 7434, 2011, doi: 10.1039/c1jm00013f.

[72] S. M. Mahurin, P. F. Fulvio, P. C. Hillesheim, K. M. Nelson, G. M. Veith, and S. Dai, "Directed Synthesis of Nanoporous Carbons from Task-Specific Ionic Liquid Precursors for the Adsorption of CO 2," *ChemSusChem*, vol. 7, no. 12, pp. 3284–3289, Dec. 2014, doi: 10.1002/cssc.201402338.

[73] N. Fechler, T. P. Fellinger, and M. Antonietti, "'Salt templating': A simple and sustainable pathway toward highly porous functional carbons from ionic liquids," *Adv. Mater.*, vol. 25, no. 1, pp. 75–79, Jan. 2013, doi: 10.1002/adma.201203422.

[74] J. Gong, J. Zhang, H. Lin, and J. Yuan, "'Cooking carbon in a solid salt': Synthesis of porous heteroatom-doped carbon foams for enhanced organic pollutant degradation under visible light," *Appl. Mater. Today*, vol. 12, pp. 168–176, 2018, doi: 10.1016/j.apmt.2018.04.008.

[75] X. Wang and S. Dai, "Ionic Liquids as Versatile Precursors for Functionalized Porous Carbon and Carbon-Oxide Composite Materials by Confined Carbonization," *Angew. Chemie Int. Ed.*, vol. 49, no. 37, pp. 6664–6668, Sep. 2010, doi: 10.1002/anie.201003163.

[76] M. Inagaki, F. Kang, M. Toyoda, and H. Konno, "Template Carbonization: Morphology and Pore Control," in *Advanced Materials Science and Engineering of Carbon*, vol. 3, Elsevier, 2014, pp. 133–163.

[77] J. P. Paraknowitsch, J. Zhang, D. Su, A. Thomas, and M. Antonietti, "Ionic Liquids as Precursors for Nitrogen-Doped Graphitic Carbon," *Adv. Mater.*, vol. 22, no. 1, pp. 87–92, Jan. 2010, doi: 10.1002/adma.200900965.

[78] L. Xie, Z. Jin, Z. Dai, Y. Chang, X. Jiang, and H. Wang, "Porous carbons synthesized by templating approach from fluid precursors and their applications in environment and energy storage: A review," *Carbon N. Y.*, vol. 170, pp. 100–118, 2020, doi: 10.1016/j.carbon.2020.07.034.

[79] Q. Zhao, T.-P. Fellinger, M. Antonietti, and J. Yuan, "A novel polymeric precursor for micro/mesoporous nitrogen-doped carbons," *J. Mater. Chem. A*, vol. 1, no. 16, p. 5113, 2013, doi: 10.1039/c3ta10291b.

[80] P. Zhang, J. Yuan, T.-P. Fellinger, M. Antonietti, H. Li, and Y. Wang, "Improving Hydrothermal Carbonization by Using Poly(ionic liquid)s," *Angew. Chemie Int. Ed.*, vol. 52, no. 23, pp. 6028–6032, Jun. 2013, doi: 10.1002/anie.201301069.

[81] M. Baccour *et al.*, "Carbonization of polysaccharides in FeCl3/BmimCl ionic liquids:

Breaking the capacity barrier of carbon negative electrodes in lithium ion batteries," *J. Power Sources*, vol. 474, p. 228575, Oct. 2020, doi: 10.1016/j.jpowsour.2020.228575.

[82] X. Huang, K. Yamasaki, S. Kudo, J. Sperry, and J. ichiro Hayashi, "Influence of ionic liquid type on porous carbon formation during the ionothermal pyrolysis of cellulose," *J. Anal. Appl. Pyrolysis*, vol. 145, no. November 2019, p. 104728, 2020, doi: 10.1016/j.jaap.2019.104728.

[83] Z.-L. Xie, X. Huang, M.-M. Titirici, and A. Taubert, "Mesoporous graphite nanoflakes via ionothermal carbonization of fructose and their use in dye removal," *RSC Adv.*, vol. 4, no. 70, pp. 37423–37430, 2014, doi: 10.1039/C4RA05146G.

[84] X. Gao, Y. Yu, Q. He, H. Li, and Y. Liu, "Transition metal assisted ionothermal carbonization of cellulose towards high yield and recycling," *Cellulose*, vol. 28, no. 7, pp. 4025–4037, 2021, doi: 10.1007/s10570-021-03808-8.

[85] M. N. Ettish, G. S. El-Sayyad, M. A. Elsayed, and O. Abuzalat, "Preparation and characterization of new adsorbent from Cinnamon waste by physical activation for removal of Chlorpyrifos," *Environ. Challenges*, vol. 5, no. May, p. 100208, 2021, doi: 10.1016/j.envc.2021.100208.

[86] G. R. Bolzan, G. Abarca, W. D. G. Gonçalves, C. F. Matos, M. J. L. Santos, and J. Dupont, "Imprinted Naked Pt Nanoparticles on N-Doped Carbon Supports: A Synergistic Effect between Catalyst and Support," *Chem. - A Eur. J.*, vol. 24, no. 6, pp. 1365–1372, Jan. 2018, doi: 10.1002/chem.201704094.

[87] R. Sun, K. M. Meek, H. C. Ho, and Y. A. Elabd, "Nitrogen-doped carbons derived from poly(ionic liquid)s with various backbones and cations," *Polym. Int.*, vol. 68, no. 9, pp. 1599–1609, Sep. 2019, doi: 10.1002/pi.5864.

[88] Q. Guo *et al.*, "Controllable construction of N-enriched hierarchically porous carbon nanosheets with enhanced performance for CO2 capture," *Chem. Eng. J.*, vol. 371, pp. 414–423, 2019, doi: 10.1016/j.cej.2019.04.062.

[89] Y. Xie *et al.*, "Hypercrosslinked mesoporous poly(ionic liquid)s with high ionic density for efficient CO2 capture and conversion into cyclic carbonates," *J. Mater. Chem. A*, vol. 6, no. 15, pp. 6660–6666, 2018, doi: 10.1039/c8ta01346b.

[90] K. Täuber, A. Dani, and J. Yuan, "Covalent cross-linking of porous poly(ionic liquid) membrane via a triazine network," *ACS Macro Lett.*, vol. 6, no. 1, pp. 1–5, Jan. 2017, doi: 10.1021/acsmacrolett.6b00782.

[91] A. V. Korobeinyk, R. L. D. Whitby, and S. V. Mikhalovsky, "High temperature oxidative resistance of polyacrylonitrile- methylmethacrylate copolymer powder converting to a carbonized monolith," *Eur. Polym. J.*, vol. 48, no. 1, pp. 97–104, 2012, doi: 10.1016/j.eurpolymj.2011.10.006.

[92] F. Rodríguez-Reinoso and A. Sepúlveda-Escribano, "Porous Carbons in Adsorption and Catalysis," in *Handbook of Surfaces and Interfaces of Materials*, vol. 5, Elsevier, 2001, pp. 309–355.

[93] M. Mukhopadhyay and D. Bhattacharya, "Application of Lignocellulosic Biomass in the Paper Industry," in *Lignocellulosic Biomass Production and Industrial Applications*, Hoboken, NJ, USA: John Wiley & Sons, Inc., 2017, pp. 265–278.

[94] S. Mopoung and N. Dejang, "Activated carbon preparation from eucalyptus wood chips using continuous carbonization–steam activation process in a batch intermittent rotary kiln," *Sci. Rep.*, vol. 11, no. 1, p. 13948, Dec. 2021, doi: 10.1038/s41598-021-93249-x.

[95] A. Sahu, S. Sen, and S. C. Mishra, "Economical way of processing activated carbon from Calotropis gigantea and its suitability for application in Lithium/Sodium ion batteries," *Diam. Relat. Mater.*, vol. 108, p. 107931, 2020, doi: 10.1016/j.diamond.2020.107931.

[96] D. Angin, E. Altintig, and T. E. Köse, "Influence of process parameters on the surface

and chemical properties of activated carbon obtained from biochar by chemical activation," *Bioresour. Technol.*, vol. 148, pp. 542–549, 2013, doi: 10.1016/j.biortech.2013.08.164.

[97] B. Chen, D. Zhou, and L. Zhu, "Transitional Adsorption and Partition of Nonpolar and Polar Aromatic Contaminants by Biochars of Pine Needles with Different Pyrolytic Temperatures," *Environ. Sci. Technol.*, vol. 42, no. 14, pp. 5137–5143, Jul. 2008, doi: 10.1021/es8002684.

[98] M. Thommes *et al.*, "Physisorption of gases, with special reference to the evaluation of surface area and pore size distribution (IUPAC Technical Report)," *Pure Appl. Chem.*, vol. 87, no. 9–10, pp. 1051–1069, Oct. 2015, doi: 10.1515/pac-2014-1117.

[99] H. F. Stoeckli, "Microporous carbons and their characterization: The present state of the art," *Carbon N. Y.*, vol. 28, no. 1, pp. 1–6, 1990, doi: 10.1016/0008-6223(90)90086-E.

[100] V. Calisto, C. I. A. Ferreira, S. M. Santos, M. V. Gil, M. Otero, and V. I. Esteves, "Production of adsorbents by pyrolysis of paper mill sludge and application on the removal of citalopram from water," *Bioresour. Technol.*, vol. 166, pp. 335–344, Aug. 2014, doi: 10.1016/j.biortech.2014.05.047.

[101] J. Soucy, A. Koubaa, S. Migneault, and B. Riedl, "The potential of paper mill sludge for wood-plastic composites," *Ind. Crops Prod.*, vol. 54, pp. 248–256, 2014, doi: 10.1016/j.indcrop.2014.01.013.

[102] R. Modolo, V. M. Ferreira, L. M. Machado, M. Rodrigues, and I. Coelho, "Construction materials as a waste management solution for cellulose sludge," *Waste Manag.*, vol. 31, no. 2, pp. 370–377, 2011, doi: 10.1016/j.wasman.2010.09.017.

[103] C. Guizani, K. Haddad, L. Limousy, and M. Jeguirim, "New insights on the structural evolution of biomass char upon pyrolysis as revealed by the Raman spectroscopy and elemental analysis," *Carbon N. Y.*, vol. 119, no. May, pp. 519–521, 2017, doi: 10.1016/j.carbon.2017.04.078.

[104] M. W. Smith *et al.*, "Structural analysis of char by Raman spectroscopy: Improving band assignments through computational calculations from first principles," *Carbon N. Y.*, vol. 100, pp. 678–692, 2016, doi: 10.1016/j.carbon.2016.01.031.

[105] P. Hu, D. Meng, G. Ren, R. Yan, and X. Peng, "Nitrogen-doped mesoporous carbon thin film for binder-free supercapacitor," *Appl. Mater. Today*, vol. 5, pp. 1–8, 2016, doi: 10.1016/j.apmt.2016.08.001.

[106] L. Xiaojiang, H. Jun-ichiro, and L. Chun-Zhu, "FT-Raman spectroscopic study of the evolution of char structure during the pyrolysis of a Victorian brown coal," *Fuel*, vol. 85, no. 12–13, pp. 1700–1707, Sep. 2006, doi: 10.1016/j.fuel.2006.03.008.

[107] A. K. Mondal *et al.*, "Nitrogen-Doped Porous Carbon Nanosheets from Eco-Friendly Eucalyptus Leaves as High Performance Electrode Materials for Supercapacitors and Lithium Ion Batteries," *Chem. - A Eur. J.*, vol. 23, no. 15, pp. 3683–3690, Mar. 2017, doi: 10.1002/chem.201605019.

[108] J. Urmos, S. K. Sharma, and F. T. Mackenzie, "Characterization of some biogenic carbonates with Raman spectroscopy," *Am. Mineral.*, vol. 76, no. 3–4, pp. 641–646, 1991.

[109] C. A. Montoya *et al.*, "Styrene carbonate synthesis from CO2 using tetrabutylammonium bromide as a non-supported heterogeneous catalyst phase," *J. Supercrit. Fluids*, vol. 100, pp. 155–159, 2015, doi: 10.1016/j.supflu.2015.01.027.

[110] K. Kiatkittipong *et al.*, "Green Pathway in Utilizing CO2 via Cycloaddition Reaction with Epoxide—A Mini Review," *Processes*, vol. 8, no. 5, p. 548, May 2020, doi: 10.3390/pr8050548.

[111] P. P. Pescarmona and M. Taherimehr, "Challenges in the catalytic synthesis of cyclic and polymeric carbonates from epoxides and CO2," *Catal. Sci. Technol.*, vol. 2, no. 11, p. 2169, 2012, doi: 10.1039/c2cy20365k.

[112] F. Zhang, Y. Wang, X. Zhang, X. Zhang, H. Liu, and B. Han, "Recent advances in the

coupling of CO2 and epoxides into cyclic carbonates under halogen-free condition," *Green Chem. Eng.*, vol. 1, no. 2, pp. 82–93, 2020, doi: 10.1016/j.gce.2020.09.008.
[113] B. Han and T. Wu, Eds., *Green Chemistry and Chemical Engineering*, vol. 52, no. 6. New York, NY: Springer New York, 2019.
[114] B. Viswanathan, P. Neel, and T. Varadarajan, *Methods of activation and specific applications of carbon materials*. 2009.
[115] J. Sun, W. Cheng, W. Fan, Y. Wang, Z. Meng, and S. Zhang, "Reusable and efficient polymer-supported task-specific ionic liquid catalyst for cycloaddition of epoxide with CO2," *Catal. Today*, vol. 148, no. 3–4, pp. 361–367, Nov. 2009, doi: 10.1016/j.cattod.2009.07.070.
[116] R. Jamil, L. C. Tomé, D. Mecerreyes, and D. S. Silvester, "Emerging Ionic Polymers for CO2 Conversion to Cyclic Carbonates: An Overview of Recent Developments," *Aust. J. Chem.*, 2021, doi: 10.1071/CH21182.
[117] X. Fu, D. Zhou, K. Wang, and H. Jing, "Pd/C as a high efficient and reusable catalyst for cycloaddition of CO2 to epoxides," *J. CO2 Util.*, vol. 14, pp. 31–36, 2016, doi: 10.1016/j.jcou.2016.02.003.
[118] V. Caló, A. Nacci, A. Monopoli, and A. Fanizzi, "Cyclic Carbonate Formation from Carbon Dioxide and Oxiranes in Tetrabutylammonium Halides as Solvents and Catalysts," *Org. Lett.*, vol. 4, no. 15, pp. 2561–2563, 2002, doi: 10.1021/ol026189w.

A. APPENDIX

A.1. Literature revision

Table A.1. Literature revision of biomass-based carbocatalysts for CO_2 conversion.

Entry	Catalytic system	Substrate[a]	P_{CO2} (bar)	Temp. (°C)	Time (h)	Yield (%)	Sel. (%)	Ref.
1	N-doped porous carbon monolith derived from alginic acid	EPCH	40	150	16	33[b]	–	[28]
			40	150	16	54[c]	–	
			40	150	16	84[d]	–	
			40	150	16	18[e]	–	
2	Imidazolium-allyl bromide grafted on rice husk derived MCM-41	BH	15	150	8	58	>99	[39]
		EH	15	150	8	14	98	
		EPCH	15	150	8	69	99	
		PO	15	150	8	72	95	
3	Imidazole and 1,2-dibromoethane grafted on rice husk derived MCM-41	EH	10	100	4	98	100	[41]–[43]
		GOH	20	90	4	100	98	
		EH	20	100	3	100	100	
		EH	20	100	4	100	100	
		PGE	20	100	3	97	100	
		EPCH	25	90	4	100	97	
		EH	30	100	4	100	100	
		SO	30	140	6	9[f]	84	
		SO	30	140	6	84	97	
		SO	40	100	4	99	99	
		AGE	60	120	6	100	100	
4	N-doped porous carbons derived from waste cow manure[g]	BGE	1	30	48	65	–	[27]
		SO	1	30	48	50	–	
		EH	1	50	48	65	–	
		BGE	1	50	48	94	–	
		EPCH	1	80	48	69	–	
		SO	1	80	48	84	–	
		PO	1	100	0.5	96	99	
		PO	5	25	48	92	99	
		PO	5	100	1.5	95	≈100	
		PO	5	100	1.5	95[h]	≈100	
		PO	5	100	1.5	95[i]	9	
		PO	5	100	1.5	26[j]	≈100	
		PO	5	100	1.5	42[k]	≈100	

Entry	Catalytic system	Substrate[a]	P_{CO_2} (bar)	Temp. (˚C)	Time (h)	Yield (%)	Sel. (%)	Ref.
5	Ag supported on N-doped porous carbons derived from walnut shells	2-Methyl-3-butyn-2-ol	10	30	0.5	21	–	[29]
			10	30	1	41	–	
			10	30	6	74	–	
			10	30	16	99	–	
			10	40	1	48	–	
			10	50	1	59	–	
			10	60	1	67	–	
6	N-doped active carbons derived from chitosan and non-food protein wastes	EPCH	15	150	5	72[l]	86	[30]
			15	150	5	88[m]	99	
			15	150	5	97[n]	87	
			15	150	15	>99[l]	93	
			15	150	15	>99[n]	94	
			15	150	15	>99[m]	99	
7	N-doped mesoporous carbon derived from glucose	SO	10	80	15	52[o]	–	[31]
			10	80	15	67[p]	–	
			10	80	15	88[q]	–	
			10	80	15	98[r]	–	
			10	80	15	98[s]	–	
			10	80	15	36[r],[t]	–	

[a] EH: 1,2-epoxyhexane. AGE: allyl glycidyl ether. BGE: butyl glycidyl ether. BH: 1,2-epoxybutane. EPCH: epichlorohydrin. GOH: glycidol. PGE: phenyl glycidyl ether PO: propylene oxide.

[b] Carbonized at 750 ˚C. [c] Carbonized at 850 ˚C. [d] Carbonized at 950 ˚C. [e] Carbonized at 1000 ˚C. [f] without 1,2-dibromoethane grafted.

[g] unless stated otherwise, the carbons in this study were used with: Co^{2+} supported on the carbon; activating agent: KOH; co-catalyst TBABr. [h] Activating agent: $NaNH_2$. [i] Zn^{2+} supported on the carbon. [j] no co-catalyst used. [k] no metal ions were supported on the carbon.

[l] carbon precursor: *Jatropha curcas* seeds. [m] carbon precursor: *Mesua ferrea L.* seeds. [n] carbon precursor: chitosan.

[o] catalyst: 20 mg. [p] catalyst: 30 mg. [q] catalyst: 40 mg. [r] catalyst: 50 mg. [s] catalyst: 60 mg. [t] without co-catalyst TBAB.

A.2. **Materials and Equipment**

Commercially available reagents were used without any further purification. Chitosan (degree of deacetylation 76%, low molecular weight), poly(diallyldimethylammonium chloride) solution − 20 wt.% in H_2O, sodium dicyanamide 96%, styrene oxide 97%, anion exchange resin Amberlyst A-26 (OH^- form), potassium chloride, tetrabutylammonium chloride >97%, and 1-butyl-1-methylimidazolium chloride were all purchased from Sigma-Aldrich (St. Louis, MO, USA). 1-Butyl-4-methylpyridinium chloride, 1-butyl-2-methylpyridinium chloride, and 1-butyl-1-methylpyrrolidinium chloride were purchased from Iolitec (Heilbronn, Germany). Chloroform-*d* and deuterium oxide were purchased from Euriso-top (Saint-Aubin, France). Ethanol 96%, acetone, and lithium chloride anhydrous were purchased from Honeywell (Charlotte, NC, USA). Trichloromethane was purchased from PanReac AppliChem ITW Reagents (Barcelona, Spain). Tetrabutylammonium bromide was purchased from TCI (Tokyo, Japan). Carbon dioxide (>99.9%) and compressed nitrogen (>99.8%) were obtained from Air Liquide. Vinylbenzyltriethylammonium chloride and poly(vinylbenzyltriethylammonium) chloride were synthesized and kindly provided by a member of this research team, Raquel Barrulas. Paper mill waste sludges − primary and biological sludge − and knots were kindly supplied by The Navigator Company (Setúbal, Portugal). The water used was MilliQ water.

1-Butyl-1-methylpyrrolidinium dicyanamide was synthetized according to the experimental details provided in Section A.3.1.

The reactor used was a 22 mL Parr 4700 General Purpose Pressure Vessel and the furnace was a Termolab tubular alumina furnace with Eurotherm 2416 and 2132 Process Controllers. The 2416 controller was used to set the ramping rate and dwell time, while the 2132 controller was used to control the temperature inside the furnace.

Raman spectra were collected using a Labram300 Jobin Yvon spectrometer, equipped with a HeNe laser 17 mW operating at 632.8 nm. The spectra were acquired in the range of 1800 to 100 cm^{-1}. Data processing was carried out with *Origin 9* software. Nuclear magnetic resonance (NMR) spectra were recorded at room temperature on a Bruker Avance III 400 spectrometer operating at 400.15 MHz Larmor frequency for hydrogen and 100.61 MHz for carbon with a Bruker High-Resolution BBO probe. This spectrometer is equipped with a temperature control unit and a pulse field gradient unit capable of producing magnetic pulsed field gradients in the z-direction of 50.0 G/cm. ^1H NMR spectra were acquired with 64 K time domain points over a spectral window of 8012.820 Hz and with 16 scans per FID. ^{13}C NMR spectra were acquired with 64 K time domain points over a spectral window of 24038.461 Hz with 512 scans per FID. HSQC-DEPT spectra were acquired with 2D H-1/X correlation via double inept transfer, using sensitivity improvement phase sensitive Echo/Antiecho -TPPI gradient selection, with decoupling during acquisition using trim pulses in inept transfer with multiplicity editing during selection step (hsqcedetgp); size of FID TD(F2) = 2048, TD(F1) =128; 4 scans per FID. ^1H, ^1H-COSY spectra were acquired using a 2D homonuclear shift correlation (cosygpppqf); size of FID TD(F2) = 4096, TD(F1) =256; 4 scans per FID. Data processing was carried out using *Bruker Topspin 3.5* software. Spectra description is presented stating the deuterated solvent used and for each signal, chemical shift value, multiplicity,

coupling constant and nuclei assignment. The following abbreviations were used to indicate signal multiplicity: s, singlet; t, triplet; m, multiplet. Deuterium oxide was the solvent for ionic liquid characterization and chloroform-*d* the solvent for catalytic conversion analysis. Nitrogen adsorption/desorption experiments and CNHS elemental analysis was outsourced to LAQV/REQUIMTE – the Associated Laboratory for Green Chemistry at NOVA School of Science and Technology (*FCT NOVA*). Nitrogen adsorption/desorption isotherms were obtained from a gas porosimeter Micromeritics ASAP 2010 at 77 K. CNHS elemental analysis was carried out in an Elemental analyzer Thermo Finnigan-CE Instruments Flash EA 1112

Scanning electron microscopy was performed a Carl Zeiss AURIGA CrossBeam workstation instrument equipped with an Oxford X-ray Energy Dispersive Spectrometer. The images were analyzed using *ImageJ* software (v1.50i).

A.3. **Additional Experimental Procedures**

A.3.1. [Bmpyr][DCA] synthesis

1-Butyl-1-methylpyrrolidinium dicyanamide ([Bmpyr][DCA]) was synthesized by anion exchange. A 1-Butyl-1-methylpyrrolidinium chloride ([Bmpyr][Cl]) methanolic solution (0.70 g, 3.94 mmol in 2.00 mL) was passed through a column packed with approximately 3.00 g of Amberlyst A-26 resin (OH^- form) that was previously loaded with 1.50 g (16.85 mmol) of sodium dicyanamide in 150 mL of water. The final compound was obtained with a yield of 87%. The structure of [Bmpyr][DCA] was confirmed by ^{1}H and ^{13}C NMR.

A.3.2. Impregnation of TBABr on sample CHI-ImCl

For co-catalyst impregnation, after degassing 50 mg of sample CHI-ImCl in vacuum for 35 min, the desired amount of tetrabutylammonium bromide (TBABr) and 200 µL of acetone were added to the carbon sample. The system was mixed and kept under nitrogen atmosphere for 3 h, until the sample took a dry aspect. The sample was then dried of any remaining acetone by vacuum until the weight was constant. The resulting powder was stored until used. The impregnated samples were designated CHI-ImCl@TBABr-X, where X is the weight percent of TBABr used relative to the carbon sample.

A.4. **NMR characterization of [Bmpyr][DCA]**

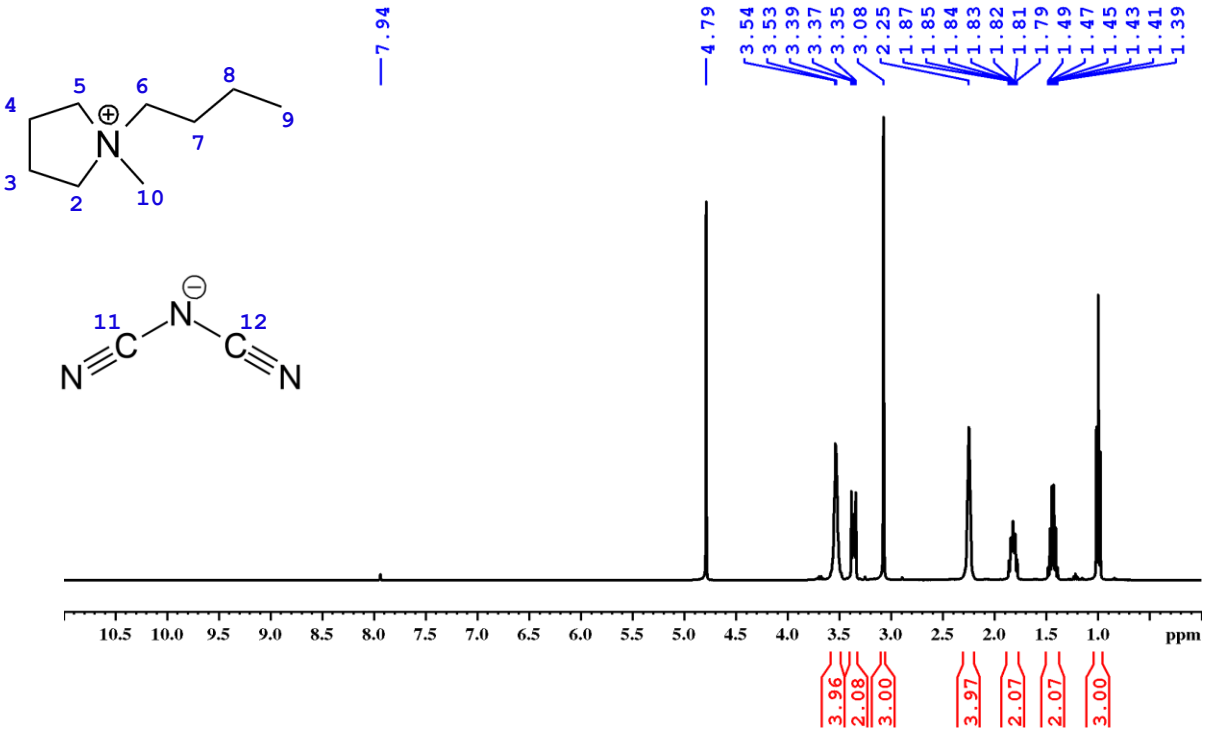

Figure A.1. ^{1}H NMR spectrum of [Bmpyr][DCA] in D_2O.

^{1}H NMR (400 MHz, D_2O) δ (ppm) 3.47-3.61 (br, 4H, C(2)H_2 and C(5)H_2), 3.37 (t, 8.51 Hz, 2H C(6)H_2), 3.08 (s, 3H, C(10)H_3), 2.18-2.33 (br, 4H, C(3)H_2 and C(4)H_2), 1.83 (m, 2H, C(7)H_2), 1.44 (m, 2H, C(8)H_2), 1.00 (t, 7.42 Hz, 3H, C(9)H_3).

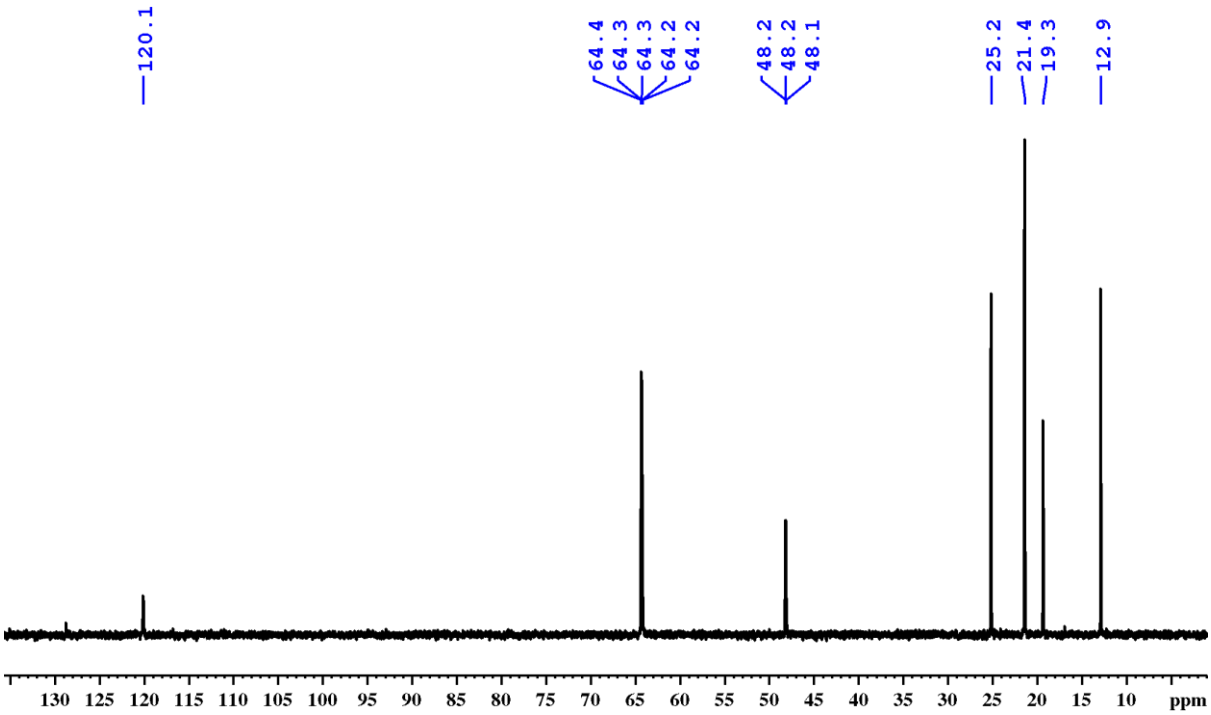

Figure A.2. ^{13}C NMR spectrum of [Bmpyr][DCA] in D_2O.

^{13}C NMR (400 MHz, D_2O) δ (ppm) 120.1 (C(11) and C(12)), 64.3 (C(2) and C(5)), 48.2 (C(10)), 25.2 (C(7)), 21.4 (C(3) and C(4)), 19.3 (C(8)), 12.9 (C(9)).

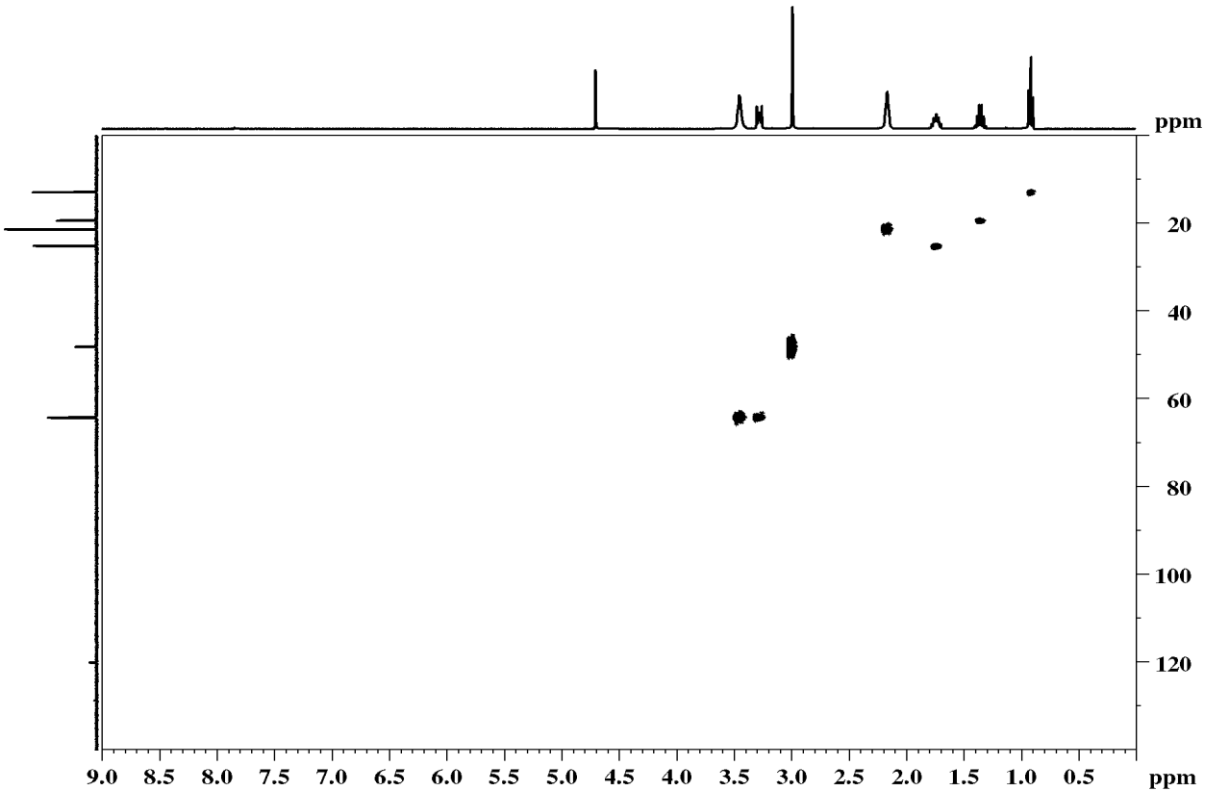

Figure A.3. ^{1}H, ^{13}C HSQC -DEPT NMR spectrum of [Bmpyr][DCA] in D_2O.

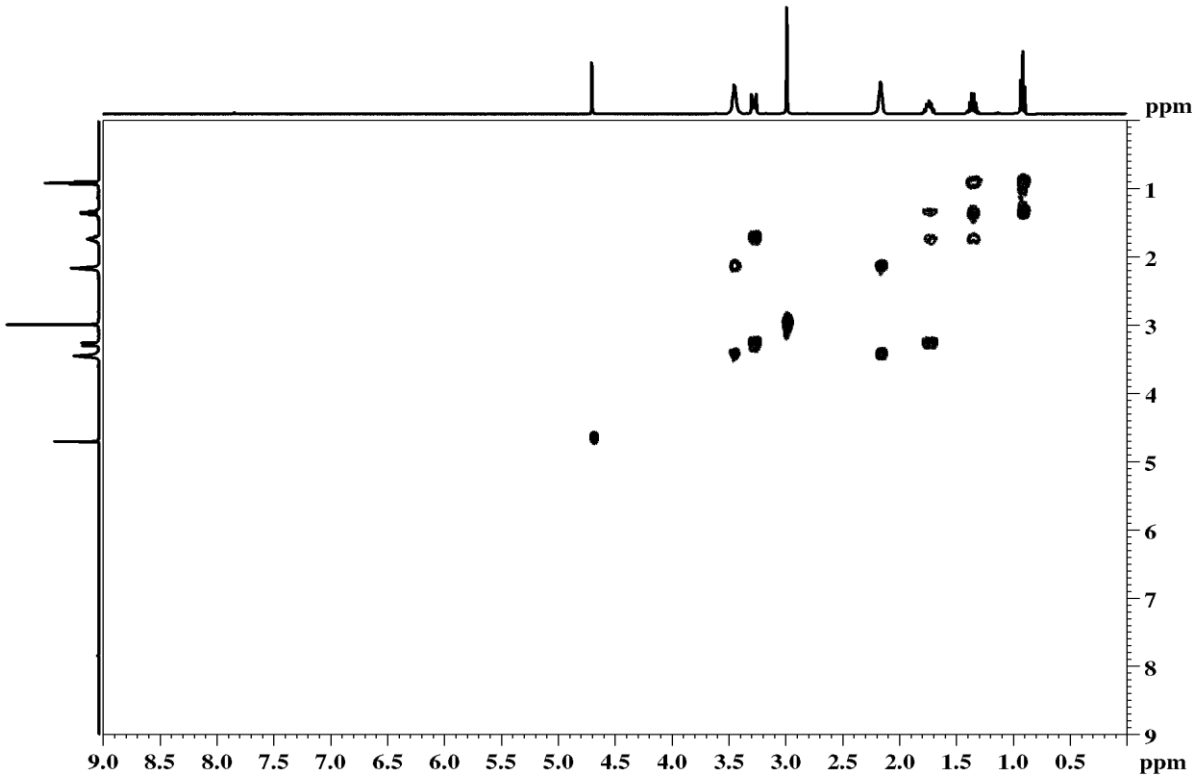

Figure A.4. ^{1}H, ^{1}H COSY NMR spectrum of [Bmpyr][DCA] in D_2O.

A.5. **List of samples**

Table A.2. Materials used in all completed carbonizations and chemical structures of the additives.

Entry	Sample designation	Biomass	Additive	
			Name	Chemical structure
1	CHI-0	CHI	–	–
2	Kno-0	Knots	–	–
3	PriS-0	Primary sludge	–	–
4	BioS-0	Biological sludge	–	–
5	BioS-ImCl	Biological sludge	[Bmim][Cl]	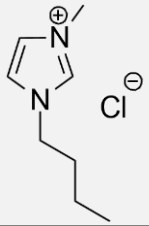
6	CHI-ImCl	CHI		
7	CHI-PyrCl	CHI	[Bmpyr][Cl]	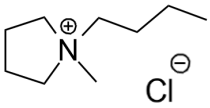
8	CHI-PyrDCA	CHI	[Bmpyr][DCA]	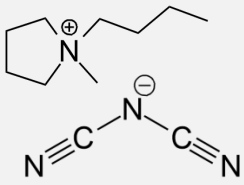
9	CHI-PDADMACl	CHI	PDADMACl	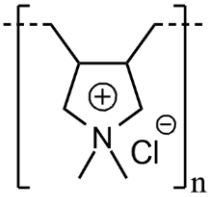
10	CHI-2PyCl	CHI	[2Bmpy][Cl]	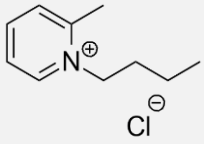
11	CHI-4PyCl	CHI	[4Bmpy][Cl]	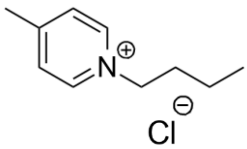
12	CHI-DES	CHI	LiCl/KCl[b]	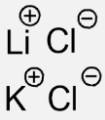
13	CHI-DES-F[a]	CHI		

[a] Carbon obtained from washing and filtering sample CHI-DES.

[b] 45:55 by weight.

A.6. **Nitrogen adsorption/desorption isotherms**

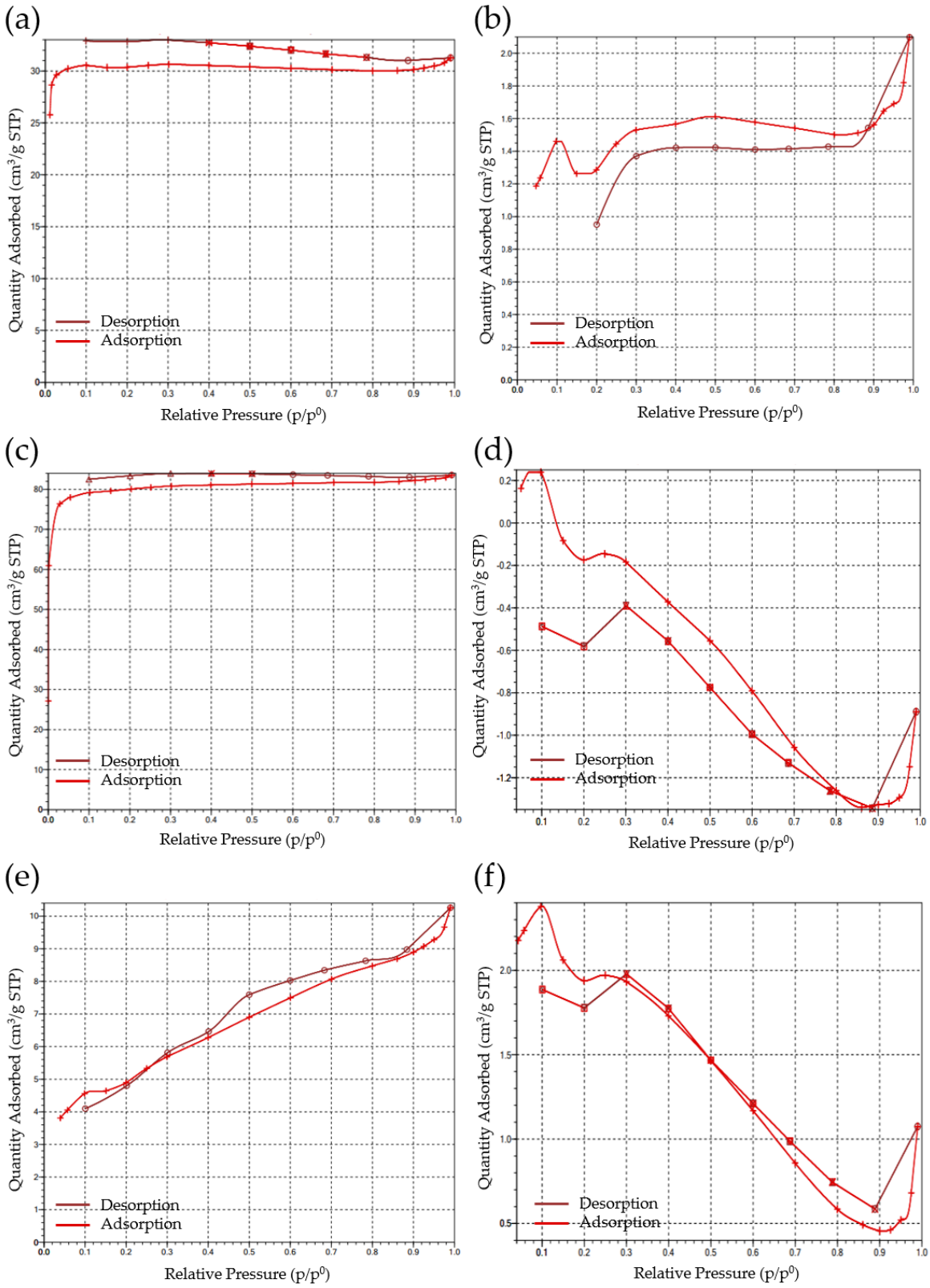

Figure A.5. N_2 adsorption/desorption isotherms at 77 K of the chitosan-based carbons: (a) CHI-0. (b) CHI-ImCl. (c) CHI-PyrCl. (d) CHI-PyrDCA. (e) CHI-PDADMACl. (f) CHI-2PyCl.

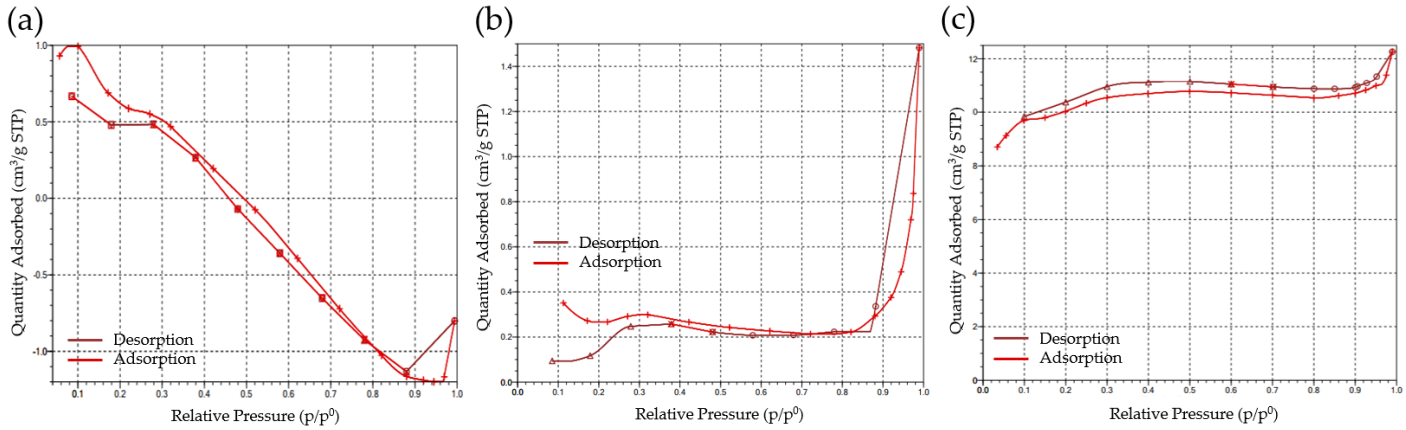

Figure A.6. N_2 adsorption/desorption isotherms at 77 K of the chitosan-based carbons: (a) CHI-4PyCl. (b) CHI-DES. (c) CHI-DES-F.

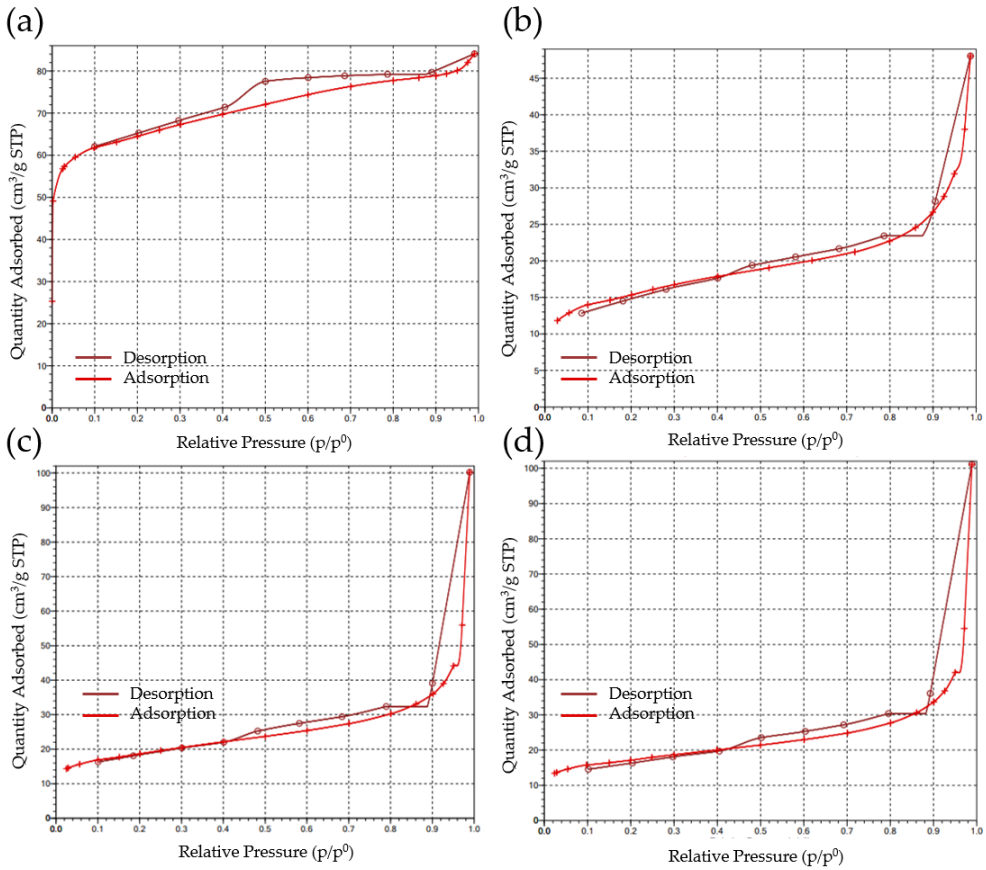

Figure A.7. N_2 adsorption/desorption isotherms at 77 K of waste biomass-based carbons: (a) Kno-0. (b) PriS-0 (c) BioS-0. (d) BioS-ImCl.

A.7. **SEM images**

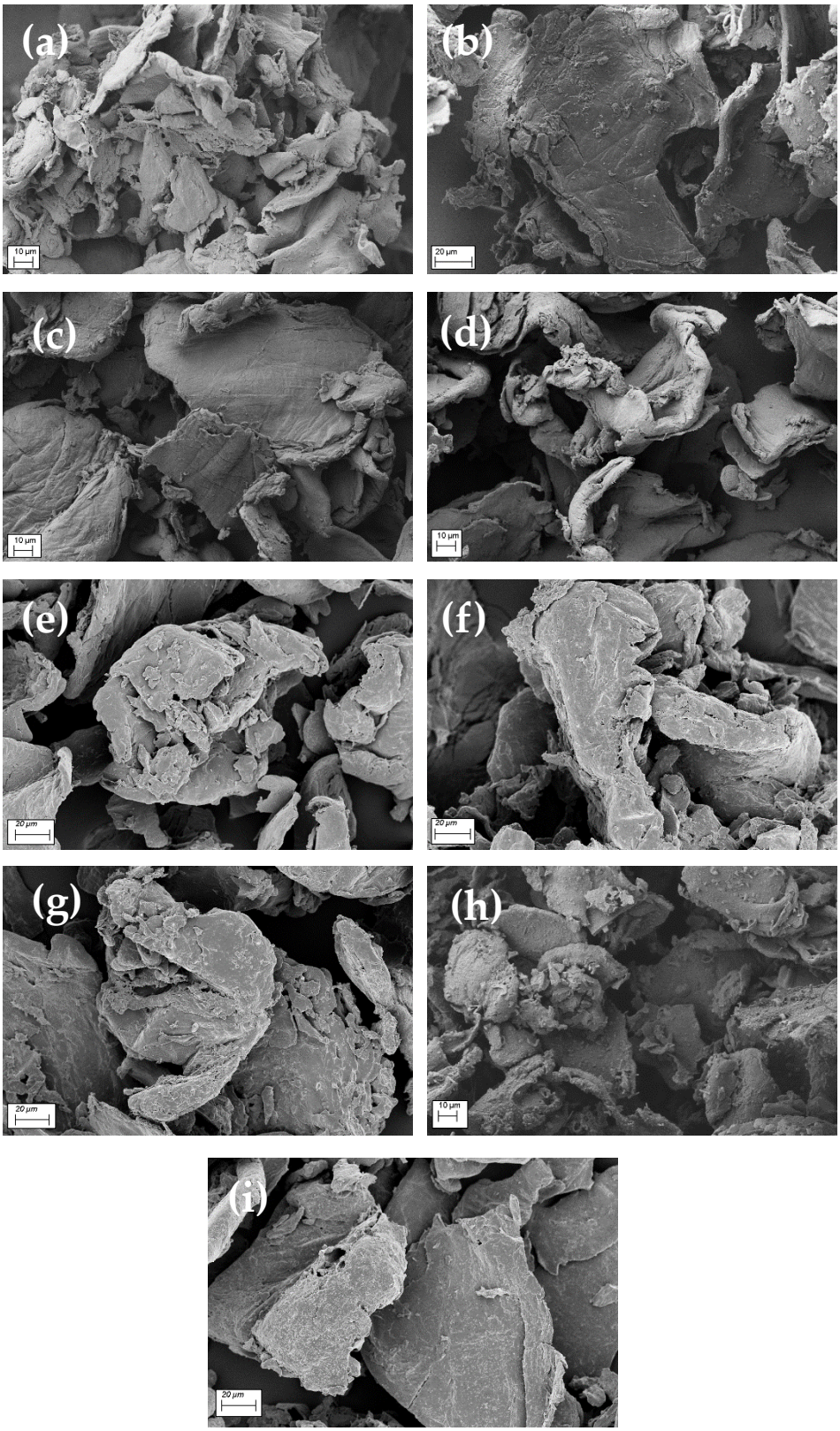

Figure A.8. SEM images of the chitosan-based carbons: (a) CHI-0. (b) CHI-ImCl. (c) CHI-PyrCl. (d) CHI-PyrDCA. (e) CHI-PDADMACl. (f) CHI-2PyCl. (g) CHI-4PyCl. (h) CHI-DES. (i) CHI-DES-F.

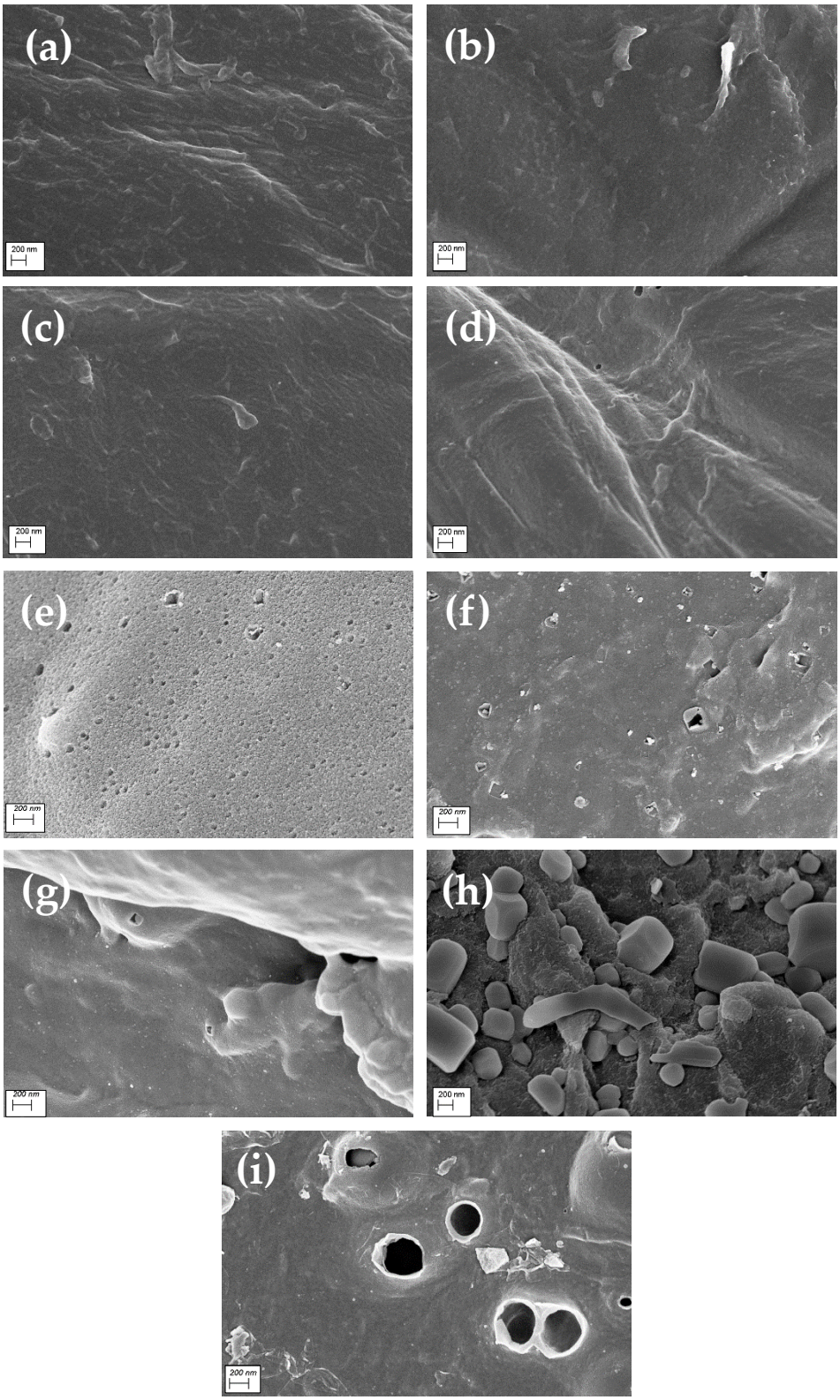

Figure A.9. SEM images with higher magnification of the chitosan-based carbons: (a) CHI-0. (b) CHI-ImCl. (c) CHI-PyrCl. (d) CHI-PyrDCA. (e) CHI-PDADMACl. (f) CHI-2PyCl. (g) CHI-4PyCl. (h). CHI-DES. (i) CHI-DES-F.

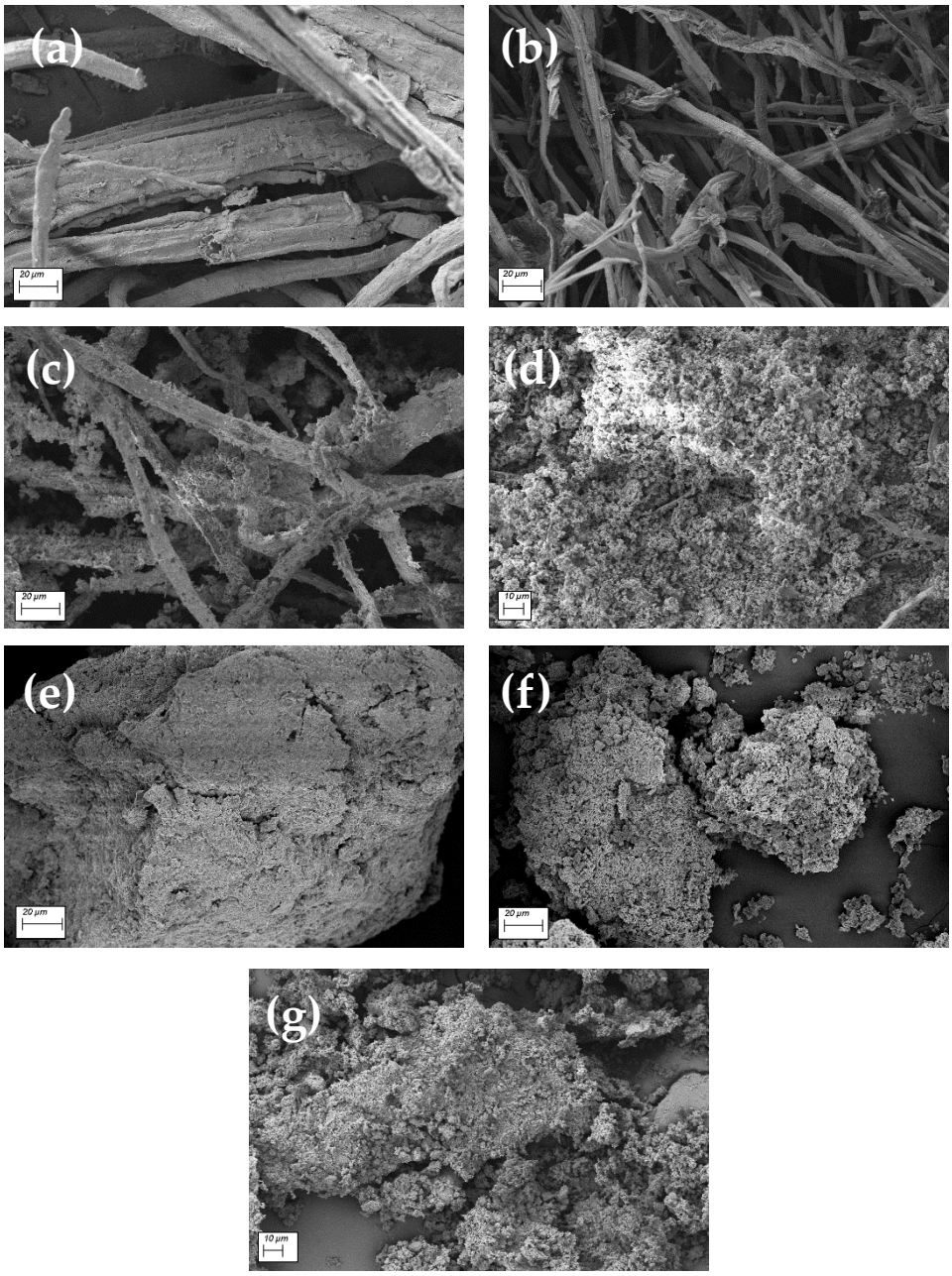

Figure A.10. SEM images of the waste biomass samples and corresponding carbons: (a) Kno. (b) Kno-0. (c) PriS. (d) PriS-0. (e) BioS. (f) BioS-0. (g) BioS-ImCl.

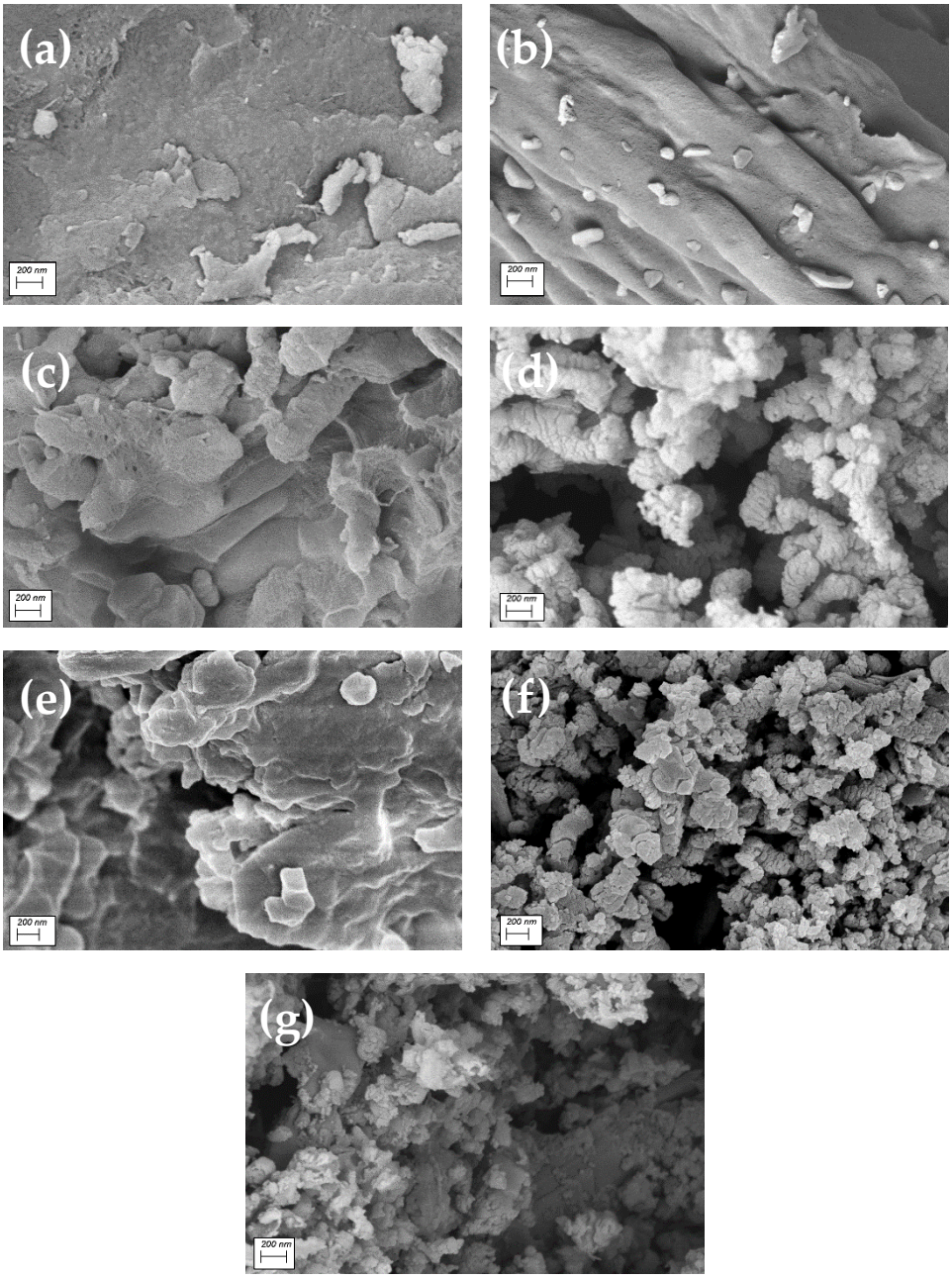

Figure A.11. SEM images with higher magnification of the waste biomass samples and corresponding carbons: (a) Kno. (b) Kno-0. (c) PriS. (d) PriS-0. (e) BioS. (f) BioS-0. (g) BioS-ImCl.

A.8. **Raman spectra**

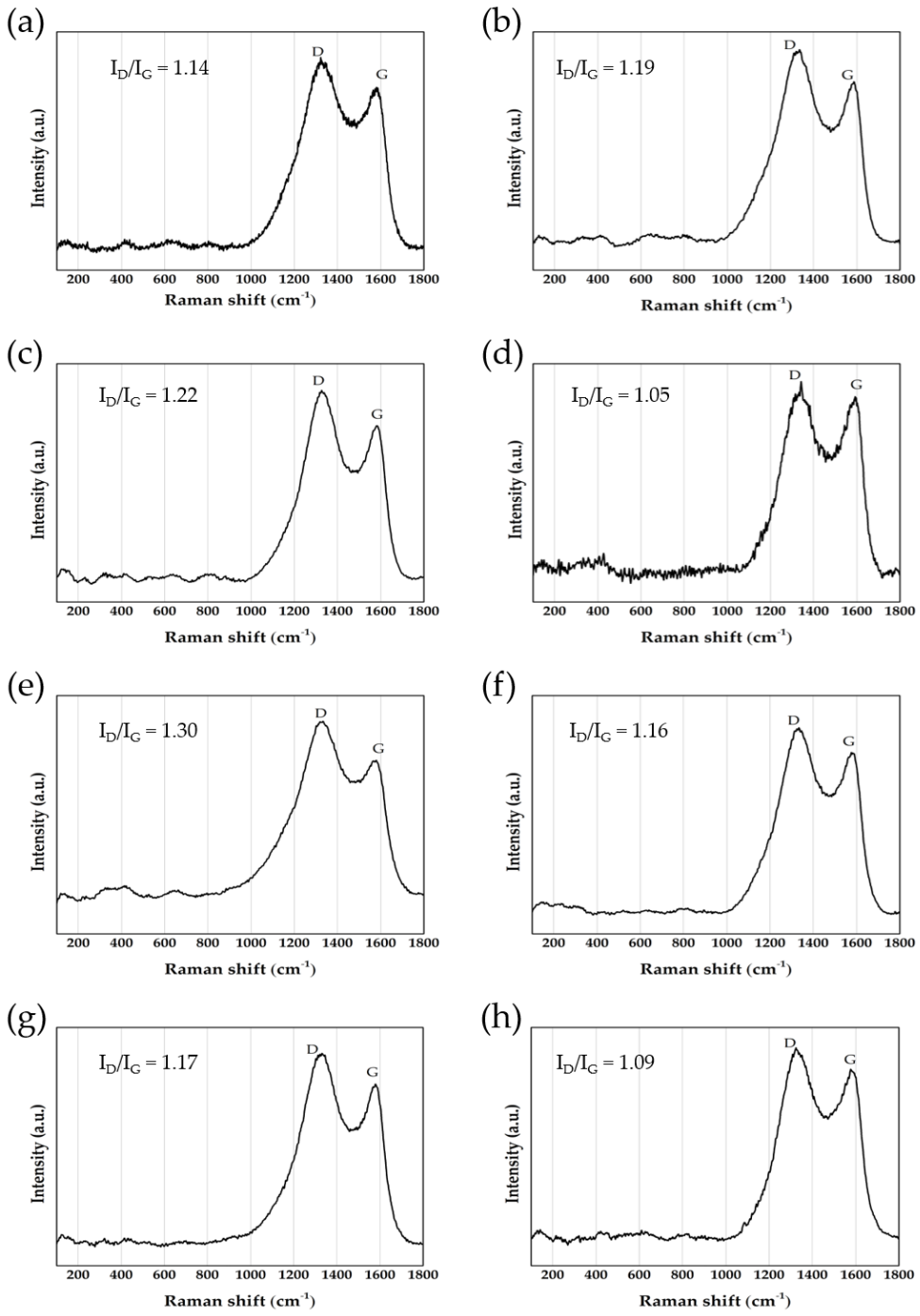

Figure A.12. Raman spectra of chitosan-based carbons: (a) CHI-0. (b) CHI-ImCl. (c) CHI-PyrCl. (d) CHI-PyrDCA. (e) CHI-PDADMACl. (f) CHI-2PyCl. (g) CHI-4PyCl. (h) CHI-DES.

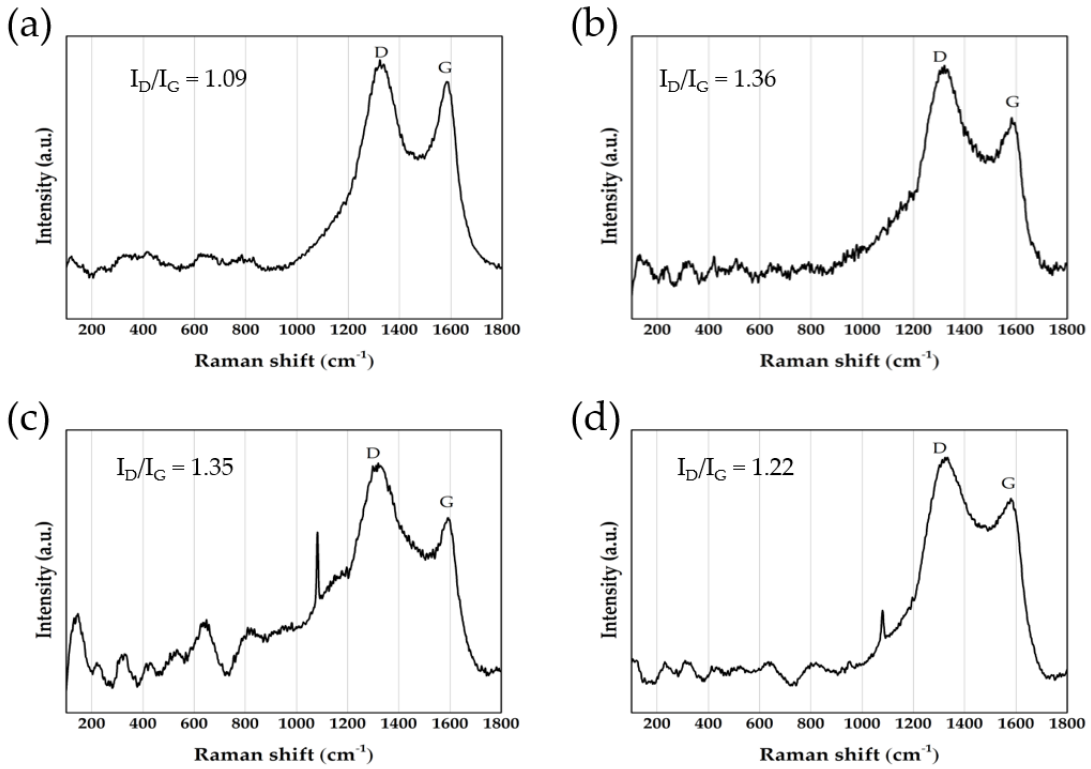

Figure A.13. Raman spectra of waste biomass-based carbons: (a) Kno-0. (b) PriS-0. (c) BioS-0. (d) BioS-ImCl.

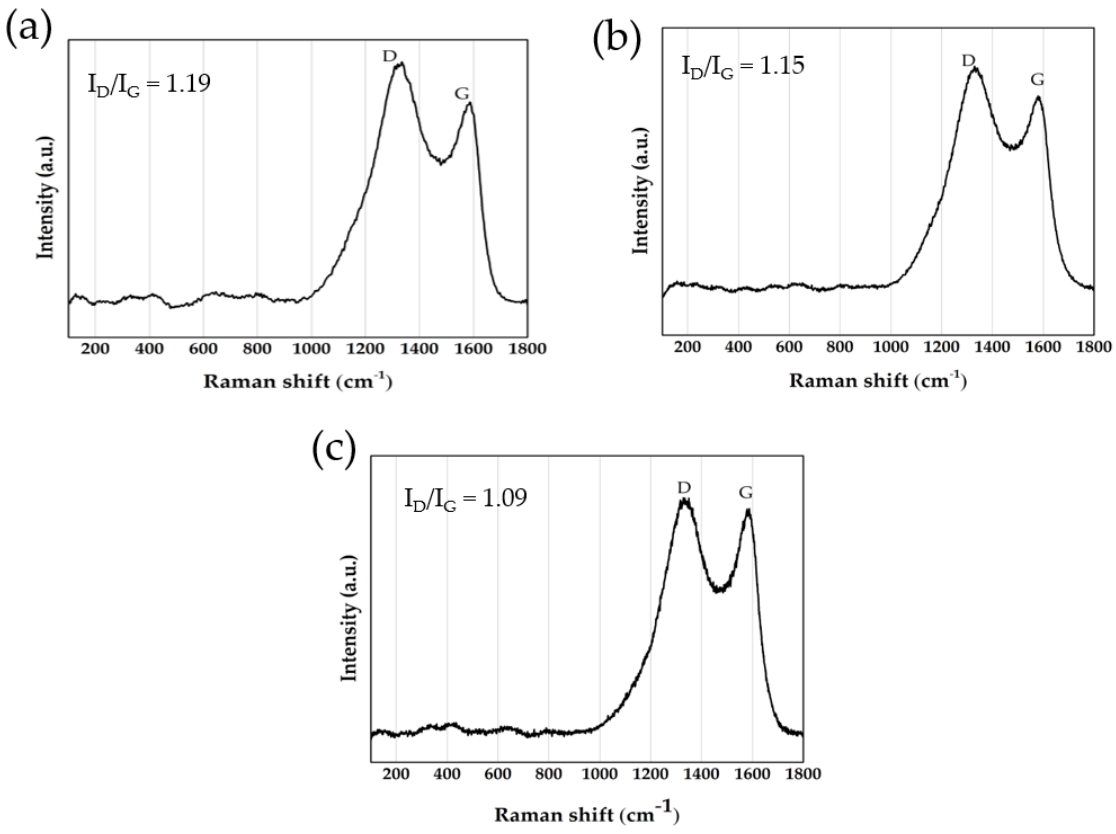

Figure A.14. Raman spectra of CHI-ImCl before (a) and after being subjected to a CO_2 flow of: (b) 5 min. (c) 30 min.

A.9. CO_2 flow system

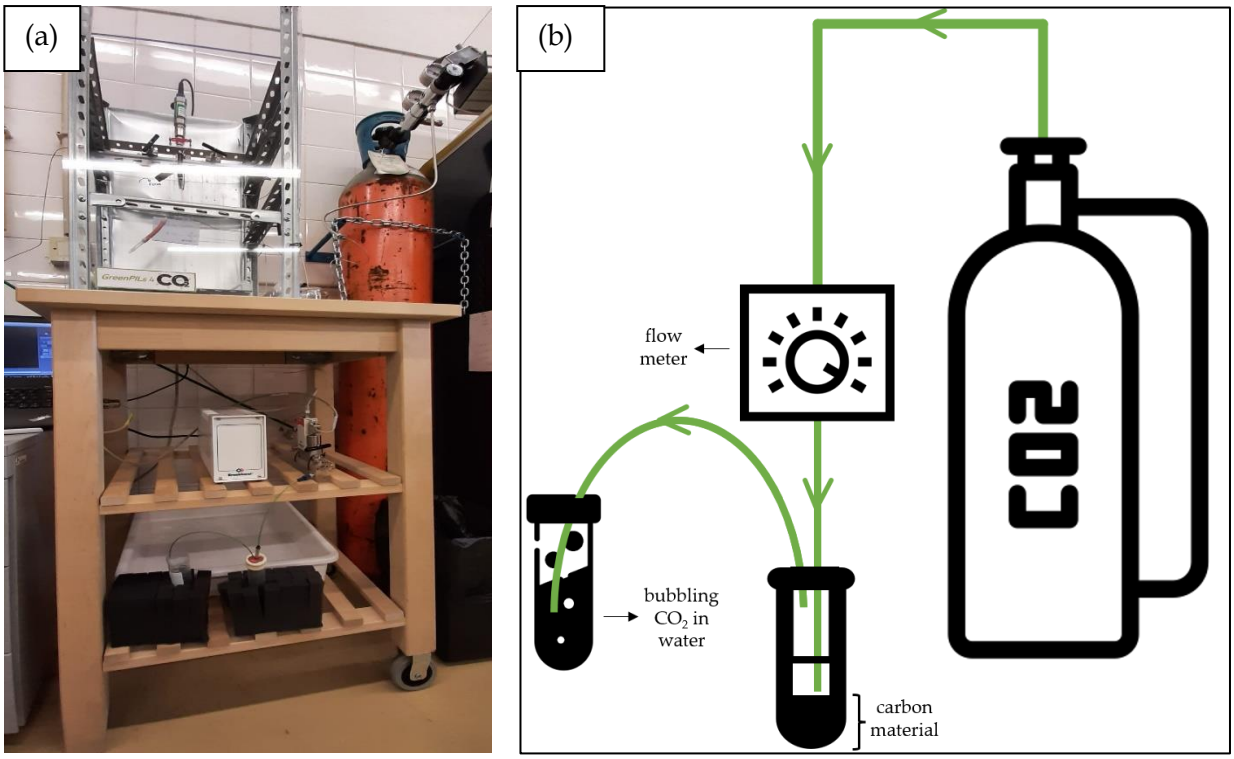

Figure A.15. (a) Photograph and (b) schematic illustration of the CO_2 flow system.

A.10. Catalytic activity results

A.10.1. List of completed reactions

Table A.3. Reaction index[a].

Entry	Reaction number (Figure)	Catalyst (mg)	Co-catalyst (mol%)	t (h)	Conversion (%)
1	1 (Figure A.16)	CHI-ImCl (10)	TBABr (7)	3	80
2	2 (Figure A.17)	CHI-ImCl@TBAB-20 (12)	–	3	5
3	3 (Figure A.18)	–	TBABr (7)	3	87
4	4 (Figure A.19)	CHI-ImCl@TBAB-50 (20)	–	3	21
5	5 (Figure A.20)	CHI-0 (10)	TBABr (7)	3	61
6	6 (Figure A.21)	CHI-DES (10)	TBABr (7)	3	74
7	7 (Figure A.22)	CHI-DES-F (10)	TBABr (7)	3	74
8	8 (Figure A.23)	PriS-0 (10)	TBABr (7)	3	47
9	9 (Figure A.24)	BioS-0 (10)	TBABr (7)	3	75
10	10 (Figure A.25)	Kno-0 (10)	TBABr (7)	3	50
11	11 (Figure A.26)	CHI-ImCl (10)	–	3	0
12	12 (Figure A.27)	CHI-PyrCl (10)	TBABr (7)	3	74
13	13 (Figure A.28)	CHI-PyrDCA (10)	TBABr (7)	3	62
14	14 (Figure A.29)	CHI-PDADMACl (10)	TBABr (7)	3	56
15	15 (Figure A.30)	CHI-2PyCl (10)	TBABr (7)	3	77
16	16 (Figure A.31)	CHI-4PyCl (10)	TBABr (7)	3	58
17	17 (Figure A.32)	CHI-ImCl (50)	TBABr (7)	3	72
18	18 (Figure A.33)	CHI-ImCl (5)	TBABr (7)	3	77
19	19 (Figure A.34)	CHI-ImCl (10)	TBABr (3.5)	3	68
20	20 (Figure A.35)	–	TBABr (3.5)	3	62
21	21 (Figure A.36)	CHI-ImCl (10)	TBABr (1.75)	3	56
22	22 (Figure A.37)	–	TBABr (1.75)	3	59
23	23 (Figure A.38)	CHI-ImCl (10)	TBABr (3.5)	24	98
24	24 (Figure A.39)	–	TBABr (3.5)	24	98
25	25 (Figure A.40)	BioS-ImCl (10)	TBABr (3.5)	3	81
26	26 (Figure A.41)	–	TBABr (3.5)	8	92
27	27 (Figure A.42)	CHI-ImCl (10)	TBABr (3.5)	8	95
28	28 (Figure A.43)	CHI-ImCl (10)	TBACl (3.5)	3	52
29	29 (Figure A.44)	CHI-ImCl (10)	VBACl (3.5)	3	41
30	30 (Figure A.45)	CHI-ImCl (10)	PVBACl (3.5)	3	3
31	31 (Figure A.47)	CHI-0 (10)	TBABr (3.5)	3	56
32	32 (Figure A.48)	CHI-PyrCl (10)	TBABr (3.5)	3	52
33	33 (Figure A.49)	BioS-0 (10)	TBABr (3.5)	3	50
34	34 (Figure A.50)	BioS-ImCl (10)	TBABr (3.5)	3	62

Entry	Reaction number (Figure)	Catalyst (mg)	Co-catalyst (mol%)	t (h)	Conversion (%)
35	35 (Figure A.51)	CHI-ImCl (10)	TBABr (3.5)	3	62
36	36 (Figure A.52)	CHI-ImCl (10)	TBABr (3.5)	3	50
37	37 (Figure A.53)	CHI-ImCl (10)	TBABr (3.5)	3	58
38	30a (Figure A.46)	CHI-ImCl (10)	PVBACl (3.5)	3	14

[a] Temperature (100 °C), CO_2 (5 bar).

A.10.2. ^{1}H NMR spectra

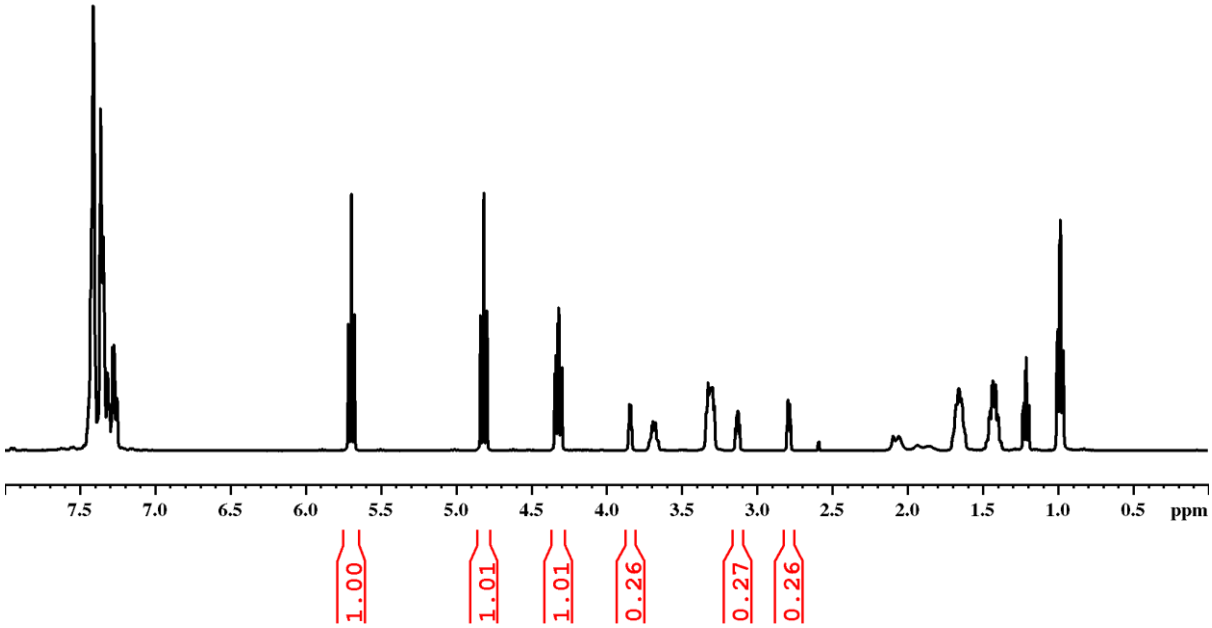

Figure A.16. ^{1}H NMR spectrum of reaction number 1 in $CDCl_3$.

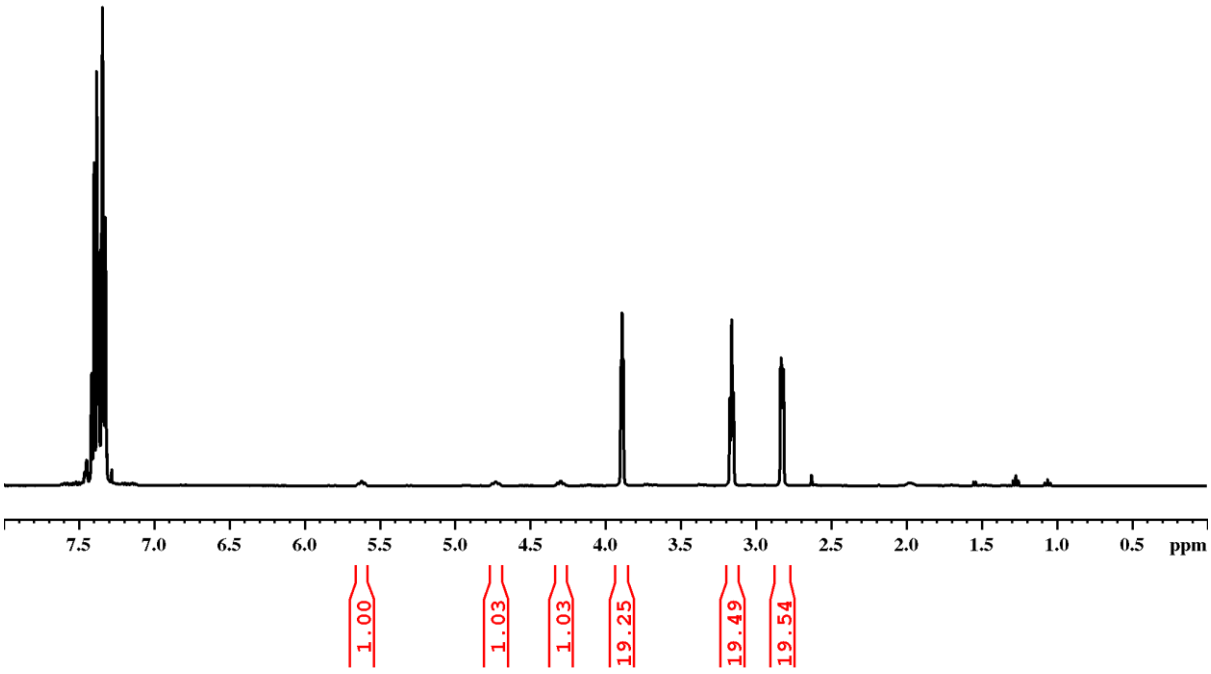

Figure A.17. ^{1}H NMR spectrum of reaction number 2 in $CDCl_3$.

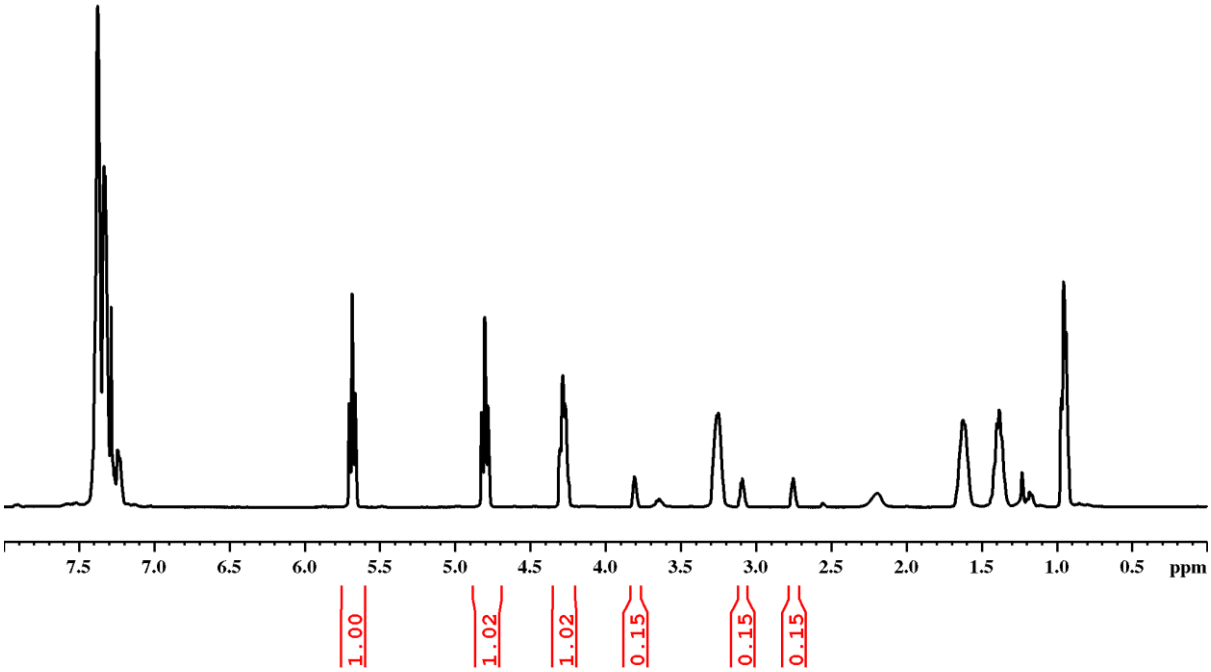

Figure A.18. ^{1}H NMR spectrum of reaction number 3 in $CDCl_3$.

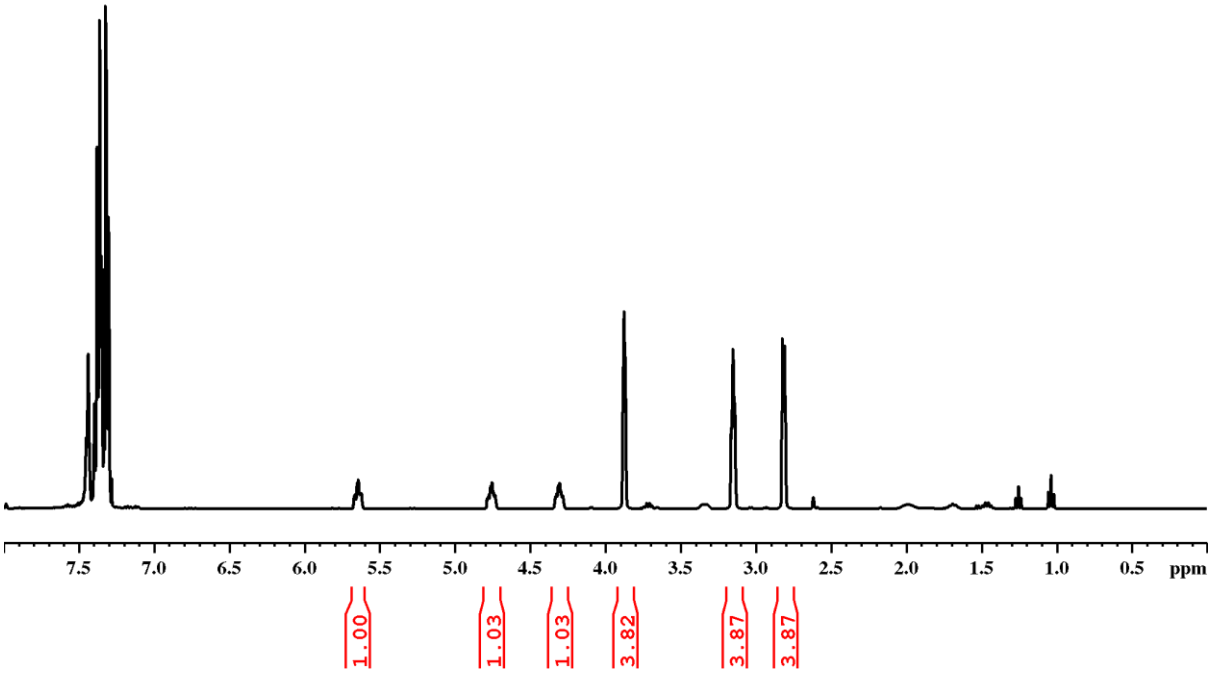

Figure A.19. ^{1}H NMR spectrum of reaction number 4 in $CDCl_3$.

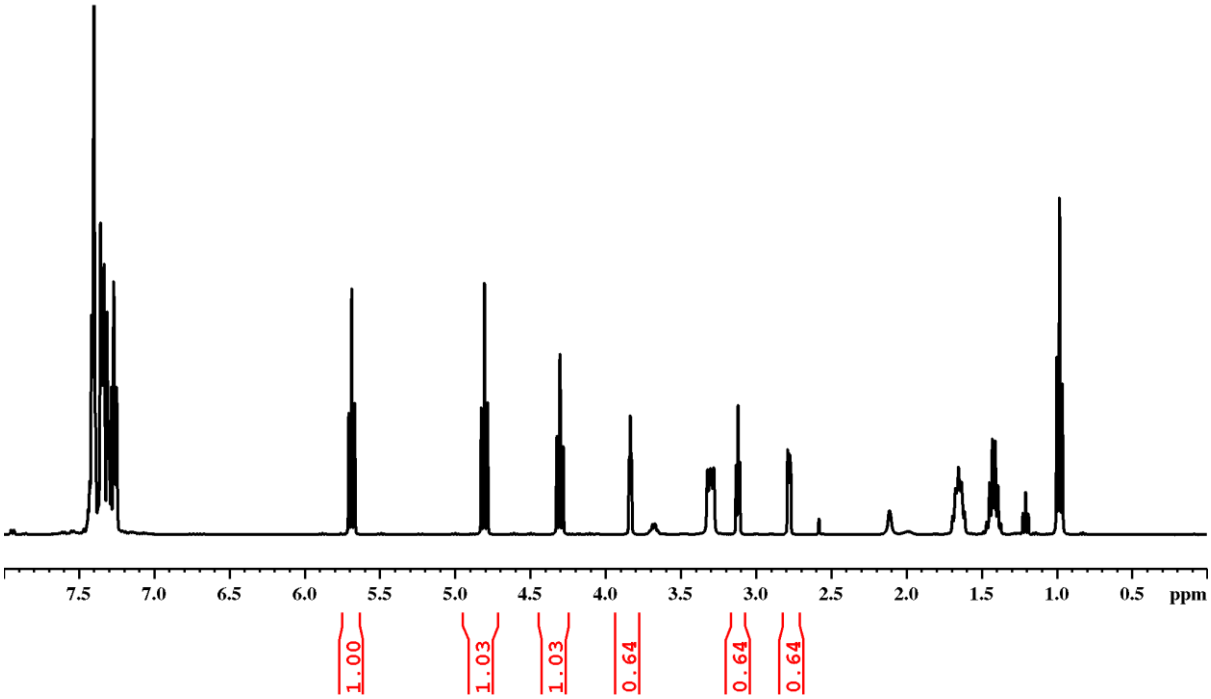

Figure A.20. ^{1}H NMR spectrum of reaction number 5 in $CDCl_3$.

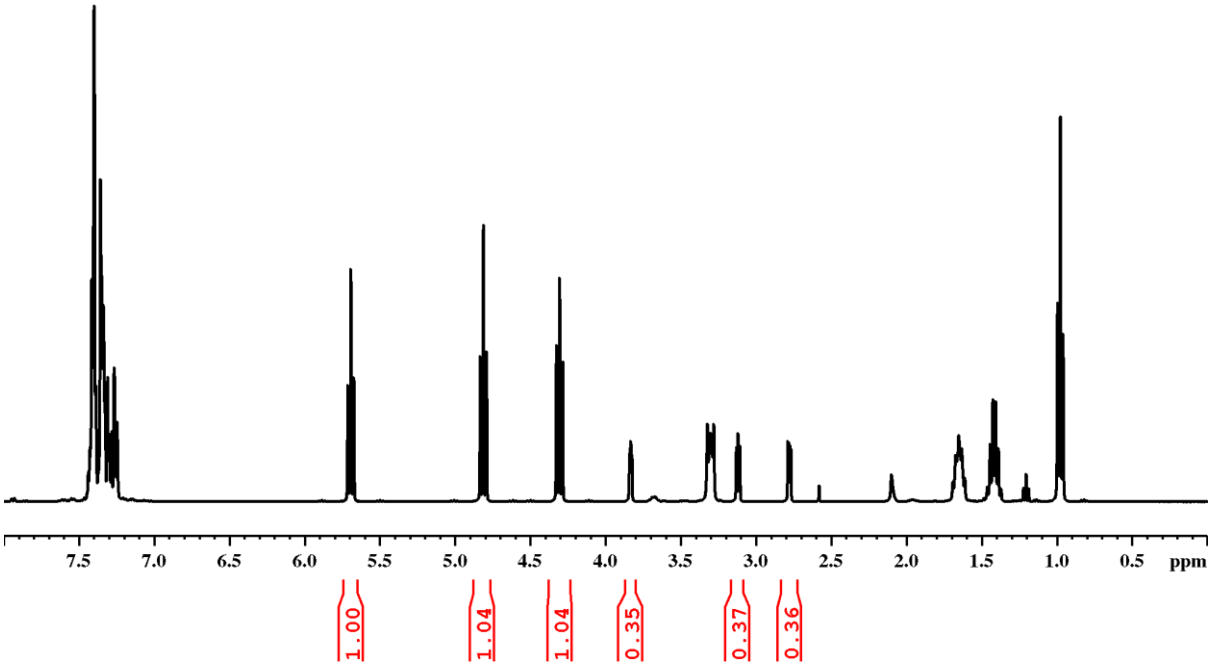

Figure A.21. ^{1}H NMR spectrum of reaction number 6 in $CDCl_3$.

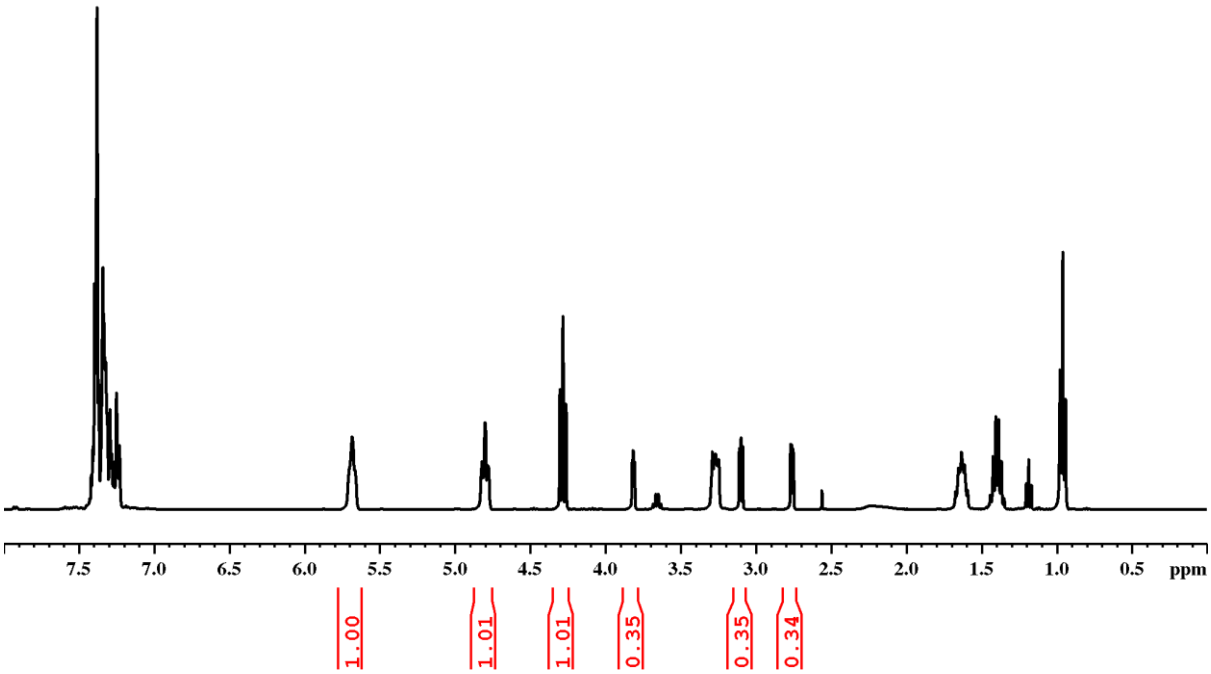

Figure A.22. ^{1}H NMR spectrum of reaction number 7 in $CDCl_3$.

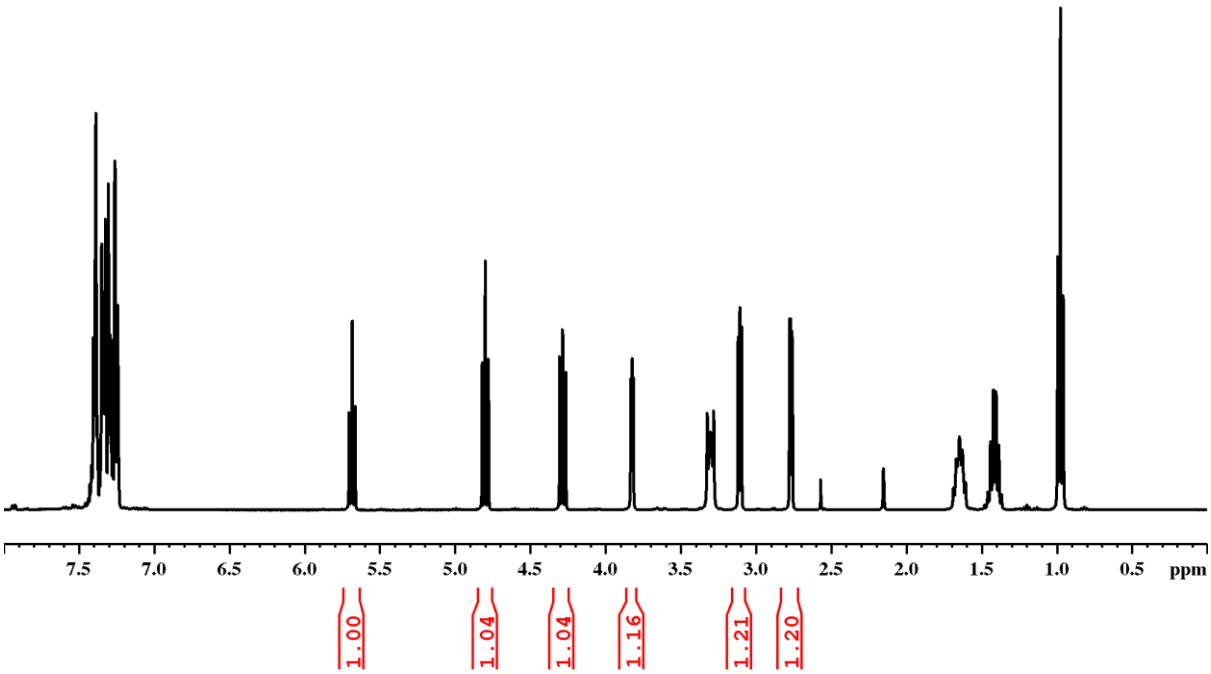

Figure A.23. ^{1}H NMR spectrum of reaction number 8 in $CDCl_3$.

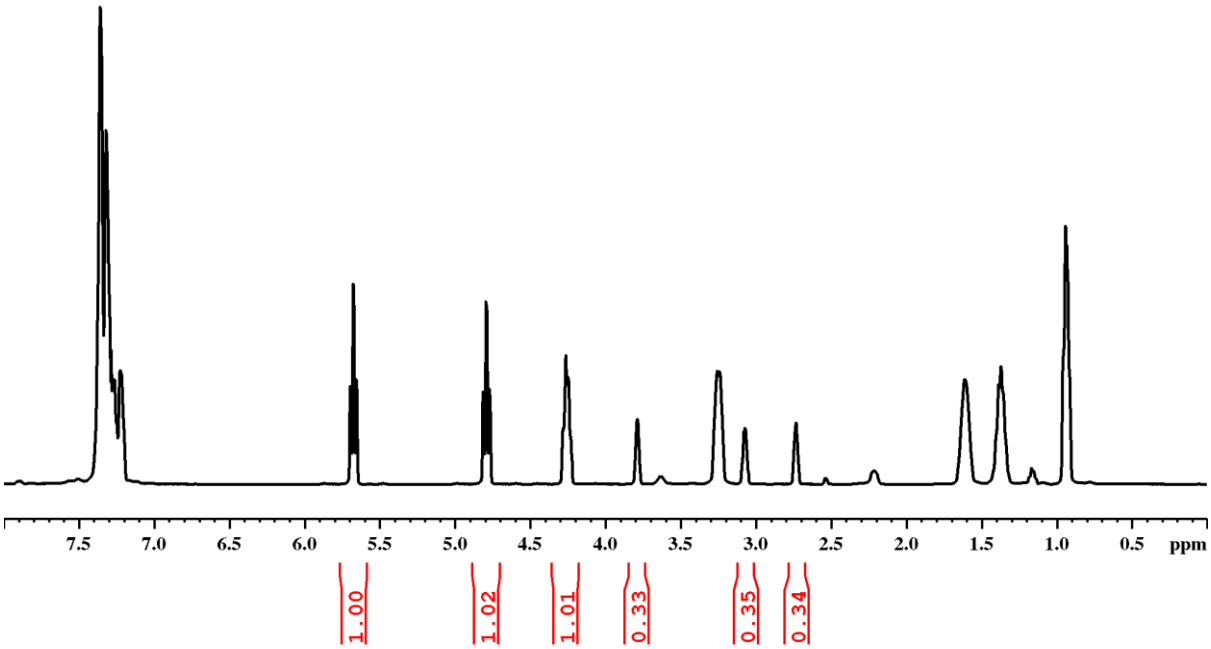

Figure A.24. ^{1}H NMR spectrum of reaction number 9 in $CDCl_3$.

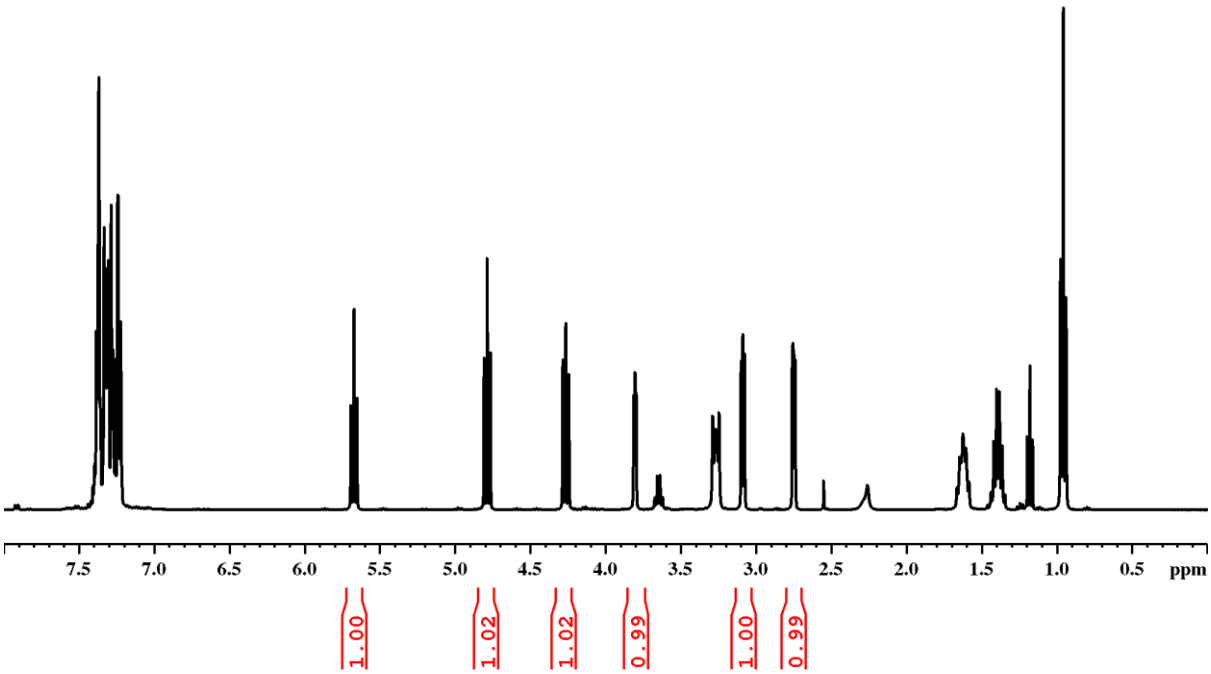

Figure A.25. ^{1}H NMR spectrum of reaction number 10 in $CDCl_3$.

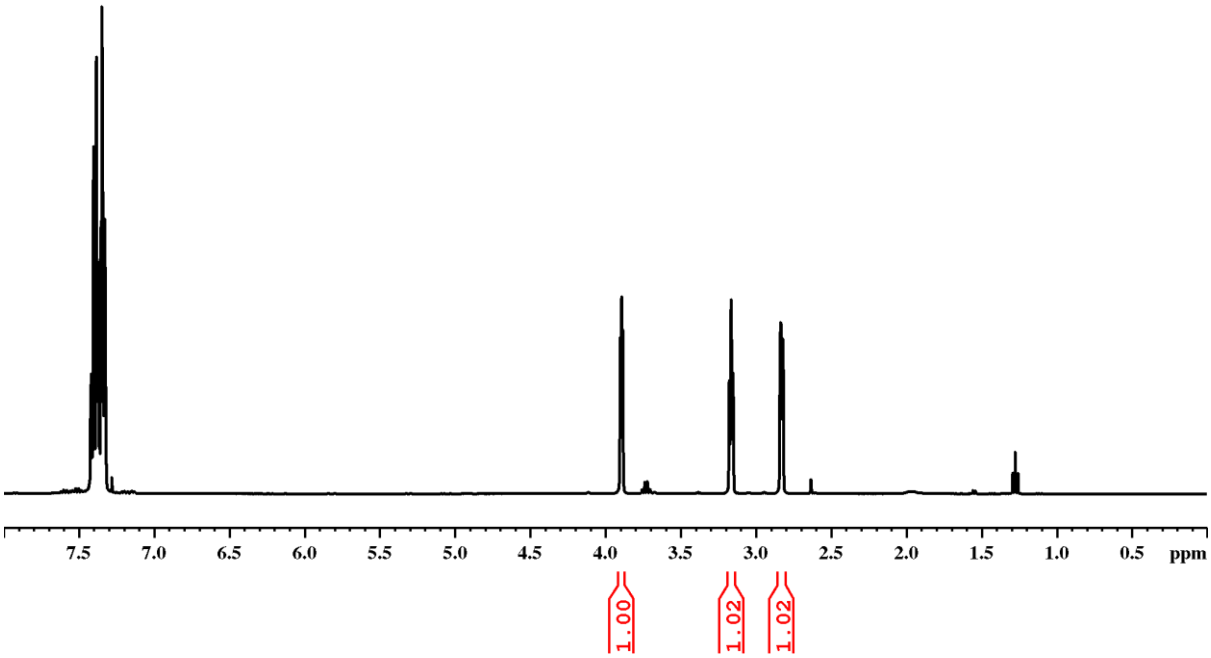

Figure A.26. ^{1}H NMR spectrum of reaction number 11 in $CDCl_3$.

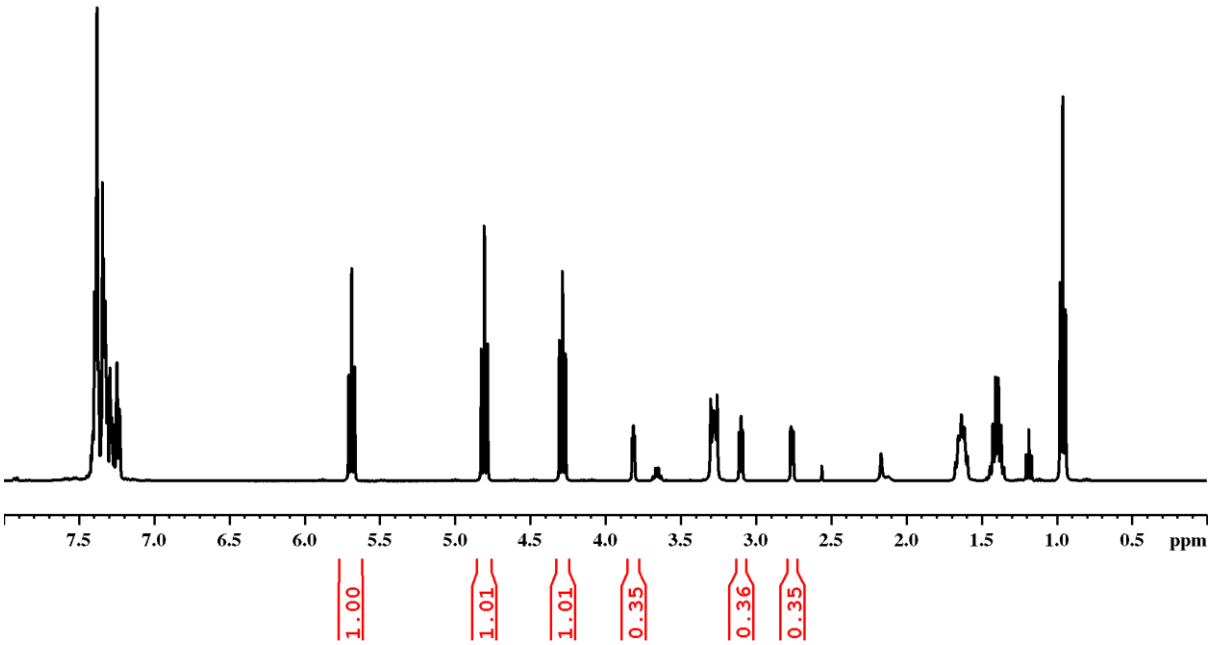

Figure A.27. ^{1}H NMR spectrum of reaction number 12 in $CDCl_3$.

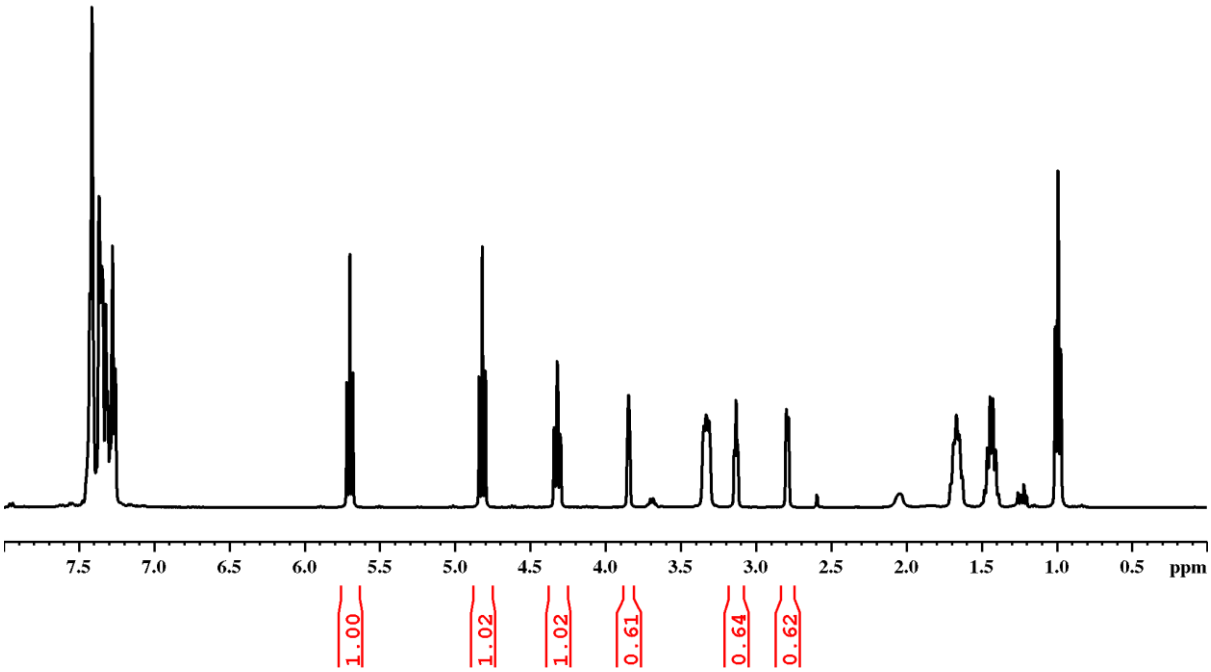

Figure A.28. ^{1}H NMR spectrum of reaction number 13 in $CDCl_3$.

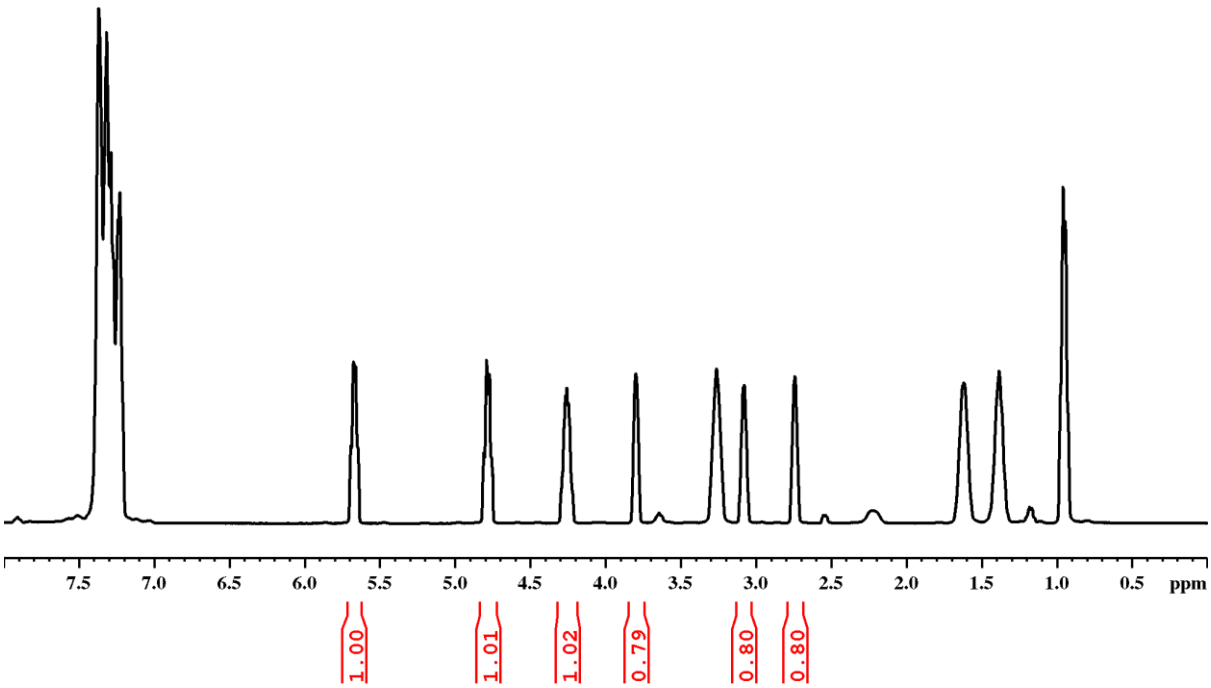

Figure A.29. ^{1}H NMR spectrum of reaction number 14 in $CDCl_3$.

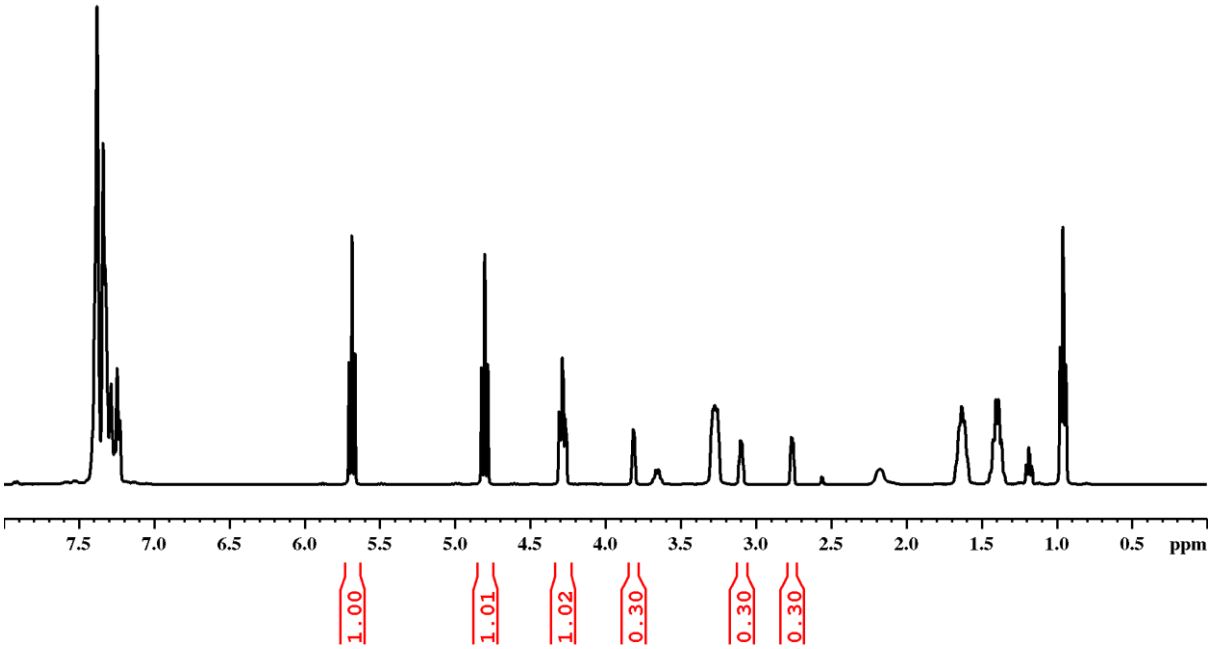

Figure A.30. ^{1}H NMR spectrum of reaction number 15 in $CDCl_3$.

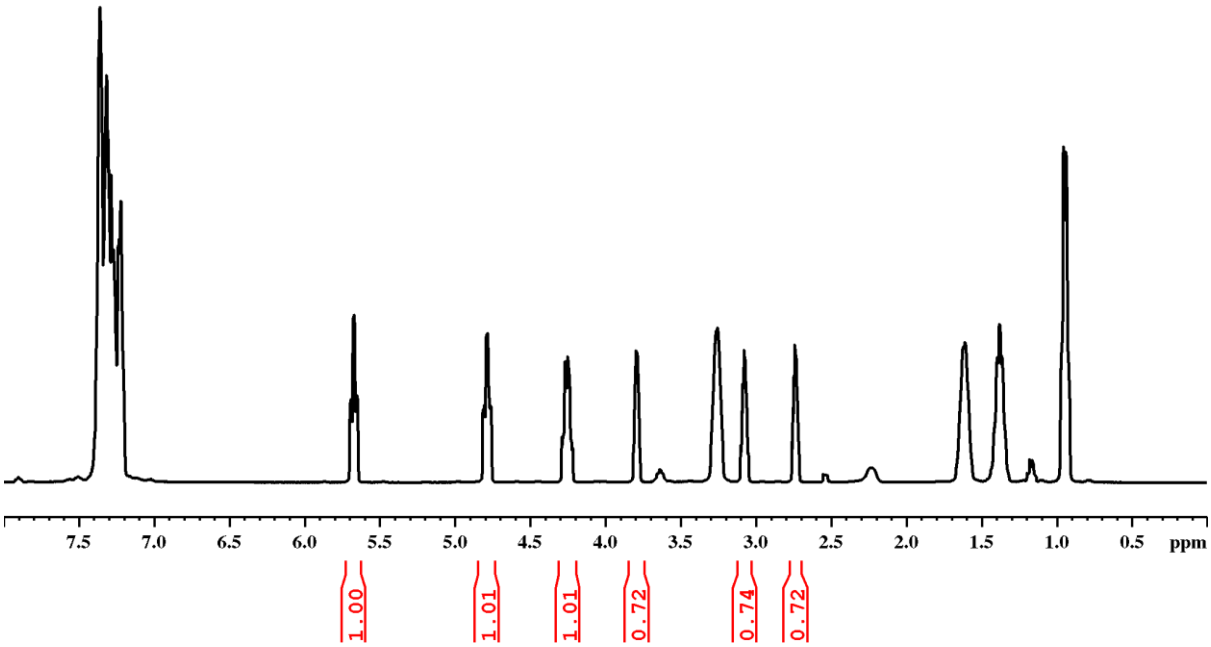

Figure A.31. ^{1}H NMR spectrum of reaction number 16 in $CDCl_3$.

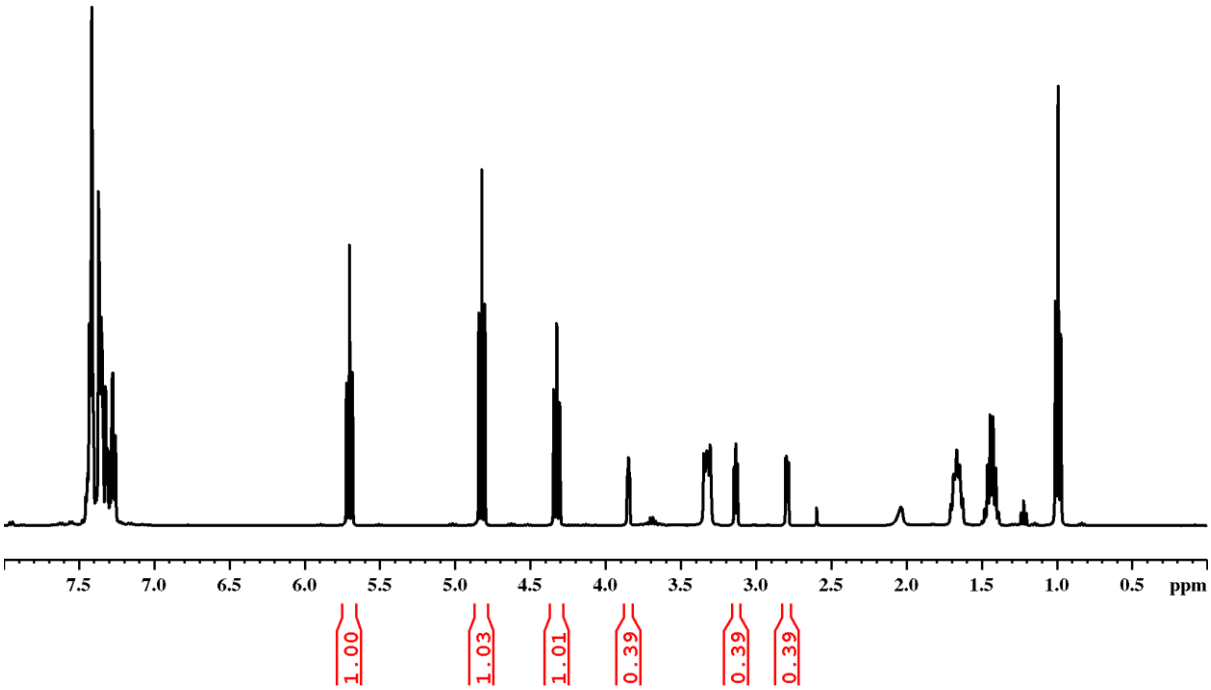

Figure A.32. ^{1}H NMR spectrum of reaction number 17 in $CDCl_3$.

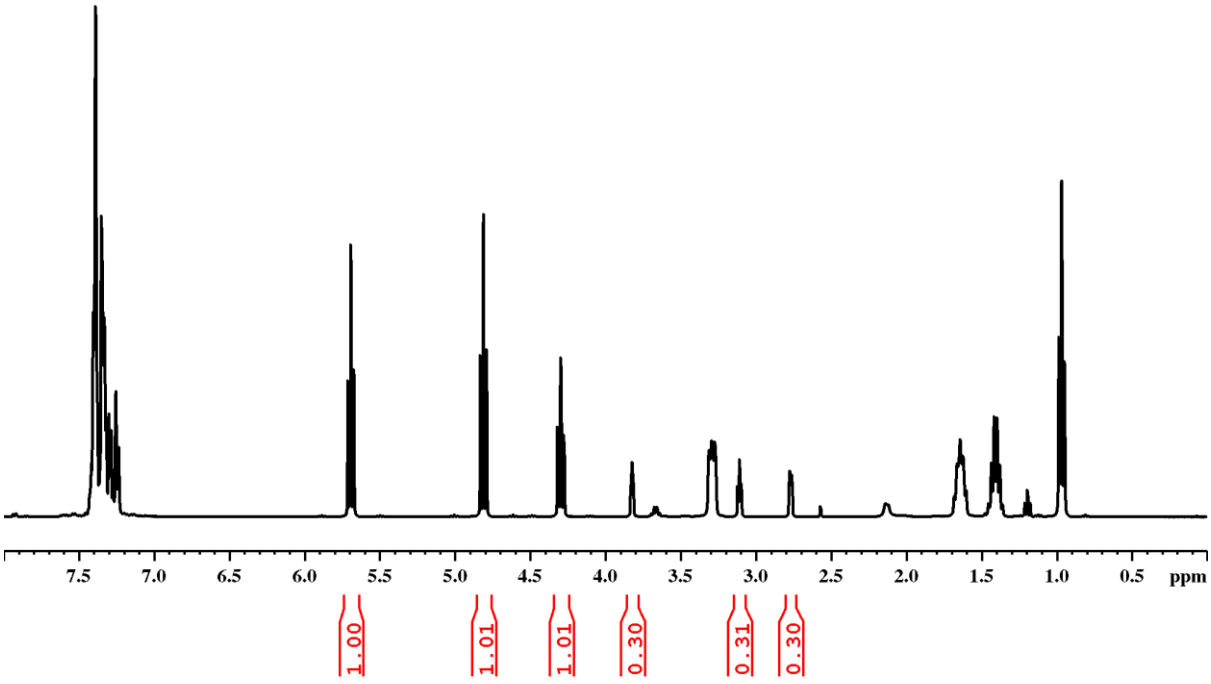

Figure A.33. ^{1}H NMR spectrum of reaction number 18 in $CDCl_3$.

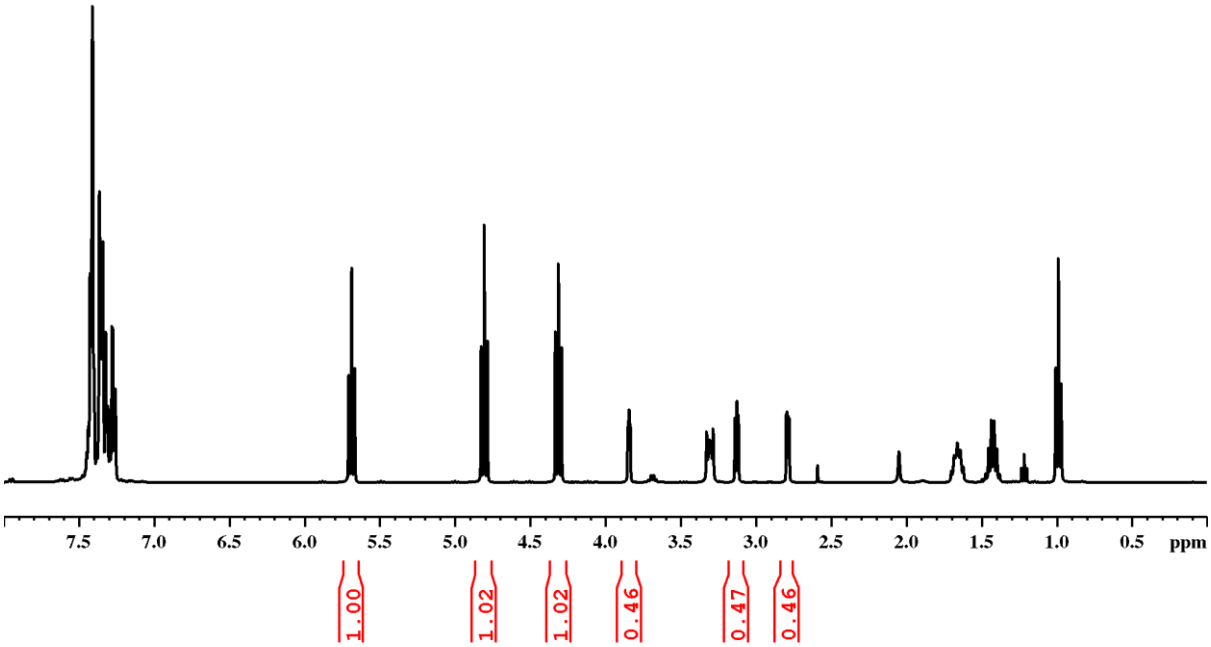

Figure A.34. ^{1}H NMR spectrum of reaction number 19 in $CDCl_3$.

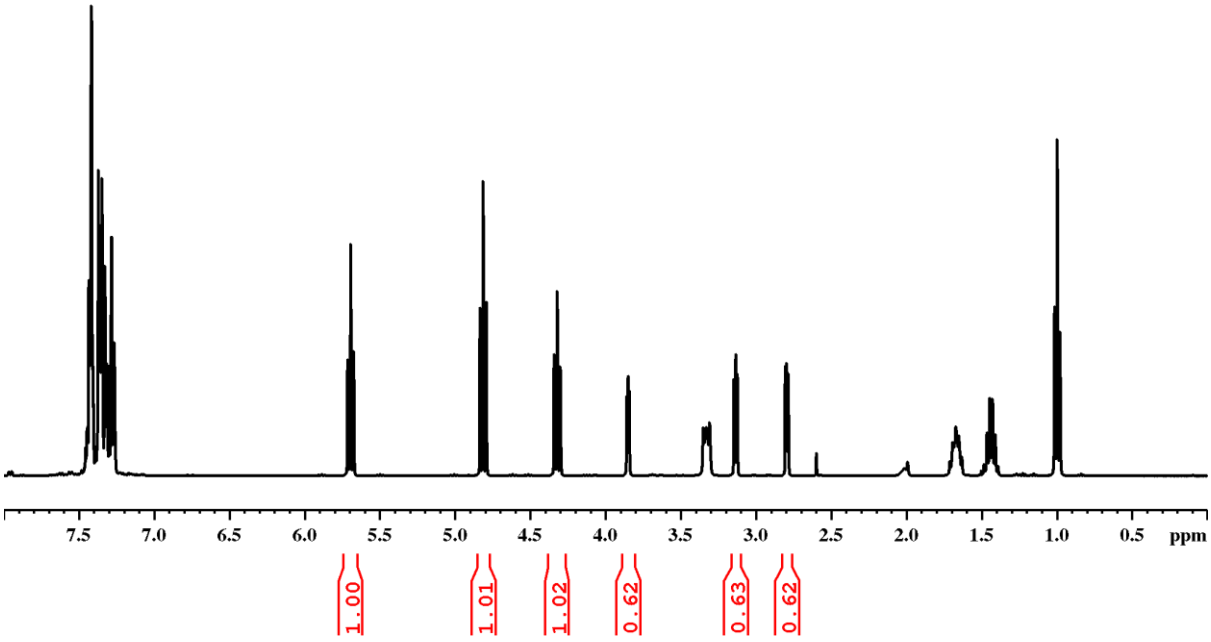

Figure A.35. ^{1}H NMR spectrum of reaction number 20 in $CDCl_3$.

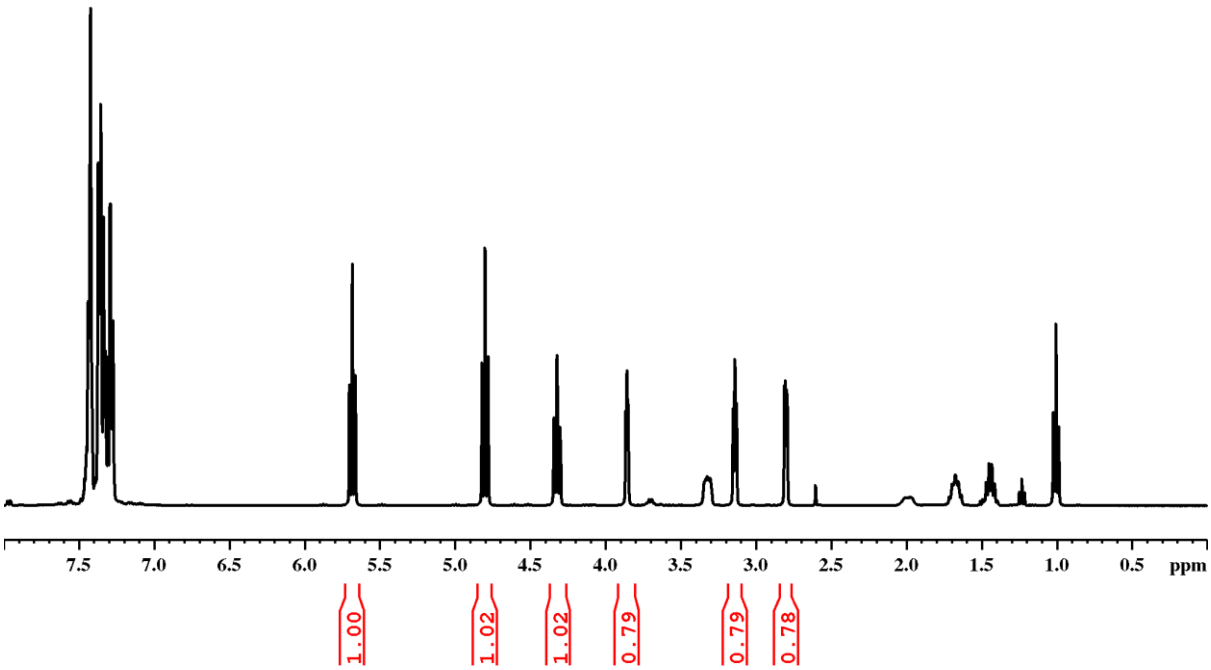

Figure A.36. ^{1}H NMR spectrum of reaction number 21 in $CDCl_3$.

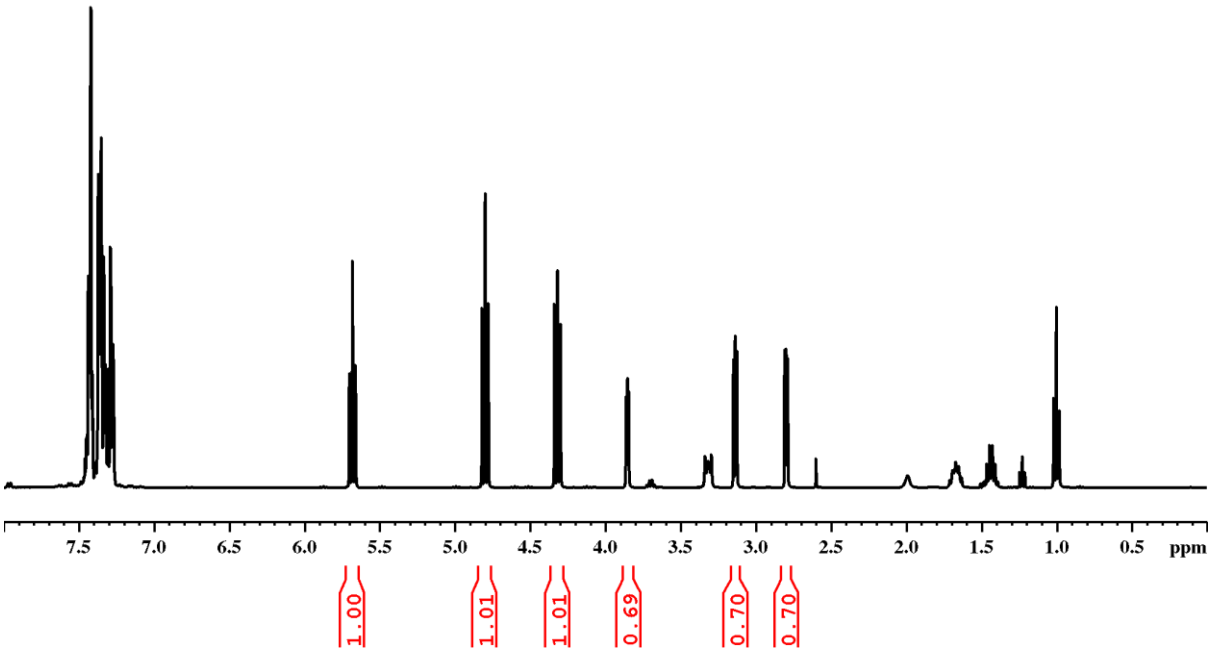

Figure A.37. ^{1}H NMR spectrum of reaction number 22 in $CDCl_3$.

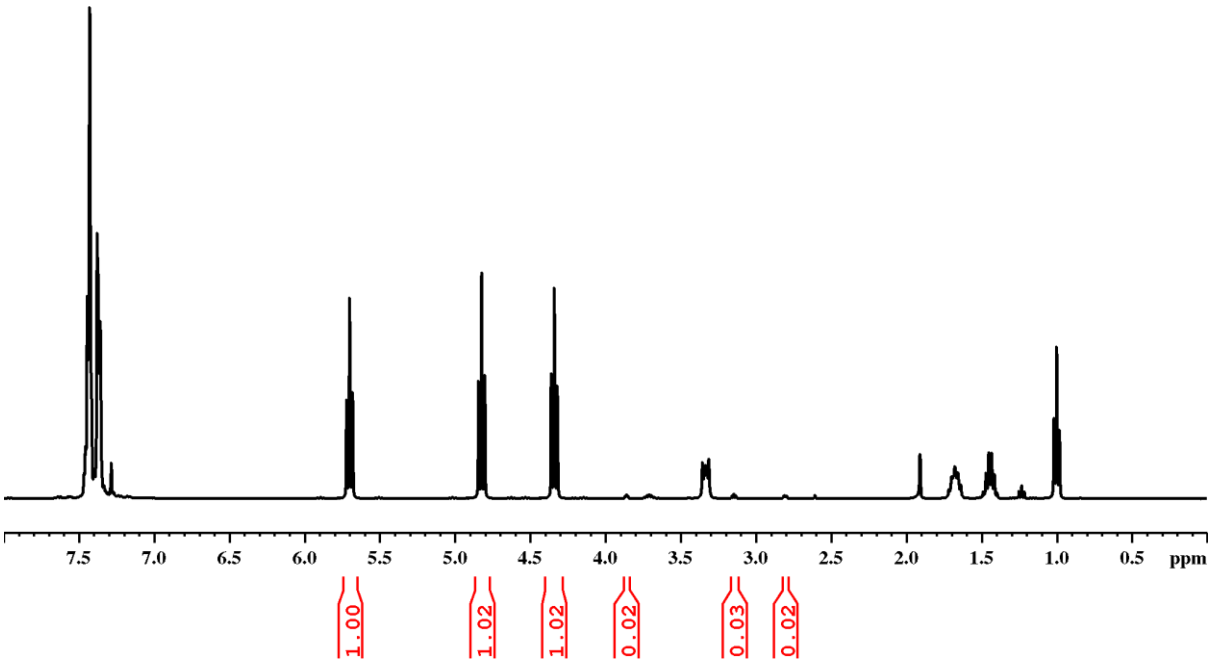

Figure A.38. ^{1}H NMR spectrum of reaction number 23 in $CDCl_3$.

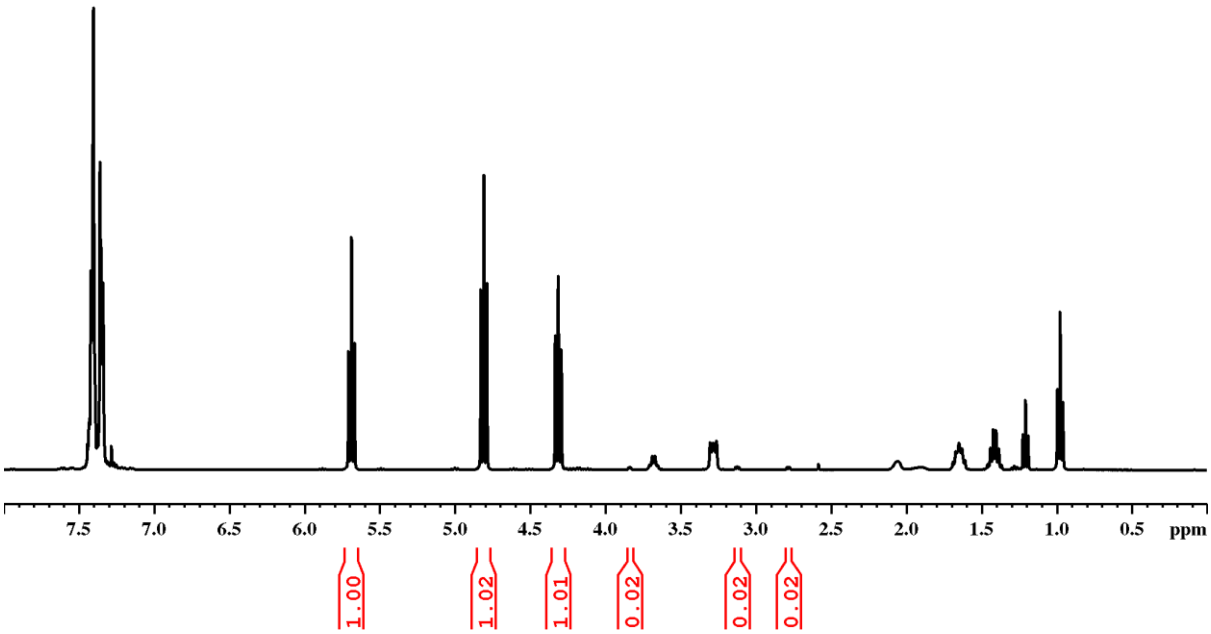

Figure A.39. ^{1}H NMR spectrum of reaction number 24 in $CDCl_3$.

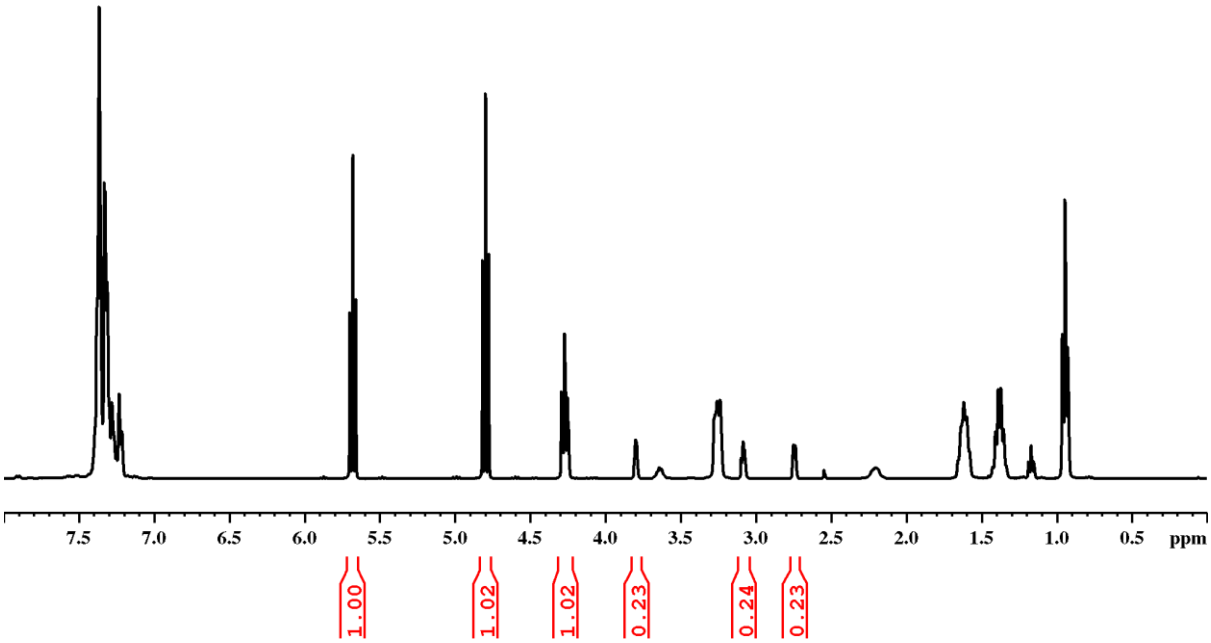

Figure A.40. ^{1}H NMR spectrum of reaction number 25 in $CDCl_3$.

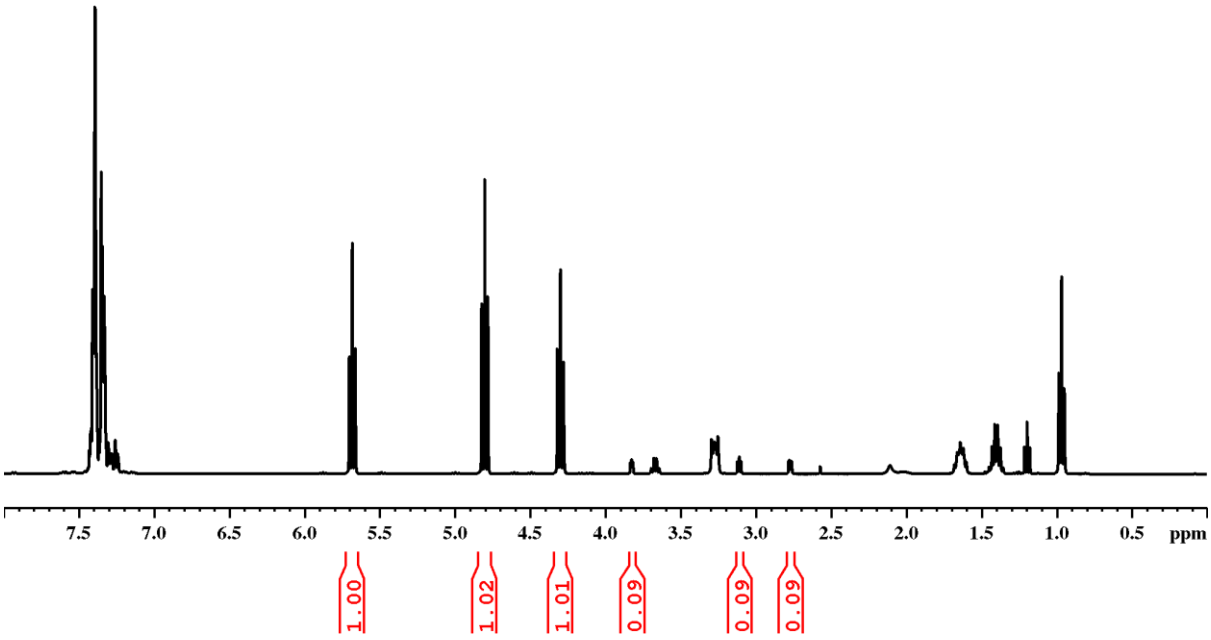

Figure A.41. ^{1}H NMR spectrum of reaction number 26 in $CDCl_3$.

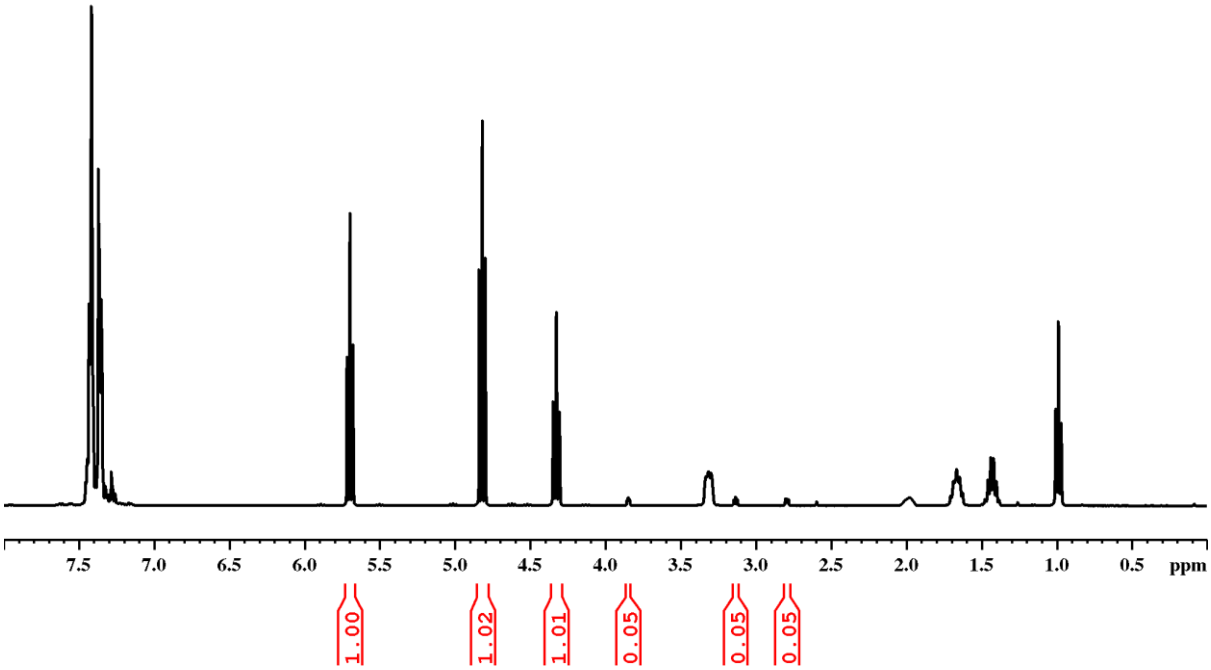

Figure A.42. ^{1}H NMR spectrum of reaction number 27 in $CDCl_3$.

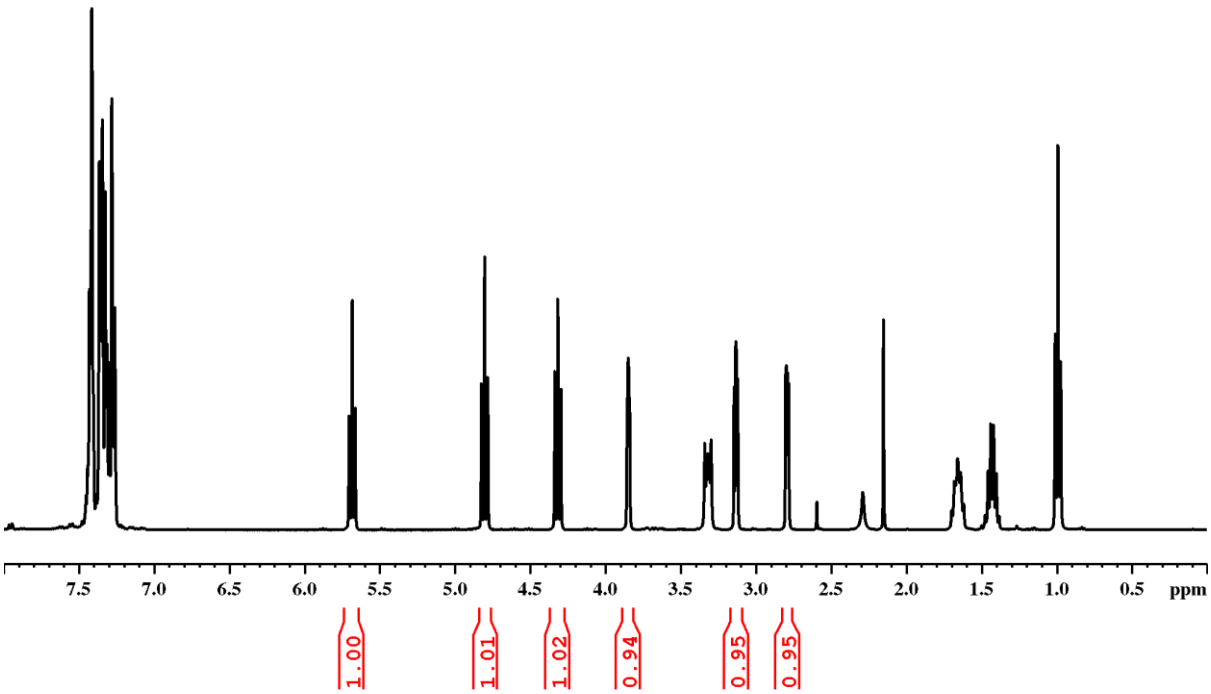

Figure A.43. ^{1}H NMR spectrum of reaction number 28 in $CDCl_3$.

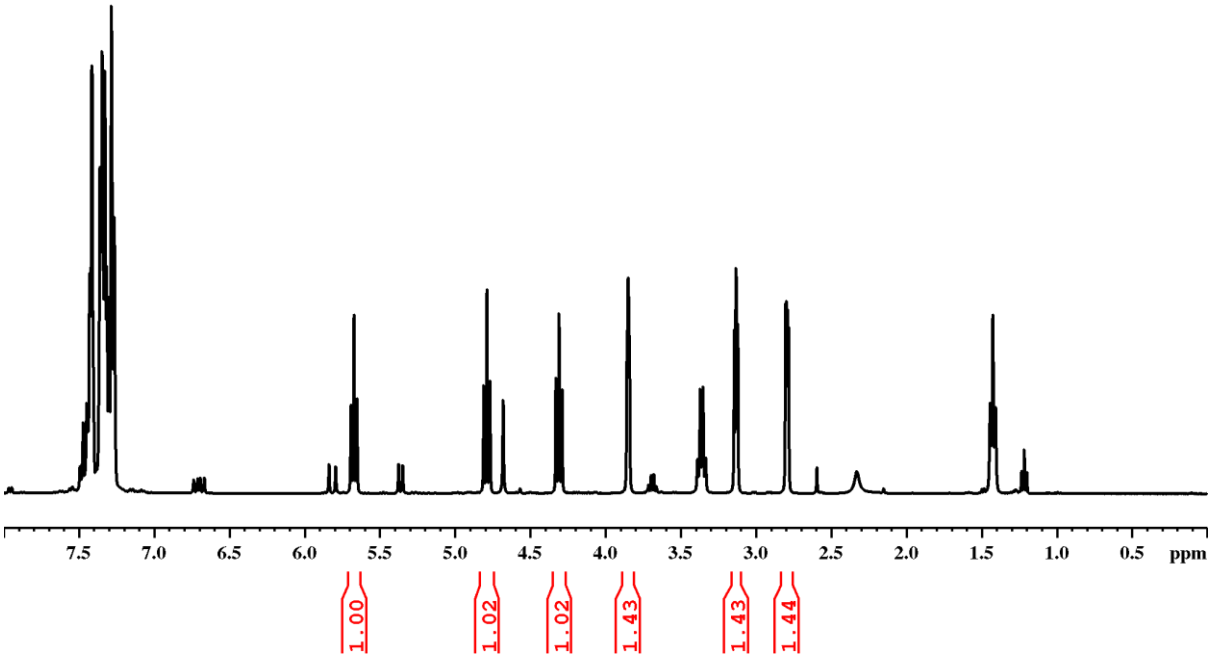

Figure A.44. ^{1}H NMR spectrum of reaction number 29 in $CDCl_3$.

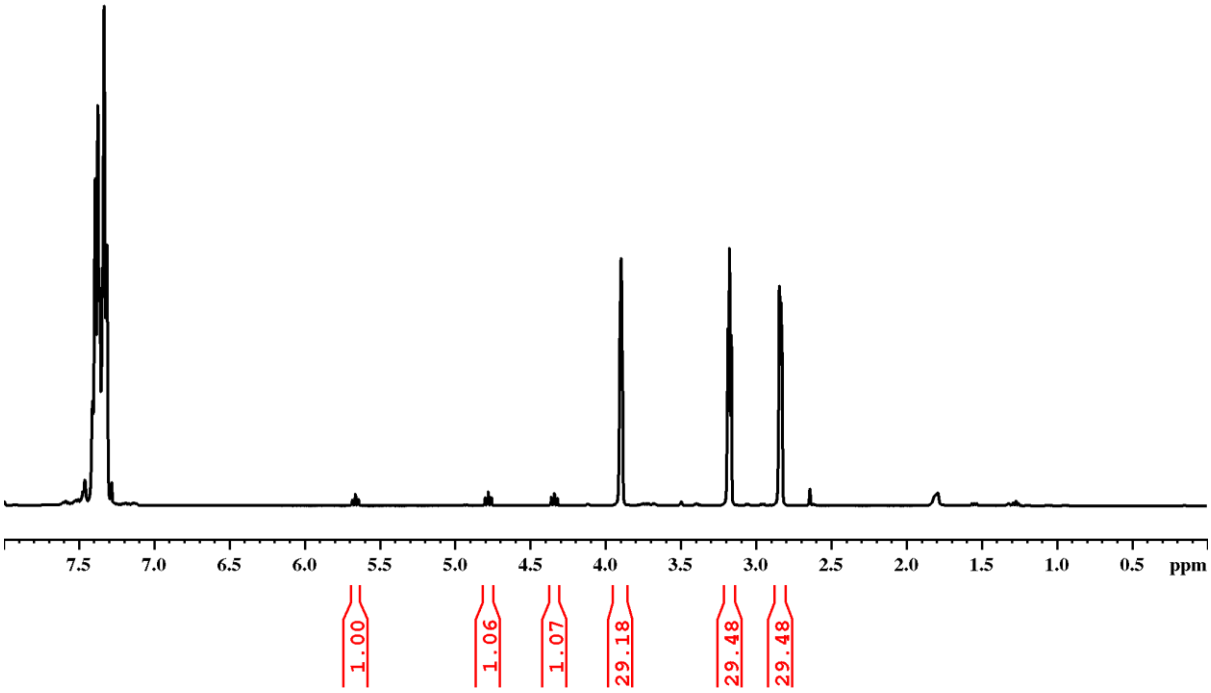

Figure A.45. ^{1}H NMR spectrum of reaction number 30 in $CDCl_3$.

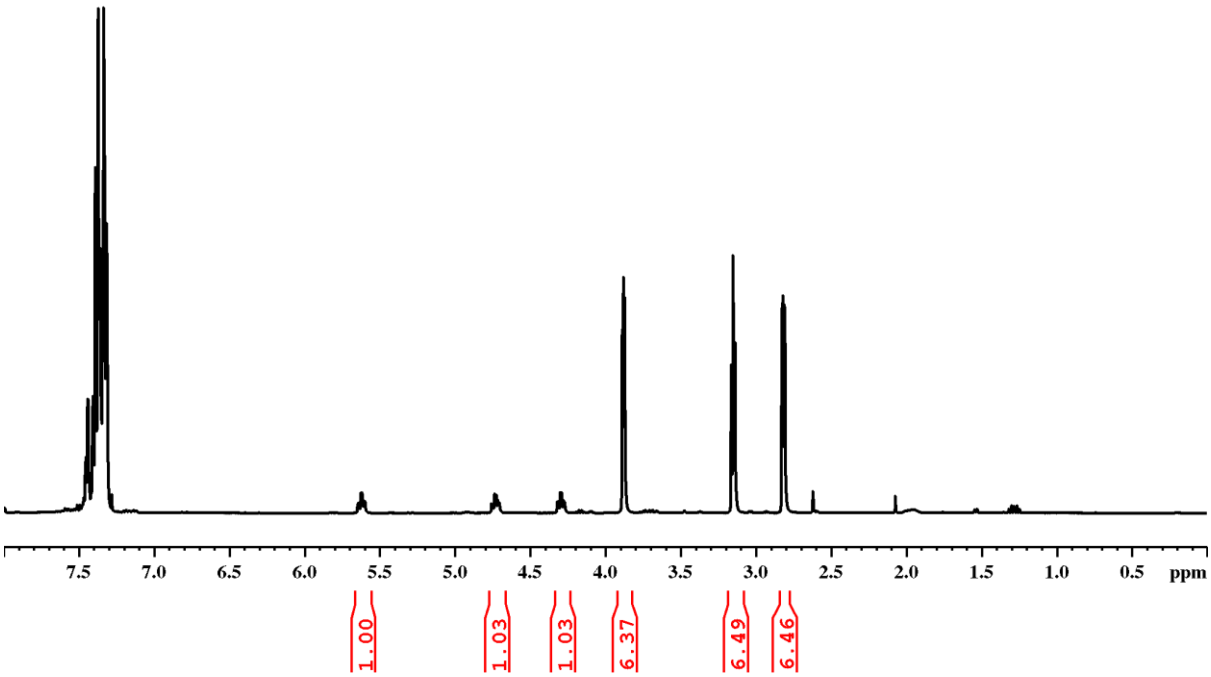

Figure A.46. ^{1}H NMR spectrum of reaction number 30a in $CDCl_3$.

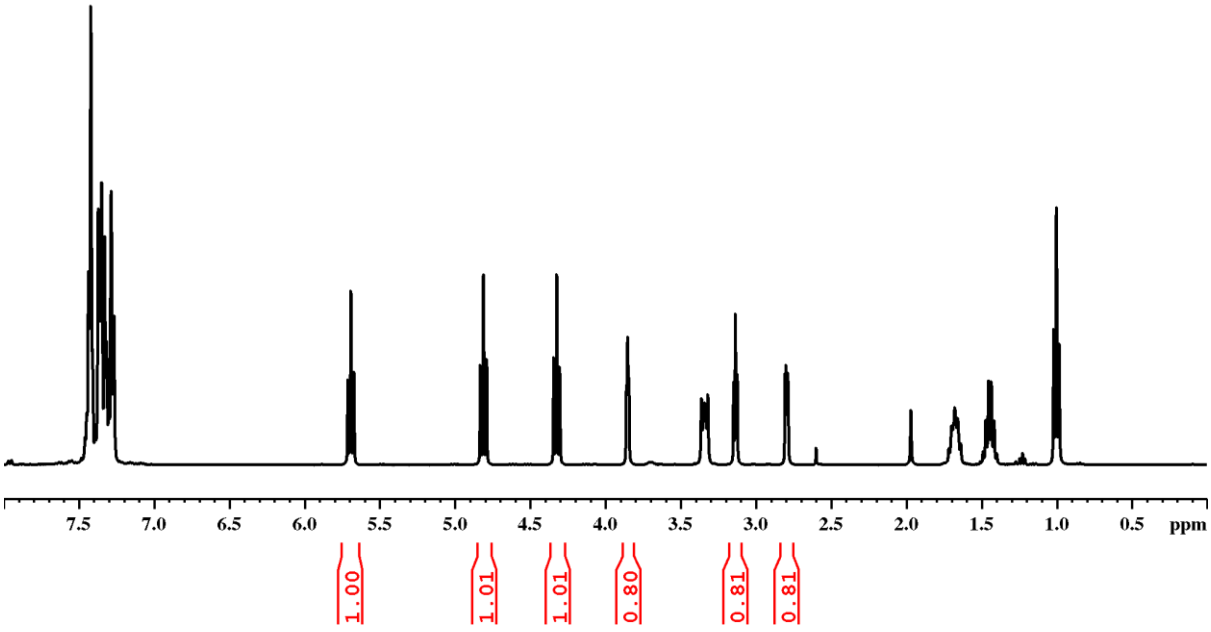

Figure A.47. ^{1}H NMR spectrum of reaction number 31 in $CDCl_3$.

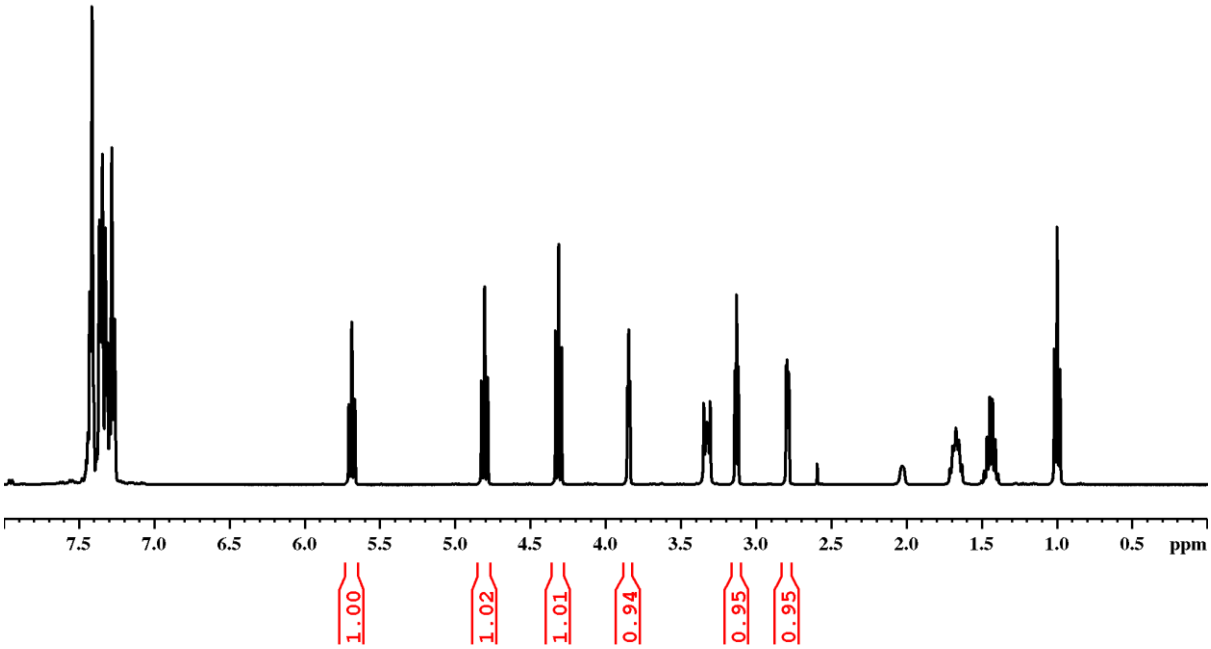

Figure A.48. ^{1}H NMR spectrum of reaction number 32 in $CDCl_3$.

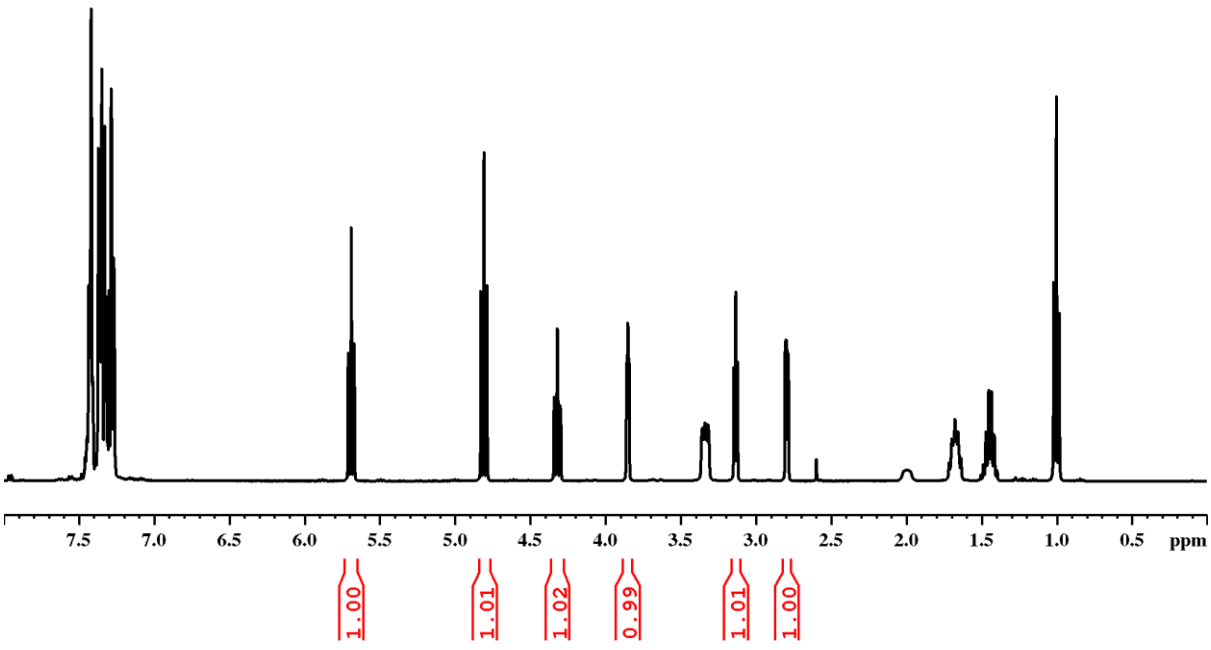

Figure A.49. ^{1}H NMR spectrum of reaction number 33 in $CDCl_3$.

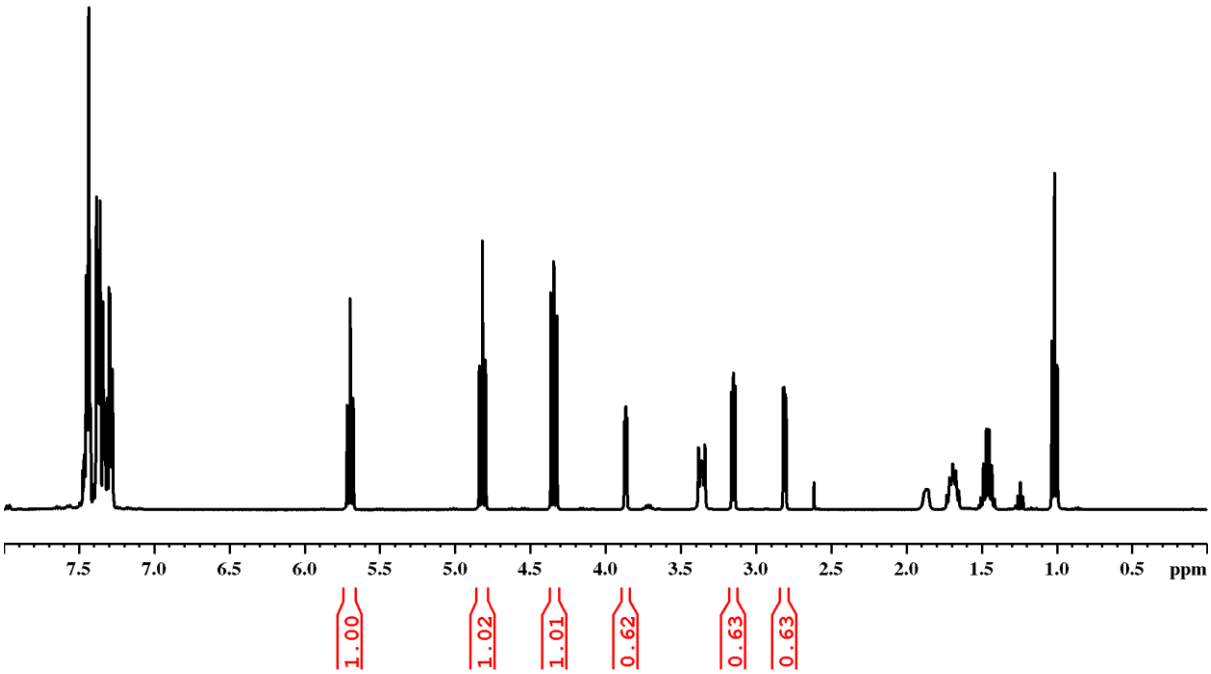

Figure A.50. ^{1}H NMR spectrum of reaction number 34 in $CDCl_3$.

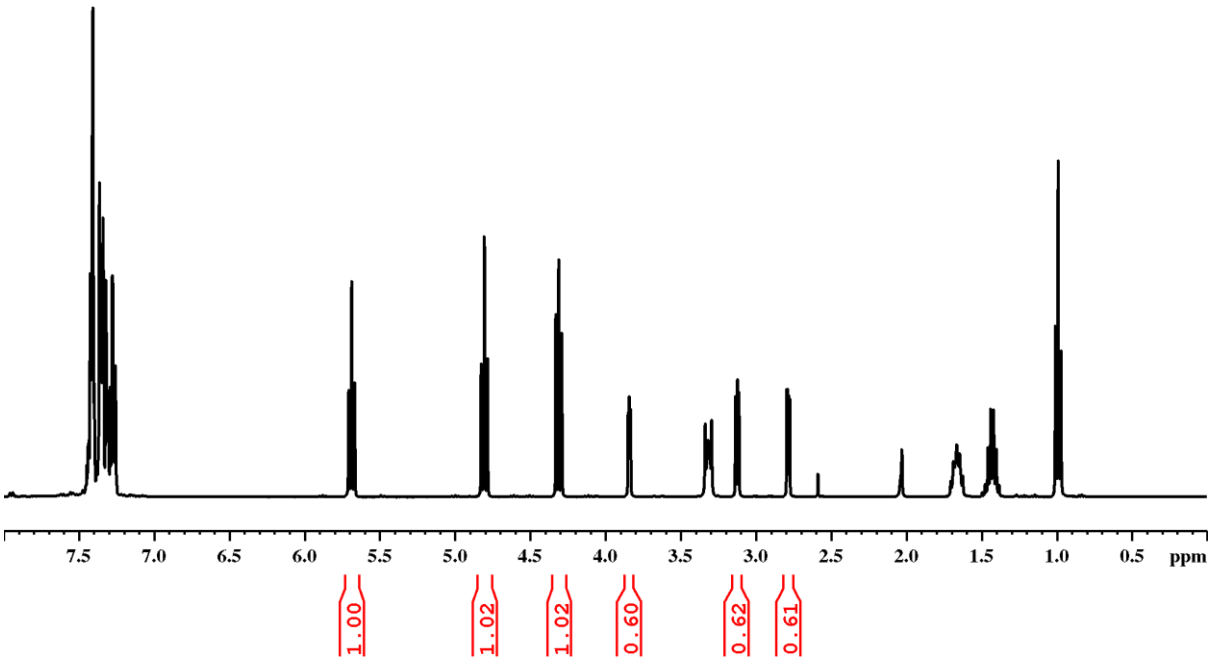

Figure A.51. ^{1}H NMR spectrum of reaction number 35 in $CDCl_3$.

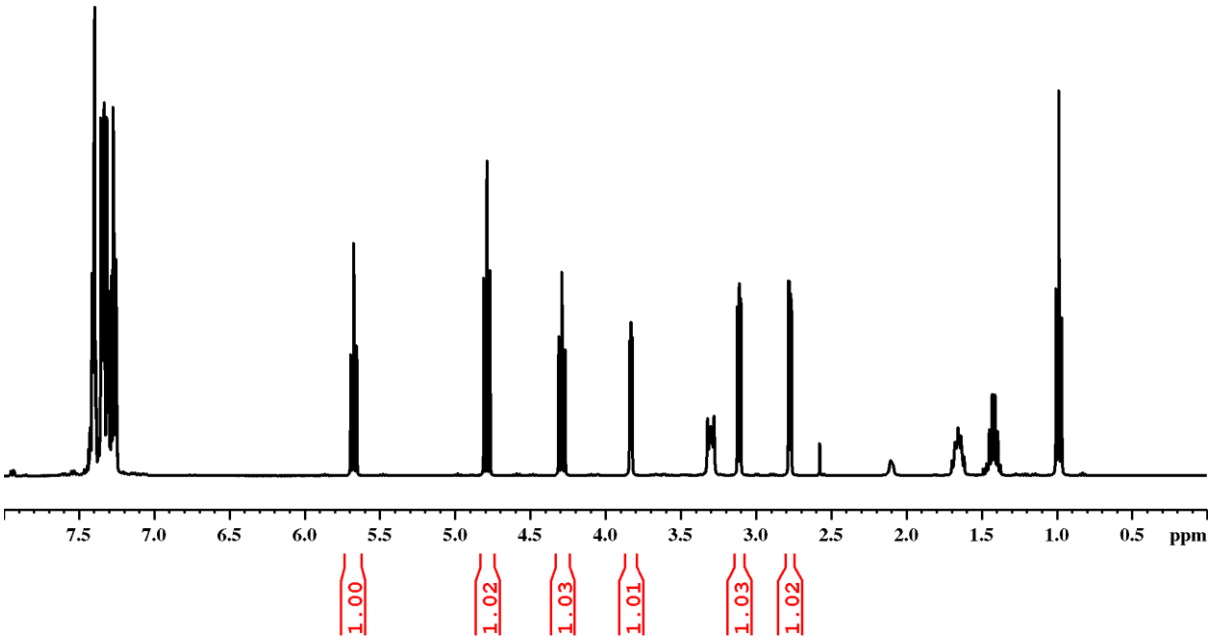

Figure A.52. ^{1}H NMR spectrum of reaction number 36 in $CDCl_3$.

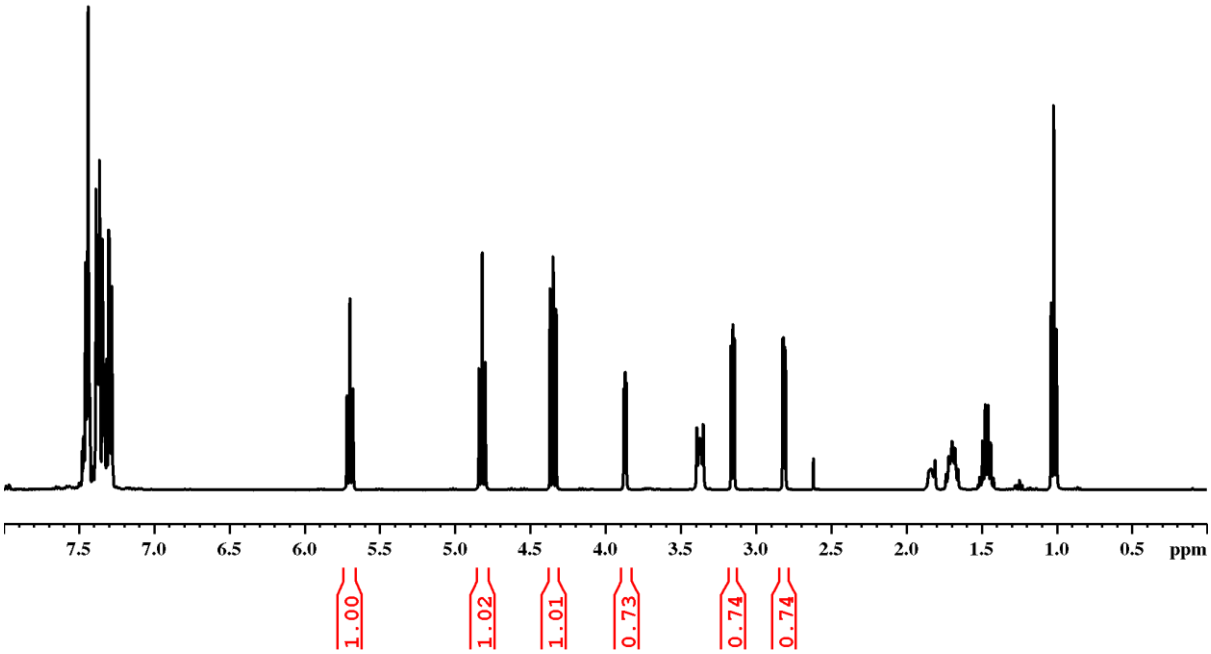

Figure A.53. ^{1}H NMR spectrum of reaction number 37 in $CDCl_3$.

2021

MÓNICA AVELÃS STANTON ARAU RIBEIRO

DEVELOPMENT OF NEW MATERIALS FOR CO_2 CONVERSION: EFFECT OF CARBONIZATION

NOVA SCHOOL OF SCIENCE & TECHNOLOGY